STEADY AND UNSTEADY HEAT AND MASS TRANSFER THROUGH POROUS MEDIA WITH PHASE CHANGE

by

Andrew P. Shapiro

B.A., Dartmouth College
(1982)

B.E., Thayer School of Engineering
(1983)

SUBMITTED IN PARTIAL FULFILLMENT

OF THE REQUIREMENTS OF THE

DEGREE OF

MASTER OF SCIENCE

IN MECHANICAL ENGINEERING

at the

MASSACHUSETTS INSTITUTE OF TECHNOLOGY

February 1987

Signature of Author _____
Department of Mechanical Engineering
February 17, 1987

Certified by _____
Shahryar Motakef
Thesis Supervisor

Certified by _____
Leon Glicksman
Thesis Supervisor

Accepted by _____
Ain A. Sonin
Chairman, Departmental Committee on Graduate Students

Acknowledgements

I wish to thank the Oak Ridge National Laboratory , which has sponsored this research contract. In addition I express my sincere gratitude to Professor Shahryar Motakef for his encouragement and guidance throughout this work. The development of the transient analytic model in this thesis is based on previous work by Prof. Motakef. My work with Prof. Motakef has been a productive learning experience. I also thank Dr. Leon Glicksman for his numerous practical suggestions which have helped direct the experimental work in this thesis.

I also appreciate the assistance given to me by the Phys-Chemical Research Corporation who took special care in providing me with polymer coated humidity transducers.

Steady and Unsteady Heat and Mass Transfer
Through Porous Media with Phase Change

by Andrew P. Shapiro

ABSTRACT

The behavior of liquid water in roof insulation is important in determining the conditions for which the insulation will tend to accumulate water or dry out.

A one-dimensional, quasi-steady, analytical model is developed to simulate transient transport of heat and mass with phase change through a porous slab subjected to temperature and vapor concentration gradients.

Small scale experiments examining the heat and moisture transport through fiberglass insulation were conducted. These experiments indicate that condensate tends to accumulate in a non-uniform manner.

In spite of the irregularities in moisture distribution, the data from these experiments indicate that the quasi-steady model is capable of predicting the transient behavior of heat and moisture transport in roof insulation. Additionally, the quasi-steady model is shown to agree well with the experimental results from other researchers.

Thesis Supervisors: Prof. Shahryar Motakef
Dr. Leon Glicksman

TABLE OF CONTENTS

1. Introduction

In recent years there has been much speculation regarding the supply of cheap energy. Because the price of end-use energy depends on many factors, it has been difficult to make accurate predictions of the long term cost of energy. It is this uncertainty which has prompted many industries to employ energy conservation techniques as a hedge against sudden increases in energy costs.

The building industry has been active in developing and implementing energy conservation measures. Improvements have been achieved in building materials, construction techniques, and building design which have greatly reduced the energy consumption requirements of both industrial and residential buildings [9,12]. In the effort to reduce energy loss (or gain) through the building shell the two major approaches have been to add thermal insulation and to reduce air infiltration.

One of the major problems associated with the resulting energy-efficient buildings is water vapor condensation within the building shell. The reduced air infiltration can cause undesirably high levels of humidity to occur inside the building. As this humid interior air comes in contact with the cold external building skin, condensation can be expected.

Another manner in which water enters the building shell is by leakage through holes and cracks in the exterior shell. The numerous penetrations in the building shell necessary for ventilation, air conditioning, and heating provide likely sites for water leakage. The flat roof, popular on industrial buildings for its low capital cost, is especially vulneralble to leaks.

These two modes of water infiltration, condensation and leakage, can be responsible for higher heat losses, due to the decreased thermal resistance of the insulating material, as well as the destruction of the building shell. Once the water gets inside the roof cavity, the chances of fungal decay of wooden components are greatly increased [10]. In many cases the roof must be replaced. To illustrate the magnitude of this problem the U.S. currently spends approximately $10 billion per year on roofing, half of which goes to repairs and maintance [11].

Therefore there is a clear need to understand the mechanisms involved in moisture transfer in roofing systems. Of primary importance is the understanding of the environmental conditions necessary to dry out a roofing system. Because of the inherent coupling of moisture transfer and heat transfer, it is also necessary to understand the effects of moisture on the heat transfer behavior of the roofing system.

A review of the previous analytical work on simultaneous heat and moisture in insulating materials indicates that it

is necessary to make simplifying assumptions to develop a reasonable model[2,3]. However it is essential that such simplification do not lose sight of the controlling parameters. The first simplification is to model the roofing system as a one-dimensional system. Secondly, the roofing insulation is treated as a uniform porous medium through which heat and vapor diffuse. The mechanism of liquid diffusion may or may not be important. The theory of liquid diffusion has been extensively applied to the field of soil mechanics. Reference [1] presents the theory of liquid diffusion in soil. It is shown that below a critical liquid content level the liquid is essentially immobile, and above this critical level the liquid is subject to diffusion.

Simultaneous transport of heat and mass through porous insulation with condensation has been studied extensively [2,3,4,5]. The analytic work of Thomas et al [2] presents a set of differential equations to simulate the simultaneous transfer of heat vapor and liquid through porous insulation. Although their transient numerical model is verified by experiment, the results cannot be generalized and the most important governing parameters are not identified. In addition their explicit solution is too complicate to be easily applied

Motakef [3] has developed a simplified analytic model of simultaneous heat and mass transport through porous media with phase change. His formulation yields a completely

generalized solution for steady-state conditions in which the parameters governing heat transfer, condensation rate, and vapor diffusion are well defined. Motakef has also shown that the steady-state solution can form the basis of a transient model.

The previous experimental work on moisture transfer in insulating materials [2,4] has clearly demonstrated the coupling of heat transfer and moisture movement. However these experiments were of limited applicability to roofing systems. The work of Katsenelenbogen[4] examining vapor diffusion in vertically oriented polystyrene, demonstrates the possibility of a zone of condensation within the insulating slab as predicted by Motakef's model. Thomas et al [2] examined moisture migration in horizontally oriented figerlass completely encased polyethylene film. His experimental results provide useful data with which to compare analytic models, but do not accurately represent a roofing system.

The objectives of this work are:

- To develop useful analytic tools capable of predicting those cases for which a horizontal roof is subject to the accumulation of condensate, and those cases for which a wet roof will dry out. The heat transfer behavior of these roofs is also of interest.

- To develop a small scale experimental apparatus to investigate the behavior of liquid and heat transport in a

sample of roofing material subjected to a variety of realistic environmental conditions.

The quasi-steady model presented in this work is based largely on the model developed by Motakef. Here, the contribution has been the implementation of the transient model and the verification of this model through numerical simulation and experimentation.

There are two major objectives to the experimental section of this work. The first is to provide a versatile tool for testing the performance of small scale roofing samples subjected to a variety of conditions. It is believed observations from such experiments will lead to an understanding of the physics involved in moisture movement. Secondly, the experimental work will provide a means to validate the analytic models developed in the following sections. It is desirable to have the capability to subject the sample to steady-state temperature and humidity conditions as well as time varying conditions. The steady-state conditions will provide information valuable to the development of an analytic model, whereas the transient conditions will be able to simulate actual weather conditions.

The experiments presented in this work can be divided in two catagories. The first two experiments have been designed to verify the ability of the test apparatus to provide a one-dimensional environment in which to test roofing

samples. The last two experiments examine the transient behavior of moisture in fiberglass insulation.

In specific, the first experiment demonstrates the ability to accurately determine the conductivity of an insulation sample if a one-dimensional temperature field is assumed. Though this ability was not employed in the subsequent experiments, it is included here as reference for future experiments. The second experiment verifies the one-dimensional behavior of heat and vapor flux through a dry insulation sample. In this experiment the failure mode of the humidity sensors is also demonstrated. The next experiment examines the movement of moisture in an insulation sample with a vapor barrier on the cold side. The last experiment is a study of the drying of an insulation sample given an initial liquid content and subjected to a temperature and concentration gradient.

2. ANALYSIS

2.1 PROBLEM STATEMENT

In this section we analyse the simultaneous transport of heat, vapor, and moisture in fiberglass roofing insulation. Assuming discontinuous, randomly oriented fibers the insulation is modeled as a one-dimensional infinite slab of a porous medium.

In this analysis we consider an infinite slab of a porous medium that is permeable to heat, vapor, and liquid water flux. The void space of the porous medium is occupied primarily by air and water vapor. The slab is placed horizontally with the high temperature reservoir below and the low temperature reservoir above the slab. With the heat transfer by conduction and radiation combined into an effective conductivity, it can be assumed that heat is transported solely by conduction from the high temperature reservoir to the low temperature reservoir. Vapor diffuses from the reservoir of higher vapor concentration to the reservoir of lower concentration. The energy flux due to diffusing vapor and air is assumed to be negligible. Depending on the values of temperature and humidity in the reservoirs, the temperature and concentration fields within the slab may form a zone of saturation conditions, where the local temperatures in this zone equal the dew-point associated with the local values of the vapor concentration.

In such a zone there will be phase change of vapor to liquid. This condensation releases latent heat which affects the temperature field. Thus the mechanisms of heat and mass transfer through porous media with phase change are coupled.

The goal of this analysis is to model the heat, vapor, and liquid transport in such a slab with steady-state and transient reservoir conditions.

2.2. HEAT AND MASS TRANSFER WITH PHASE CHANGE IN POROUS MEDIA: SPATIALLY STEADY ANALYSIS

In this secton we consider the case in which the reservoirs surrounding the slab are characterized by constant temperature and humidity. In both reservoirs the relative humidity is below 100 %. The reservoirs below and above the slab are identified by (T_h, C_h) and (T_c, C_c) respectively:

T_h - temperature of the hot reservoir
C_h - vapor concentration of the hot reservoir
T_c - temperature of the cold reservoir
C_c - vapor concentration of the cold reservoir

with $T_h > T_c$ and $C_h > C_c$

2.2.1 HEAT AND VAPOR TRANSPORT IN THE DRY REGIONS

Given that neither reservoir has a relative humidity of 100%, if condensation occurs it will be in a region sandwiched between two dry zones. In each dry zone there are no heat or vapor sources so the heat flux, q/A, is given by Fourier's Law and the vapor flux, J_v, is given by Fick's Law:

$$q/A = -k\ dT/dz \qquad (1)$$

$$J_v = -D_v\ dc/dz \qquad (2)$$

where z is the distance across the slab measured from the hot side. Integration of eqs. (1) and (2) show that the dry regions on each side of the wet zone have linear temperature and concentration profiles for steady-state conditions. Let the wet zone have boundaries at z_0 and z_1 ($z_0 < z_1$) and the temperatures at these boundaries be T_0 and T_1. Since these boundaries mark the edges of the region of condensation the vapor concentration at z_0 is the saturation concentration at T_0, namely:

$$c_0 = c^*(T_0)$$

and similarly,

$$c_1 = c^*(T_1)$$

Hence the temperature and concentration profiles in the dry zone adjacent to the high temperature reservoir are given by:

$$T = T_h - z/z_0 \ (T_h - T_0) \qquad (3)$$

$$C = C_h - z/z_0 \ (T_h - T_0) \qquad (4)$$

For the dry region adjacent to the low temperature reservoir we have:

$$T = T_c + (L_t - z)/(L_t - z_1) \ (T_1 - T_c) \qquad (5)$$

$$C = Cc + (L_t - z)/(L_t - z_1) \ (C_1 - Cc) \qquad (6)$$

where L_t is the total length of the slab.

2.2.2 HEAT AND VAPOR TRANSPORT IN THE CONDENSATION REGION

Let the region of condensation in a slab of a porous medium, possibly between two dry regions, be characterized by width L_w, and temperatures T_0 and T_1 at the boundaries, with $T_0 > T_1$. The entire region being at saturation requires that the temperature and concentration profile are coupled such that

$$C(x) = C^{*}(T(x))$$

where C^{*} is the saturation concentration of water vapor.

Vapor and heat diffuse from the hot side (x=0) to the cold side ($x=L_w$). Heat is also conducted from the hot side to the cold side.

The differential equation describing the steady-state heat flow in the region is:

$$-k \frac{d^2T(x)}{dx^2} = w(x) \qquad (7)$$

where w denotes the rate of heat generation per unit volume. Steady-state vapor flux is given by:

$$D_v \frac{d^2C(x)}{dx^2} = \Gamma(x) \qquad (8)$$

where Γ denotes the rate of condensation per unit volume.

The energy released by condensation is the source at heat generation, thus:

$$w(x) = h_{fg} \Gamma(x)$$

where h_{fg} is the latent heat of condensation.

The condensation rate, Γ, couples eqns. (7) and (8). Eliminating Γ from them forms one differential equation:

$$\frac{d^2T}{dx^2} + (hfg\ Dv\ /\ k) \frac{d^2C}{dx^2} = 0 \qquad (9)$$

To non-dimensionalize eq.(9), we define the following terms:

$$T_r' = (T_0 + T_1)/2$$

$$\Delta T' = T_0 - T_1$$

$$C_r' = (C_0 + C_1)/2$$

$$\Delta C' = C_0 - C_1$$

$$\eta' = (T - T_r') / \Delta T'$$

$$\overline{C} = (C - C_r') / \Delta C'$$

$$\Omega' = h_{fg} \Delta C'/\rho\, c_p\, T_r' \quad \text{[Kossovitch number]}$$

$$\beta' = \Delta T'/T_r'$$

$$Le = \alpha / D_v$$

$$\overline{x} = x / L_w$$

The resulting non-dimensionalization of eq.(9) yields:

$$d^2\eta'/dx^2 + (\Omega'/Le\ \beta')\ d^2C/dx^2 = 0 \qquad (10)$$

C is a function of η determined by the equation of state of liquid water in saturation with its vapor. Thus eq.(10) is a second order nonlinear equation whose boundary conditions are:

$$\eta'(\bar{x}=0) = .5$$

$$\eta'(\bar{x}=1) = -.5$$

Note that in this geometry, $\bar{x}$ measures distance from the hot side of the wet zone.

2.2.2.1 ANALYTICAL SOLUTION

Motakef[3] has solved eq.(10) in an analytic form using a perturbation solution around a linear temperature profile. In this formulation ideal gas behavior of the air/vapor mixture is assumed, and the Clausius-Clapeyron relation is invoked to express C as a function of Á'.

$$C/C_r' = \exp(\phi)$$

where $\phi = \gamma'\beta'\eta' / (1 + \beta'\eta')$

$\gamma' = h_{fg}/(R\ T_r')$

Motakef's approximation of $\eta'(x)$ is given by:

$$\eta' = .5\left[1 - x - \frac{\exp(\lambda x) - 1}{\exp(\lambda) - 1}\right]^2 \qquad (11)$$

where $\lambda = \dfrac{2\ \gamma'\ \beta'\Omega'}{Le + \gamma'\Omega'}$

This simple form of $\eta'(x)$ is a function of the parameter λ. This parameter is composed of the physical properties of air and water, and the boundary conditions T_0,T_1, and L_w. Motakef[3] has shown that λ represents the ratio of the heat released by condensation to the heat that would be conducted through the medium if no condensation occurred.

2.2.2.2. NUMERICAL SOLUTION

Eq.(10) can be also solved numerically. The advantages of a well-formed numerical solution are increased accuracy, and flexibility in incorporating realistic changes in physical properties resulting from condensation. An additional use of the numerical solution is to verify the accuracy of the analytic solution. Here the Clausius-Clapeyron relation is used to approximate the rate of change of saturation concentration of a vapor with temperature:

$$dC^*/dT = h_{fg} C^* / R T^2 \qquad (12)$$

In this numerical approach C is determined from saturation data at each step, whereas in the analytic solution eq.(12) is integrated to give C as a simple function of Tr' and Cr', the mean temperature and concentration of the wet zone. The magnitude of the error induced by this approximation is examined in section 2.2.2.3.

Using eq.(12), eq.(10) is recast in a finite difference form using centered approximations for all derivatives:

$$\frac{T(i-1)-2T(i)+T(i+1)}{\Delta x^2} F(T(i)) + \frac{T(i+1)-T(i-1)}{2\ \Delta x}^2 K(T(i))=0 \qquad (13)$$

where

$F(T(i)) = 1 + h_{fg}Dv/k)\ (h_{fg}\ C(T)^2/(RT))$

$K(T(i)) = h_{fg}^2 Dv\ C(T)\ /\ (k\ R\ T^3\ )\ (h_{fg}/RT - 2)$

$C(T)$ is obtained from saturation data.

This second order nonlinear differential equation requires two boundary conditions. If the temperature at the boundaries, T_0 and T_1, are known then the problem is fully specified.

The method of solution is an iterative process based on Newton's Method. The region of condensation is divided into n sections (n=50 in our program). In this method, G(i) is defined by the left hand side of eq.(13). The idea is to set G(i) equal to zero for all n. In matrix notation Newton's Method can be expressed by:

$$J^k\ \Delta T^{k+1} = -G^k$$

where

$$J(i,i)=\frac{\partial G(i)}{\partial T(i)} = -2\ \frac{F(T(i))}{\Delta x^2} + \frac{T(i+1)-2T(i)+T(i-1)}{\Delta x^2}\ \frac{\partial F}{\partial T(i)} + \left[\frac{T(i+1)\ -\ T(i-1)}{4\ \Delta x^2}\right]\ \frac{\partial K}{\partial T(i)}$$

$$J(i,i-1)=\frac{\partial G(i)}{\partial (T(i-1))} = \frac{F(T(i))}{\Delta x^2} - K(T(i))\ \left[\frac{T(i+1)\ -\ T(i-1)}{2\ \Delta x^2}\right]$$

$$J(i,i+1)=\frac{\partial G(i)}{\partial (T(i+1))} = \frac{F(T(i))}{\Delta x^2} + K(T(i))\ \left[\frac{T(i+1)\ -\ T(i-1)}{2\ \Delta x^2}\right]$$

J is the Jacobian matrix whose (i,j) component is $\partial G(i)/\partial T(j)$, and ΔT is the incremental change in the T matrix. Since J is tridiagonal, it can be inverted efficiently by elimination. Thus the ΔT matrix for step k+1 is given by:

$$\Delta T^{k+1} = - G^{k} (J^{k-1})$$

In practice the $\tilde{O}T$ matrix is multiplied by a scalar, α ($0<\alpha<1$), to ensure convergence. The solution is reached in approximately ten iterations.

2.2.2.3. COMPARISON OF ANALYTICAL AND NUMERICAL SOLUTION TO TEMPERATURE PROFILE IN WET ZONE

Figure 1 shows the reduced temperature profile in a region of condensation as determined by the analytic method described in section 2.2.2.1 and the numerical method described in section 2.2.2.2. The relatively steep temperature and concentration gradients in this case represents an extreme condition at which to test the analytical solution, because the rate of condensation will be considerably higher than in most practical cases involving roof insulation. The agreement between the methods indicates that the approximations incorporated in the analytical model, namely the use of the Clausius-Clapeyron relation for determining the saturation

concentration and the perturbation solution of eq.(9), do not introduce significant error into the solution of the temperature field.

There are two advantages to the analytical solution. First of all, its solution is fast and straightforward. Once the boundary temperatures and wet zone thickness are determined, the parameter λ can be calculated and the temperature field is given by eq.(11). Secondly the parameter λ provides immediate information regarding the rate of overall condensation. The numerical model gives no such insight.

As an illustrative example, the condensation rate in the case depicted in fig. 1 is determined as follows:

$$T_0 = 305 \qquad T_1 = 274 \qquad L_w = 0.1 \text{ m}$$

$$\lambda = \frac{2\,\gamma'\,\beta'\Omega'}{Le + \gamma'\Omega'} = \frac{2\,(17.9)^2\,(.107)\,(29.5)}{1 + (17.9)\,(29.5)} = 3.82$$

$$\lambda = \frac{2\,H_{fg}\,\bar{\Gamma}}{k\,(T_0 - \bar{T}_1)/L_w}$$

$$\bar{\Gamma} = 0.023 \quad kg/m^2hr$$

W E T Z O N E T E M P E R A T U R E P R O F I L E

Comparison of Analytical and Numerical Solutions

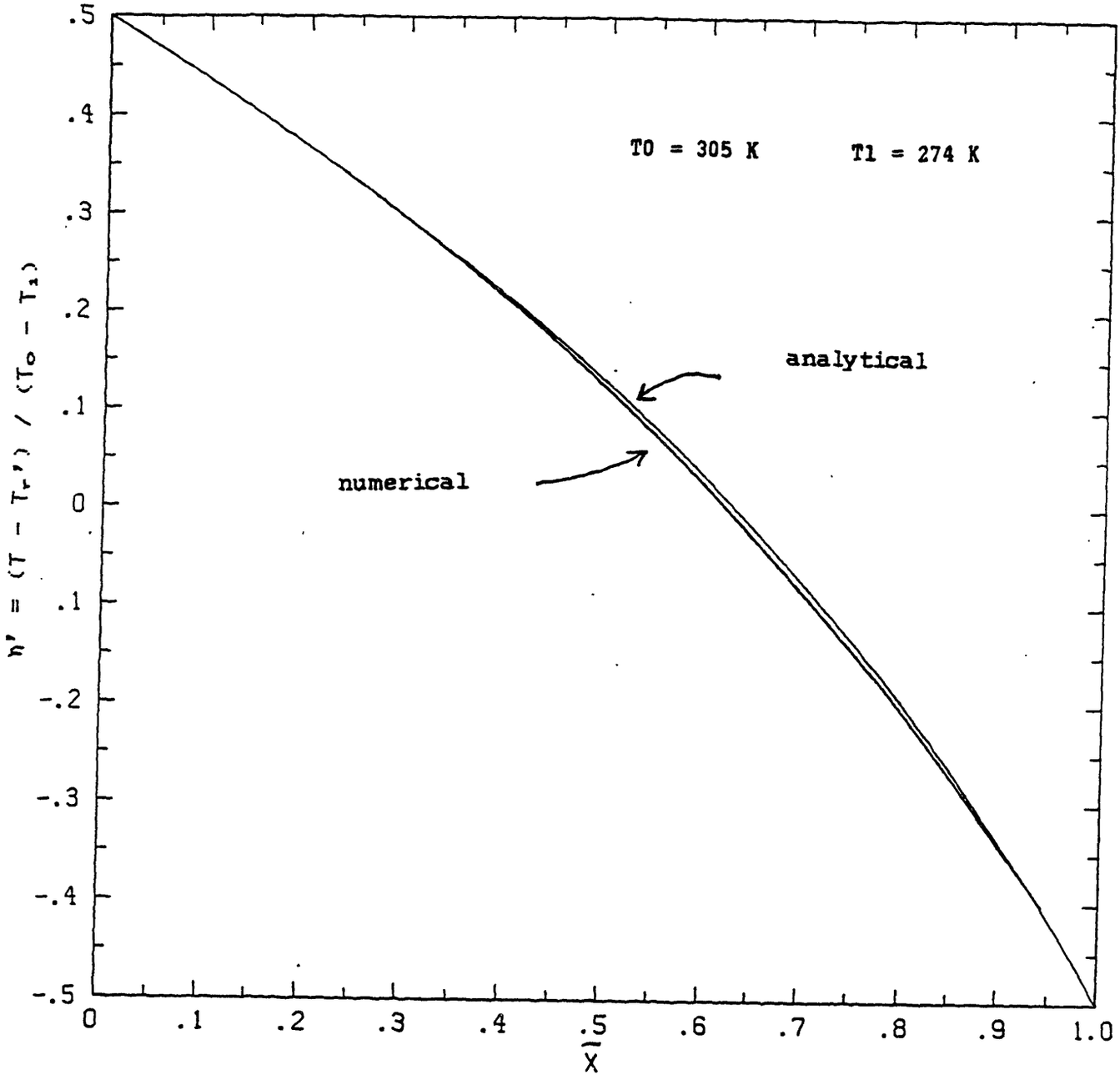

FIG 1

2.3 ZONE MATCHING - SPATIALLY STEADY REGIMES

In sections 2.2.1 and 2.2.2 the temperature and concentration profiles in a slab of a porous medium with condensation were determined in the dry and wet regions respectively. In each regime the temperatures and positions of the boundaries were assumed. In this section we consider the conditions at the wet/dry interfaces in order to determine the temperatures and positions of these boundaries. Two scenarios are examined: one in which the condensate is in pendular form and is essentailly immobile; and another in which the condensate moves against the gradient of liquid content in a liquid diffusion process.

The case of immobile condensate corresponds to the onset of condensation and subsequent low liquid content levels. In this case there is an accumulation of condensate. As the liquid content grows there is a tendency for capillary forces to act on the droplets of condensate. The effect of the capillary forces is to make the condensate mobile. When all of the condensate is subjected to these capillary interactions, the resulting mechanism of liquid mobility can be modeled as liquid diffusion [1,3]. This is the behavior assumed for the case of mobile condensate.

2.3.1 IMMOBILE CONDENSATE

Consider a slab of porous medium exposed to constant temperature and vapor concentration boundary conditions, such that there exists a region of condensation. If the liquid content in the wet zone is below a critical level, determined by the porous medium stucture, the condensate will accumulate in small droplets and remain stationary. The rate of condensation is given by eq.(8). The boundary conditions at the wet/dry interface are determined by heat and mass balances at the interfaces:

$$\begin{aligned} \frac{T_h - T_0}{z_0} &= -\,dT/dz \\ \frac{C_h - C_0}{z_0} &= -\,dC/dz \end{aligned} \qquad \text{at } z=z_0$$

$$\begin{aligned} \frac{T_1 - T_c}{1-z_1} &= -\,dT/dz \\ \frac{C_1 - C_c}{1-z_1} &= -\,dC/dz \end{aligned} \qquad \text{at } z=z_1 \qquad (20)$$

The four unknowns, T_0, T_1, z_0, z_1 are therefore specified by the four boundary conditions. These boundary equation are valid assuming the conductivity and diffusivity of the insulation is unaffected by liquid content.

2.3.1.1. MATCHING ZONES in the ANALYTIC SOLUTION

Motakef[3] has combined the four boundary conditions, using the Clausius-Clapeyron relation and dropping high order terms , into two implicit equations with two unknowns, $\eta 0$ and $\eta 1$:

$$1 - h_h \exp(u_h) + u_h = 0$$
$$1 - h_c \exp(u_c) + u_c = 0 \qquad (21)$$

where

$u_h = \eta_h - \eta_0$

$u_c = \eta_c - \eta_1$

$h_h = C_h / C_{sat}(T_h)$ = relative humidity of hot side

$h_c = C_c / C_{sat}(T_c)$ = relative humidity of cold side

$T_r = (T_h + T_c)/2$

$\Delta T = T_h - T_c$

$\eta = (T - T_r)/\Delta T$

Figure 2 is a plot of u for a given relative humidity, h_h or h_c. The positive value of u is used when determining uh, the negative value corresponds to u_c. Thus if given T_h, T_c, h_h, h_c, then the temperature at the wet/dry interface can be found from eq.(21). With T_0 and T_1 known eq.(11) can be used with the boundary conditions to solve for z_0 and z_1:

$$z_0 = \frac{\Pi 2}{\Pi 2 + \frac{.5+\eta 1}{.5-\eta 0}\,\Pi 1 - \frac{\eta 0-\eta 1}{.5-\eta 0}\,\Pi 1\,\Pi 2} \qquad (22)$$

$$z_1 = \frac{\Pi 2\,(\,1-(\eta 0-\eta 1)/(.5-\eta 0))}{\Pi 2 + \frac{.5+\eta 1}{.5-\eta 0}\,\Pi 1 - \frac{\eta 0-\eta 1}{.5-\eta 0}\,\Pi 1\,\Pi 2}$$

where

$$\Pi 1 = -.5 \frac{\lambda}{\exp(\lambda) - 1}$$

$$\Pi 2 = -.5 \frac{\lambda \exp(\lambda)}{\exp(\lambda) - 1} + 1$$

With T_0, T_1, z_0, z_1 determined, the temperature and vapor concentration distributions are obtained using the analyses of sections 2.2.1 and 2.2.2.

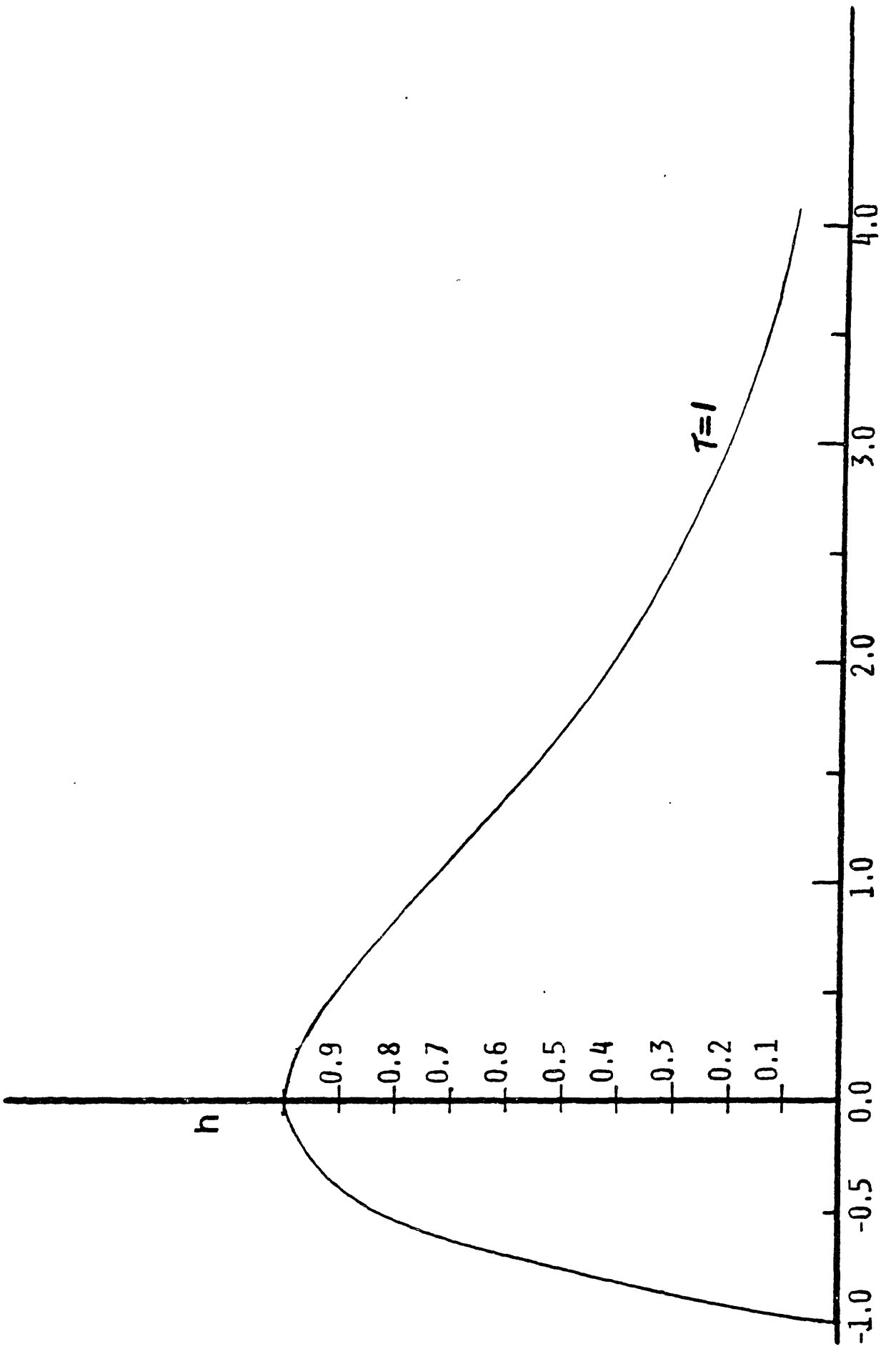

Fig. 2 Plot of the boundary equation variable u versus humidity from [3]

2.3.1.2. MATCHING ZONES IN THE NUMERICAL SOLUTION

As in the analytic solution, the numerical solution satisfies continuity of heat and vapor flux at the wet/dry interfaces. Those boundary conditions are given by eqs.(20). For the boundary at z_0, the first two conditions given in eq.(20) are combined to eliminate z_0:

$$\frac{T_h - T_0}{C_h - C_0(T_0)} = \left(\frac{dT}{dC}\right)^* \qquad \text{at} \quad z = z_0 \qquad (23)$$

Since C_0 and $(dT/dC)^*$ are both functions of T_0 and are obtained from saturation data, the only unknown in eq.(23) is T_0, which can be obtained by iterative solution of eq.(23). Similarly T_1 can be obtained by iteration on the following equation:

$$\frac{T_1 - Tc}{C_1(T_1) - C_c} = \left(\frac{dT}{dC}\right)^* \qquad \begin{array}{l}\text{at} \quad z = z_1 \\ \text{and} \quad T = T_1\end{array} \qquad (24)$$

The method chosen for converging on the correct values of T_0 and T_1 was a modified Newton's Method. For obtaining T_0, let G and J be defined as follows:

$$G = \frac{T_h - T_0}{C_h - C_0(T_0)} - \left(\frac{dT}{dC}\right)^*$$

$$J = \Delta G \; / \; \Delta T_0$$

The goal of Newton's method is to set G equal to zero. After each guess of T_0, J is calculated. The subsequent guess of T_0 is given by:

$$T_0^{k+1} = T_0^k - G / J$$

This algorithm converges to within 0.01 degree K of the final value of T_0 in approximately 15 iterations. T_1 is obtained similarly.

Once T_0 and T_1 are determined the position of the wet/dry interfaces, z_0 and z_1 can be found using a similar modified Newton's algorithm. By balancing the heat generated by condensation with the vapor condensed in the wet zone, the following relation is derived:

$$z_1 = 1 - z_0 \left[\frac{T_c - T_1 + (h_{fg} D_v/k)(C_c - C_1)}{T_0 - T_h + (h_{fg} D_v/k)(C_0 - C_h)} \right] \qquad (24)$$

The numerical scheme used to determine z0 and z1 is again iterative. Define $G(z_0)$ as the discrepancy of the temperature gradient across the wet/dry interface at z1, and define J as the unit change in G per unit change in z1:

$$G^k = \frac{T_c - T_1^k}{1 - z_1} - \frac{dT}{dz} \qquad \text{at } z = z_1$$

$$J^k = \Delta G^k / \Delta z_0^k$$

where ΔG^k is the change in G resulting from the change in z_0 at iteration k. The first guess of z_0 implies z_1 via eq.(24). Newton's method determines the next guess of z_0 as follows:

$$\Delta z_0^{k+1} = - G(z_0)^k / J^k$$

In practice the incremental change in z_0 is multiplied by .5. This has the effect of ensuring convergence while sacrificing speed. Nevertheless the final value of z_0 is reached in typically 20 iterations. Thus we have determined T_0, T_1, z_0, and z_1 for the spatially steady case of immobile condensate. The temperature and concentration distributions are determined via the analyses in sections 2.2.1 and 2.2.2.3.

2.3.1.3. COMPARISON OF ANALYTICAL AND NUMERICAL WITH IMMOBILE CONDENSATE

The complete solution for three examples of spatially steady condensation occurring within a porous slab with immobile condensate are presented in figures 3 - 5. The three profiles represent relative humidities in both reservoirs of 90 %, 80 %, and 70 %. Because the analytical solution is based on a perturbation of a linear profile, the resulting error increases with the degree of curvature of these profiles. Therefore the relatively high temperature drop across the slab used in these simulations will show a high error compared to a more moderated temperaure drop. There is some discrepancy between the analytical and numerical results for the temperature distribution in the slab. However the important quantities of heat flux entering and leaving the slab are in agreement.

This discrepancy in the temperature profiles arises because of the high sensitivity of the positon of z_0 and z_1 on the gradients of the temperature profile at the wet/dry interfaces (see eq.(20)). In the analytical solution, the temperature of the wet zone boundaries are determined from eq.(21). In that formulation, high order terms were discarded. This approximation introduces a small error into the calculated values of η_0, η_1, z_0, and z_1. Table 1 compares the boundary conditions of the wet zone with Hh and Hc = 90 %, as determined by the analytical and numerical methods.

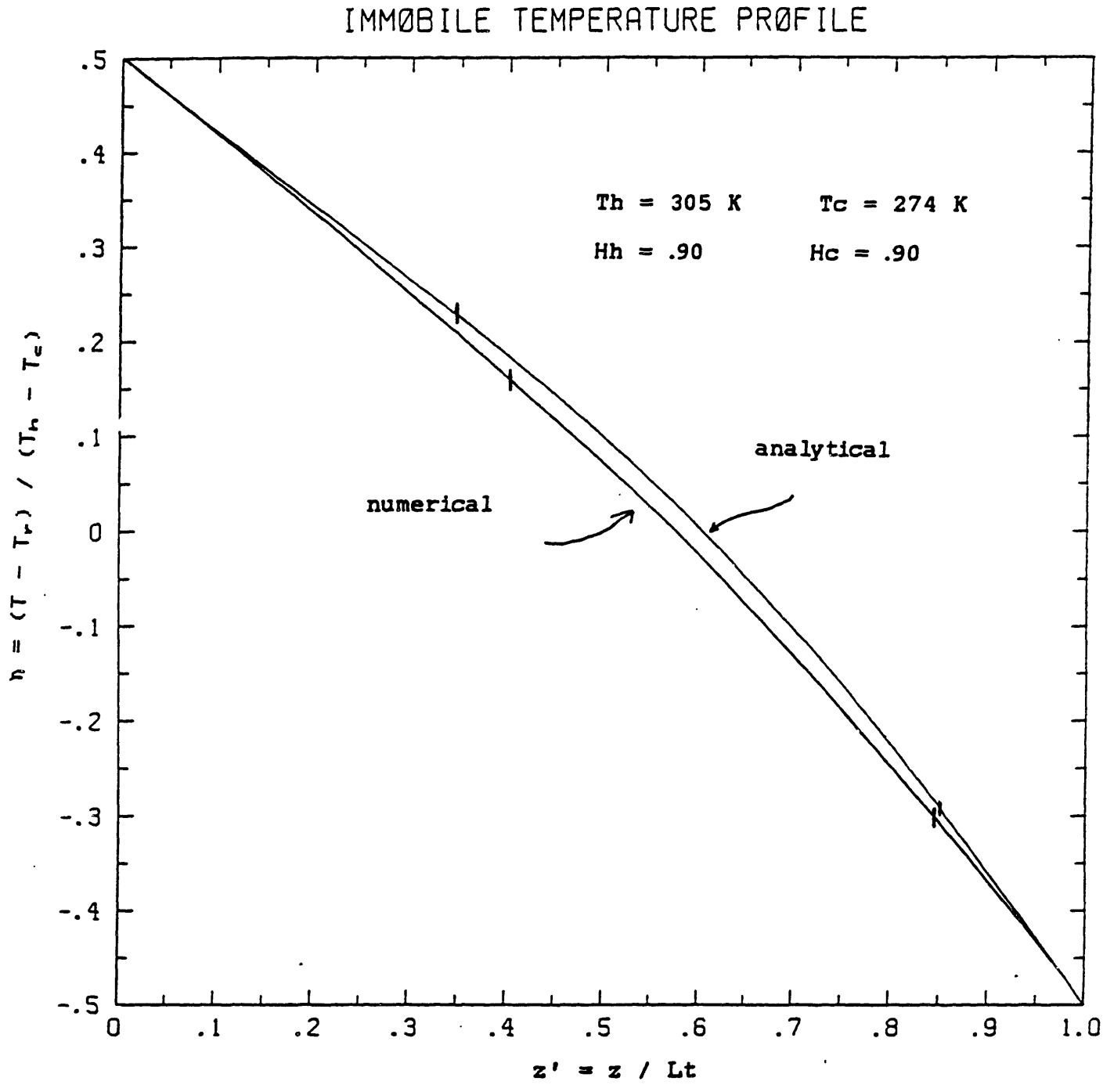
IMMØBILE TEMPERATURE PRØFILE
Th = 305 K
Tc = 274 K
Hh = .90
Hc = .90
analytical
numerical
θ = (T - Tc) / (Th - Tc)
z' = z / Lt
.5
.4
.3
.2
.1
0
-.1
-.2
-.3
-.4
-.5
0
.1
.2
.3
.4
.5
.6
.7
.8
.9
1.0

FIG 3

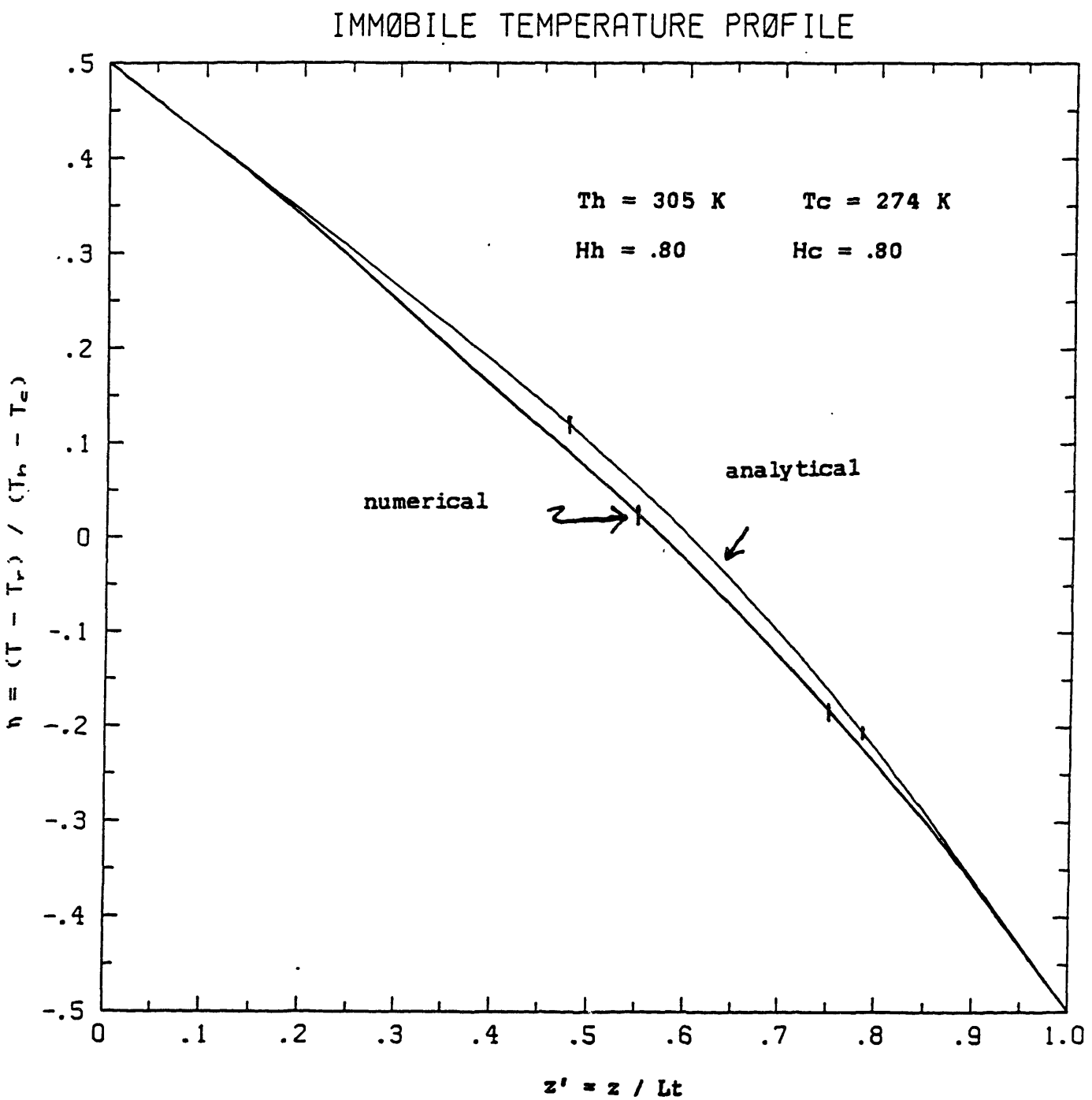
IMMØBILE TEMPERATURE PRØFILE
Th = 305 K
Tc = 274 K
Hh = .80
Hc = .80
numerical
analytical
.5
.4
.3
.2
.1
0
-.1
-.2
-.3
-.4
-.5
0
.1
.2
.3
.4
.5
.6
.7
.8
.9
1.0
z' = z / Lt

FIG 4

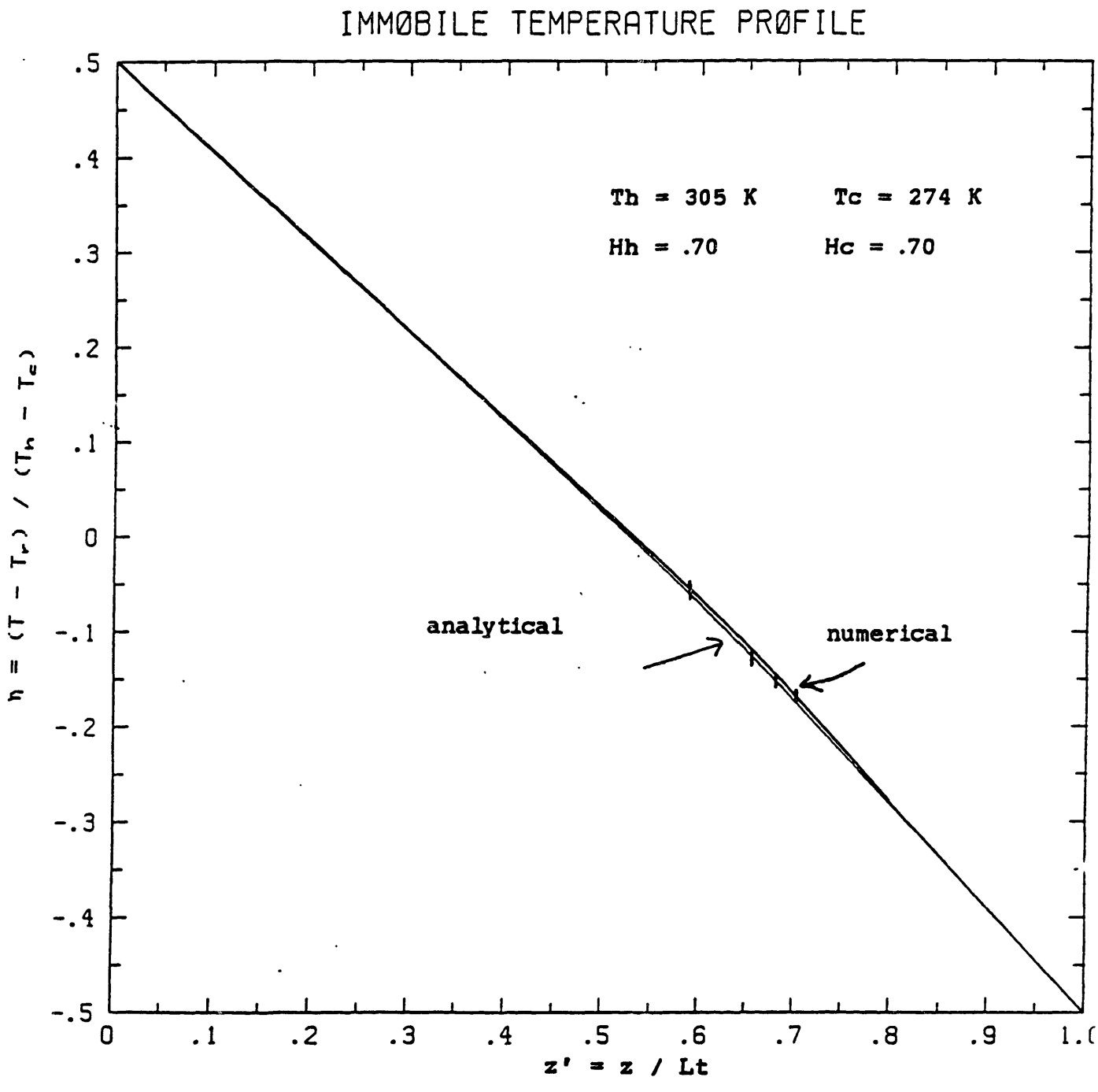
IMMØBILE TEMPERATURE PRØFILE
Th = 305 K
Tc = 274 K
Hh = .70
Hc = .70
analytical
numerical
η = (T - Tc) / (Th - Tc)
z' = z / Lt
.5
.4
.3
.2
.1
0
-.1
-.2
-.3
-.4
-.5
0
.1
.2
.3
.4
.5
.6
.7
.8
.9
1.0

FIG 5

TABLE 1: COMPARISON OF ANALYTICAL AND NUMERICAL SOLUTIONS

Immobile Condensate

Hh = Hc = 0.90

	ANALYTICAL	NUMERICAL
T_h	305 K	305 K
T_c	274 K	274 K
T_0	296.6 K	294.4 K
T_1	280.2 K	280.2 K
$\bar{z}_0$	0.343	0.401
$\bar{z}_1$	0.858	0.843
$\bar{Q}$in	0.79	0.85
$\bar{Q}$out	1.40	1.32

note: $\bar{Q} = Q \quad (T_h - T_c)/ k L_t$

For many practical problems, the quantity of primary interest is the heat tranfer across the slab. In these applications, such as determining the heat flux in a partially wetted slab, the analytical and numerical solutions agree well. In cases of more moderate temperature drops across the slab, the models agreement is even better.

2.3.2. MOBILE CONDENSATE

If the liquid content in the condensate region is above a critical level, θc, the condensate can become mobile by the mechanism of liquid diffusion [1,3]. Condensate can also move by dripping due to gravity. This work examines only the affects of liquid diffusion by capillarity. In this section the temperature and concentration profiles of a condensate region with mobile condensate are matched to the surrounding dry zones. As in the previous case of immobile condensate, we consider a slab of porous medium exposed to constant temperature and vapor concentration boundary conditions, and solve for the spatially steady temperature and concentration profiles.

The liquid content profile is coupled to the vapor concentration profile which in turn is coupled to the temperature profile. With θ defined as the ratio of the volume of liquid condensate to the volume of air in the media, and ϵ defined as the porosity of the media, conservation of water yields:

$$\rho \epsilon D_l \frac{d^2\theta}{dz^2} = -D_v \frac{d^2C}{dz^2} \qquad (25)$$

$$-D_v \frac{d^2C}{dz^2} = k/h_{fg} \frac{d^2T}{dz^2} \qquad (26)$$

Combining eqs.(25) and (26) we have:

$$\frac{d^2\theta}{dz^2} = k/\ (\rho\epsilon D_l h_{fg})\ \frac{d^2T}{dz^2} \qquad (27)$$

The boundary conditions for the liquid content at the edge of the wet region are $\theta = \theta c$. These boundary conditions are determined from the following condition: if $\theta(z_0;z_1))$ is less than θc, the condensate is immoblie and this analysis does not apply; if $\theta(z_0;z_1)$ is greater than θc, then the liquid will diffuse into the dry region and the problem is not spatially steady. With the liquid content, θ, specified at the two boundaries, eq.(27) can be integrated twice to solve for $\theta(z)$:

$$\theta(z) = \theta_c + M\ C_r\ Le\ \beta\ /\ (\rho\epsilon\Omega)\ [T + \Delta Tz - (T_r+\Delta T/2)] \qquad (28)$$

At steady-state there is no net accumulation of condensate in the wet zone. Therefore the condensing vapor is exactly balanced by evaporation of condensate at the wet/dry interfaces. The liquid flux at each boundary, J0 and J1, can be determined by integrating eq.(27) once and applying Fick's Law for diffusion:

$$J = -\ (\rho\epsilon D_l)\ d\theta/dz \qquad (29)$$

The evaporation of liquid at the boundaries creates both a source of vapor and a sink for heat. Therefore the gradients of temperature and concentration will be discontinuous at the wet/dry interfaces. Balancing heat

flux and vapor flux at these interfaces provides the criteria for matching the solutions of the temperature and concentration profiles in the wet zone to the dry zone.

$$-k\ (T_h-T_0)/z_0 = -k\ dT/dz + J_0\ h_{fg} \quad \text{at} \quad z=z_0 \quad (30)$$

$$-D_v\ (C_h-C_0)/z_0 = -D_v\ dC/dz - J_0 \quad \text{at} \quad z=z_0 \quad (31)$$

$$-k\ (T_1-T_c)/(1-z_1) = -k\ dT/dz + J_1\ h_{fg} \quad \text{at } z=z_1 \quad (32)$$

$$-D_v\ (C_1-C_c)/(1-z_1) = -D_v\ dC/dz - J_1 \quad \text{at } z=z_0 \quad (33)$$

The following two sections describe the methods used in satisfying eqs.(30) through (33) in analytical and numerical methods of solution.

2.3.2.1. MATCHING ZONES IN THE ANALYTIC SOLUTION WITH MOBILE CONDENSATE

The analytic solution for the temperature profile in a slab of a porous medium with a region of mobile condensate begins by solving for the liquid content profile in terms of the analytic solution of the temperature filed given in section 2.2.2.3. Recall that

$$T = .5\left[1-x-\frac{\exp(\lambda x)-1}{\exp(\lambda)-1}\right]\Delta T' + T_r' \qquad (34)$$

Eq.(34) gives the temperature profile in the region of condensation. This expression is substituted into eq.(28) to yield:

$$\theta(x) = \theta c + .5\,\frac{M\,C_r'\,Le\,\beta'}{\rho\,\epsilon\,\Omega'}\left[x-\frac{\exp(\lambda x)-1}{\exp(\lambda)-1}\right] \qquad (35)$$

where M is the ratio of vapor diffusivity to liquid diffusivity. Having solved for θ in the wet zone, the liquid fluxes at the wet/dry interfaces,J0 and J1, are determined from eq.(29):

$$J_0 = \frac{Le\,\beta'}{\Omega'}\,\frac{\exp(\lambda-1)-\lambda}{2\exp(\lambda-1)} \qquad (36)$$

$$J_1 = \frac{Le\,\beta'}{\Omega'}\,\frac{(\lambda-1)\exp(\lambda)+1}{2\exp(\lambda-1)}$$

Under steady-state conditions there is no net accumulation of liquid and hence no net accumulation of

vapor or heat in the wet zone. Therefore the vapor flux entering the region of condensation equals the vapor flux leaving. The same can be said for the heat flux. It follows that:

$$\frac{C_1 - C_c}{L_t - z_1} = \frac{C_h - C_0}{z_0} \qquad (37)$$

$$\frac{T_1 - T_c}{L_t - z_1} = \frac{T_h - T_0}{z_0}$$

By substituting the values for J_0 and J_1, obtained by eq.(36), into the boundary conditions given by eqs.(30)-(33) it can be shown after some algebra that:

$$\frac{T_1 - T_c}{L_t - z_1} = \frac{T_h - T_0}{z_0} = \frac{T_h - T_c}{L_t}$$

or in reduced temperature and length scales:

$$\frac{\eta_h - \eta_0}{z_0} = \frac{\eta_1 - \eta_c}{1 - z_1} = 1 \qquad (38)$$

This indicates that the heat flux entering and leaving the porous slab is the same as if no condensation had taken place. The same analysis applies to the vapor flux entering and leaving the slab. Thus:

$$\frac{\bar{C}_h - \bar{C}_0}{z_0} = \frac{\bar{C}_1 - \bar{C}_c}{1 - z_1} = 1 \qquad (39)$$

It can shown that any smooth temperature distribution in the wet zone will lead to the same conclusion[3]: The overall steady state heat and vapor transfer through porous media with phase change and mobile condensate is identical to the case in which no condensation occurs. This conclusion is of

course dependent on the validity of the one dimensional, constant property assumptions inherent in this analysis.

By non-dimensionalizing and eliminating the length scale from eqs.(30)-(33) and invoking the Clausius-Clapeyron relation, Motakef[3] has derived the following simultaneous equations in which the only two unknowns are η_0 and η_1:

$$\frac{hh\ \exp(\phi_h) - \exp(\phi_0)}{\eta_h - \eta_0} =$$

$$.5\ \gamma\ \beta\left[\left[1+\frac{\lambda}{\exp(\lambda)-1}\right](1+\eta_0\beta)^2\exp(\phi_0) - \mathrm{Le}/\Omega\gamma\left[1-\frac{\lambda}{\exp(\lambda)-1}\right]\right] \qquad (40)$$

$$\frac{hc\ \exp(\phi_c) - \exp(\phi_1)}{\eta_c - \eta_1} =$$

$$.5\ \gamma\ \beta\left[\left[1+\frac{\lambda\ \exp(\lambda)}{\exp(\lambda)-1}\right](1+\eta_1\beta)^2\exp(\phi_1) - \mathrm{Le}/\Omega\gamma\left[1-\frac{\lambda\exp(\lambda)}{\exp(\lambda)-1}\right]\right] \qquad (41)$$

These equations can be solved by successive iteration to yield the temperatures at the wet/dry interfaces.

With T_0 and T_1 known all that remains to be specified are the positions of the wet zone boundaries. The length scales can be readily obtained from eq.(38):

$$z_0 = \eta_h - \eta_0$$

$$z_1 = 1 - (\eta_1 - \eta_c) \qquad (42)$$

Section 2.3.2.3. shows various worked expamles and compares them to the numerical solution descibed in the following section.

2.3.2.2. MATCHING ZONES IN THE NUMERICAL SOLUTION WITH MOBILE CONDENSATE

The method of matching the boundary conditions at the wet/dry interfaces with mobile condensate differs from the method used in the case of immobile condensate in that T_0, T_1, z_0, and z_1 are determined simultaneously in this case. In the previous section it was shown that the temperature and concentration profiles in the dry zones are identical to the linear profile found in a slab with no condensation. This result is a consequence of the balances of heat, vapor and liquid flux and is independent of whether the solution is arrived at by numerical or analytic techniques.

The algorithm to satisfy the interface boundary conditions uses a Modified Newton's Method and proceeds as follows:

1) z_0^k and z_1^k are guessed at step k.

2) T_0^k and T_1^k are obtained from the linear temperature profiles in the dry zone:

$$T_0^k = T_h - (T_h - T_c) / z_0^k$$
$$T_1^k = T_h - (T_h - T_c) / z_1^k$$

3) Given T_0, T_1, z_0, z_1 at step k, the technique for solving for the temperature field in the wet zone described in section 2.2.3 is used to obtain:

dT/dz_{z0} and dT/dz_{z1} at the wet zone boundaries

4) Eqs.(30) and (31) are used to calculate J0 and J1:

$$J0^k = k/h_{fg} \left[T_h - T_c + dT/dz\big|_{z_0,k}\right]$$
$$J1^k = -k/h_{fg} \left[T_h - T_c + dT/dz\big|_{z_1,k}\right]$$

5) Define functions G0 and G1 from eqs.(31) and (33) which the Modified Newton's Method drives to zero:

$$G0^k = D_v \left[(C_h - C_c) + dC/dz_{z_0,k}\right] + J0^k$$
$$G1^k = D_v \left[(C_h - C_c) + dC/dz_{z_1,k}\right] + J1^k$$

6) Let $\Delta G0^k = G0^k - G0^{k-1}$

$\Delta G1^k = G1^k - G1^{k-1}$

The next guess for z0 and z1 are determined as follows:

$$\Delta z_0^k = - G0^k / (\Delta G0^k / \Delta z_0^k)$$
$$\Delta z_1^k = - G1^k / (\Delta G1^k / \Delta z_1^k)$$

$$z_0^{k+1} = z_0^k + \Delta z_0^k$$
$$z_1^{k+1} = z_1^k + \Delta z_1^k$$

To ensure convergence $\Delta z_{0,1}$ are reduced by a factor of 2. This algorithm converges in typically 20 steps. The sucess of this somewhat crude technique lies in the fact that the sensitivity of G0 is dominated by z_0 and G1 is dominated by z_1.

2.3.2.3 COMPARISON OF THE ANALYTICAL AND NUMERICAL SPATIALLY-STEADY SOLUTIONS WITH MOBILE CONDENSATE

The complete spatially steady solution for the temperature profiles in a porous slab with mobile condensate in the interior of the slab are presented in figures 6 - 8. These plots represent reservoir humidities of 90 %, 80%, and 70 %, respectively. There is excellent agreement between the two techniques.

It is important to note the effect of mobile condensate on the heat transfer through the slab. In general, when compared to the case of immobile condensate (figs 3 - 5), the heat flux entering the hot side is less and the heat flux leaving is greater. Thus the mobility of the condensate has the effect of moderating the changes in overall heat flux that occur from condensation. In practical experiments it may be the case that the condensate is partially mobile, and therefore the actual heat flux would be expected to fall between the heat fluxes determined by the immobile and mobile models.

One other effect of mobile condensate is to spread out the region of condensation. Table 2 compares the location of the wet zone for cases of identical reservoir conditions with mobile and immobile condensate.

TABLE 2
COMPARISON OF WET ZONE BOUNDARY LOCATIONS
WITH IMMOBILE AND MOBILE CONDENSATE

NUMERICAL SOLUTIONS

Relative Humidity	Immobile		Mobile	
	z_0	z_1	z_0	z_1
90 %	0.401	0.843	0.126	0.967
80 %	0.550	0.750	0.282	0.917
70 %	0.666	0.674	0.546	0.780

ANALYTICAL SOLUTIONS

Relative Humidity	Immobile		Mobile	
	z_0	z_1	z_0	z_1
90 %	0.343	0.858	0.121	0.971
80 %	0.478	0.782	0.261	0.922
70 %	0.585	0.709	0.456	0.822

Expanding of the wet zone by mobile condensate may be significant when analyzing transient experimental data. This effect is considered when examining the data presented in section 3.

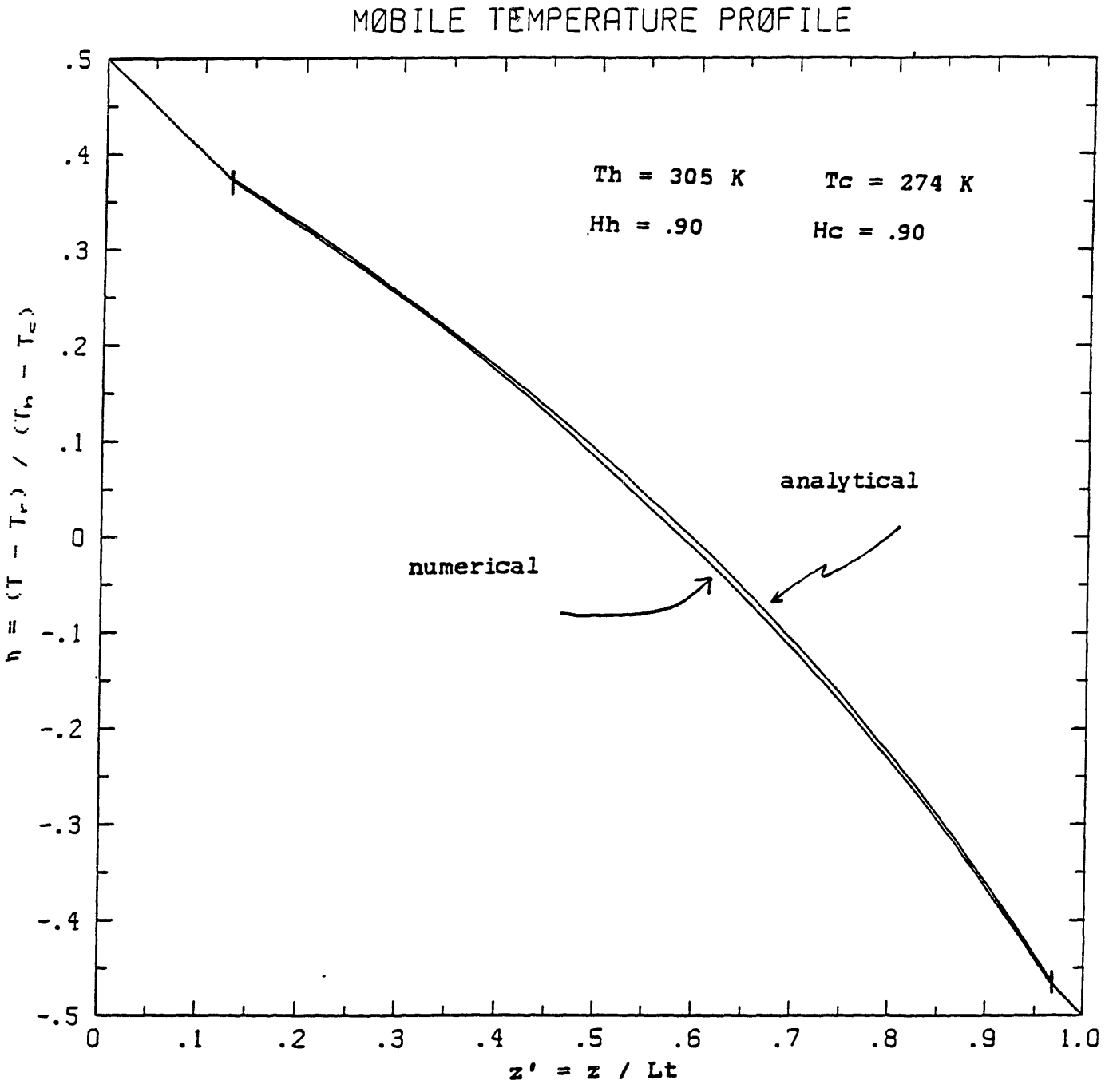
MØBILE TEMPERATURE PRØFILE
Th = 305 K
Tc = 274 K
Hh = .90
Hc = .90
analytical
numerical
.5
.4
.3
.2
.1
0
-.1
-.2
-.3
-.4
-.5
0
.1
.2
.3
.4
.5
.6
.7
.8
.9
1.0
z' = z / Lt

FIG 6

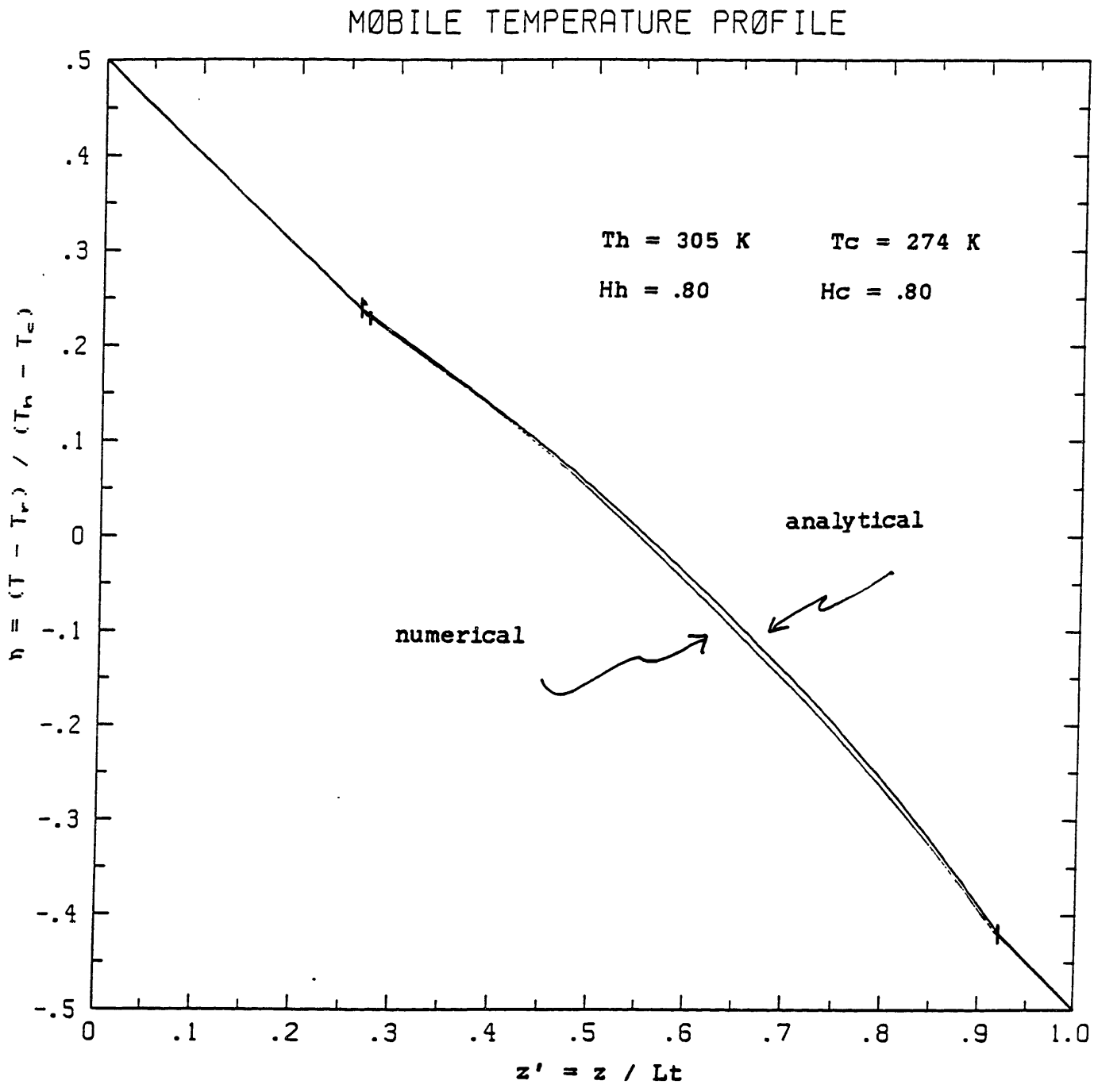
MØBILE TEMPERATURE PRØFILE
Th = 305 K
Tc = 274 K
Hh = .80
Hc = .80
analytical
numerical
h = (T - Tr) / (Th - Tc)
z' = z / Lt
.5
.4
.3
.2
.1
0
-.1
-.2
-.3
-.4
-.5
0
.1
.2
.3
.4
.5
.6
.7
.8
.9
1.0

FIG 7

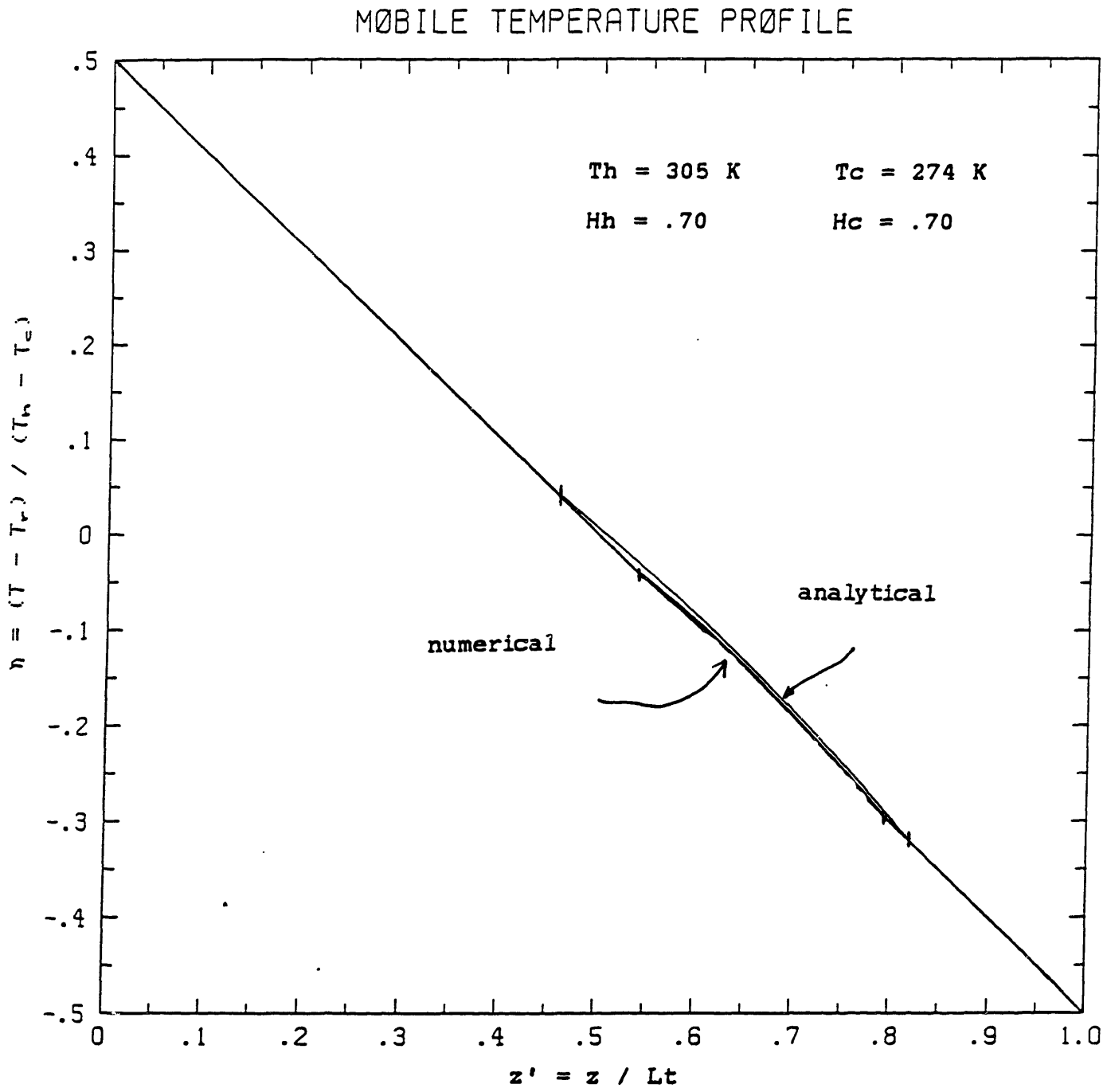
MØBILE TEMPERATURE PRØFILE
Th = 305 K
Tc = 274 K
Hh = .70
Hc = .70
analytical
numerical
h = (T - Tc) / (Th - Tc)
z' = z / Lt
.5
.4
.3
.2
.1
0
-.1
-.2
-.3
-.4
-.5
0
.1
.2
.3
.4
.5
.6
.7
.8
.9
1.0

FIG 8

2.4. HEAT AND MASS TRANSFER WITH PHASE CHANGE IN POROUS MEDIA: SPATIALLY UNSTEADY ANALYSIS

In this section the effects of time dependent boundary conditions and of an arbitrary initial liquid content distribution are examined. The goal of this analysis is to develop a model to determine whether a wet porous slab will dry out completely or redistribute its moisture when exposed to given time-varying boundary conditions. The case of moderate liquid content level that is not prone to liquid diffusion is studied.

Consider the drying of a slab of porous media with an arbitrary liquid content distribution in the wet zone as depicted in fig 9. A mass balance at the wet/dry interface at the hot side of the wet zone involves diffusion of vapor from the dry region, diffusion of vapor out of the wet region, and evaporation at the boundary.

$$D_v\left(\left.\frac{dC}{dz}\right|_{z_{0-}} - \left.\frac{dC}{dz}\right|_{z_{0+}}\right) = \rho\,\epsilon\,\theta(z_0,t)\,\frac{dz_0}{dt} \qquad (1)$$

The heat balance yields:

$$k\left(\left.\frac{dT}{dz}\right|_{z_{0-}} - \left.\frac{dT}{dz}\right|_{z_{0+}}\right) = -\,h_{fg}\,\rho\,\epsilon\,\theta(z_0,t)\,\frac{dz_0}{dt} \qquad (2)$$

Similarly, for the wet/dry interface at the cold side of the slab, the mass and heat balances yield:

Illustration of an Arbitrary Liquid Content Distribution

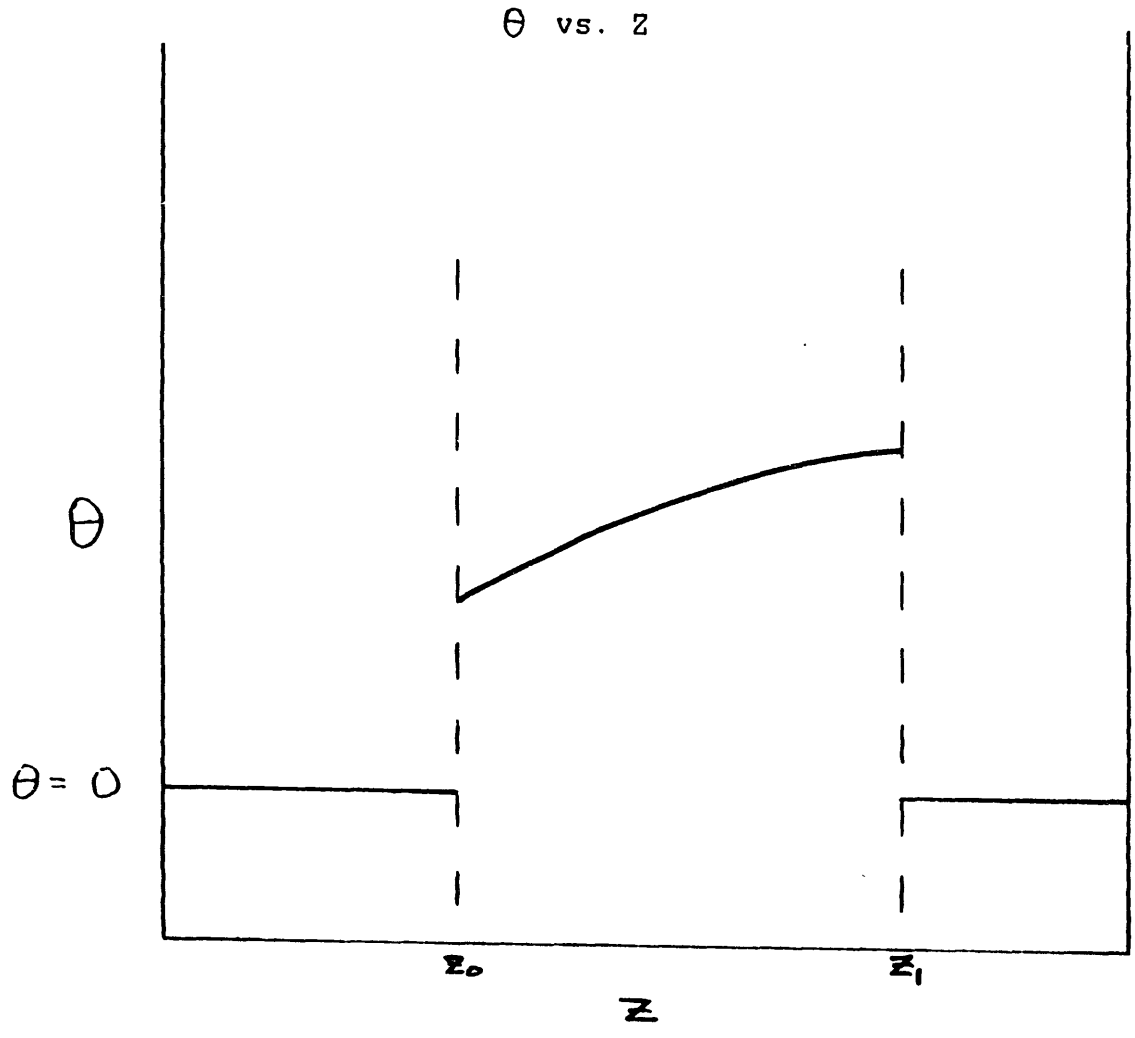

FIG 9

$$Dv\left(\frac{dC}{dz}_{z1-} - \frac{dC}{dz}_{z1+}\right) = -\rho\,\epsilon\,\theta(z_1,t)\,dz_1/dt \qquad (3)$$

$$k\left(\frac{dT}{dz}_{z_1-} - \frac{dT}{dz}_{z_1+}\right) = h_{fg}\,\rho\,\epsilon\,\theta(z_1,t)\,dz_1/dt \qquad (4)$$

2.4.1. ANALYTICAL SOLUTION TO THE SPATIALLY UNSTEADY PROBLEM

The analytical solution to heat and mass transport through porous media with phase change and time dependent boundary conditions proceeds by assuming the time scale for the wet zone boundary movement, τ_e, is much greater than the time scale associated with vapor diffussion and heat conduction through the dry zone, τ_d and τ_c respectively. With this assumption, at each time step the temperature and concentration profiles in the dry zones are linear, and the solution for the temperature and concentration profiles in the wet zone is given by the analysis presented in section 2.3.2.

The basis for the quasi-steady assumption is $_e >> \tau_{c,d}$ where:

$$\tau_{c0} = z_0^2/\alpha \qquad \tau_{c1} = (1-z_0)^2/\alpha \qquad (5)$$

$$\tau_{d0} = z_0^2/Dv \qquad \tau_{d1} = (1-z_0)^2/Dv \qquad (6)$$

The time constant of the wet zone boundary movement is given in the following analysis. Those cases for which $\tau_e << \tau_{c,d}$ are subject to this quasi-steady analysis. For all

other cases, numerical solution of the coupled unsteady heat and mass transfer equations is required.

With the aforementioned assumptions, the temperature and concentration gradients in the dry zones are:

$$\left.\frac{dT}{dz}\right|_{z_0^-} = -(T_h - T_0)/z_0 \; ; \quad \left.\frac{dT}{dz}\right|_{z_0^+} = -(T_1 - T_c)/(1-z_1) \tag{7}$$

$$\left.\frac{dC}{dz}\right|_{z_0^-} = -(C_h - C_0)/z_0 \; ; \quad \left.\frac{dC}{dz}\right|_{z_0^+} = -(C_1 - C_c)/(1-z_1) \tag{8}$$

Introducing eqs.(7) and (8) into eqs.(1)-(4) and eliminating the dz_0/dt term results in:

$$\frac{D_v h_{fg}}{k}\frac{C_h - C_0}{z_0} + \frac{T_h - T_0}{z_0} = \left[\frac{D_v h_{fg}}{k}\left.\frac{dC}{dT}\right|_{T_0} + 1\right]\left.\frac{dT}{dz}\right|_{z_0} \tag{9}$$

$$\frac{D_v h_{fg}}{k}\frac{C_1 - C_c}{1-z_1} + \frac{T_1 - T_c}{1-z_1} = \left[\frac{D_v h_{fg}}{k}\left.\frac{dC}{dT}\right|_{T_1} + 1\right]\left.\frac{dT}{dz}\right|_{z_1} \tag{10}$$

Non-dimensionalizing eq. (9) yields:

$$\frac{\eta_h - \eta_0}{z_0} + \frac{\Omega}{Le\ \beta}\frac{h_h \exp(\phi_h) - \exp(\phi_0)}{z_0} = \left[1 + \frac{\Omega\gamma}{Le\beta}(1+\eta_0\beta)^{-2}\exp(\phi_0)\right]\frac{dx}{dz}\frac{d\eta}{d\eta'}\frac{d\eta'}{dz} \tag{11}$$

where

$dx/dz = z_1 - z_0$

$d\eta/d\eta' = (T_h - T_c)/(T_0 - T_1)$

and

$d\eta'/dx$ is obtained from differentiating the solution to

the temperature profile given in section 2.2.2.2:

$$d\eta'/dx = -.5 \quad 1 + \frac{\lambda \exp(\lambda x)}{\exp(\lambda)-1} \qquad (12)$$

The same analysis is applied to the wet/dry interface at the cold side of the wet zone. Motakef has manipulated eqs.(11) and (12) and their cold side counterparts to derive the following two equations involving η_0 and η_1:

$$\eta_h-\eta_o + \frac{\Omega}{Le\beta} h_h\exp(\phi_h)-\exp(\phi_o) = -.5\left[1+\Omega\gamma(1+\eta_o\beta)^{-2}\exp(\phi_o)\right] * \frac{z_o}{z_1-z_o}\frac{\Delta T'}{\Delta T}\left[(1+\lambda/(\exp(\lambda)-1)\right]$$

$$\eta_1-\eta_c + \frac{\Omega}{Le\beta}\exp(\phi_1)-h_c\exp(\phi_c) = -.5\left[1+\Omega\gamma(1+\eta_1\beta)^{-2}\exp(\phi_1)\right] * \frac{1-z_1}{z_1-z_o}\frac{\Delta T'}{\Delta T}\left[1 + \frac{\lambda\exp(\lambda)}{(\exp(\lambda)-1)}\right]$$

(13 a,b)

Motakef has obtained the following equation for the hot side wet zone boundary movement rate by introducing the expression for $(\eta_h-\eta_0)/z_0$ from eq.(11) into eq.(1) to yield:

$$\theta(z_o,t')\, dz_o^2/dt' = \frac{-2\,\exp(\phi_o)-h_h\exp(\phi_h) + (1+\eta_o\beta)^{-2}\exp(\phi_o)(\eta_h-\eta_o)}{1 + \Omega\,\gamma/Le\,(1+\eta_o\beta)^{-2}\exp(\phi_o)}$$

Similarly for the cold side: (14a,b)

$$\theta(z_1,t')\, d(1-z_1)^2/dt' = \frac{2\,\exp(\phi_1)-h_c\exp(\phi_c) - (1+\eta_1\beta)^{-2}\exp(\phi_1)(\eta_1-\eta_c)}{1 + \Omega\,\gamma/Le\,(1+\eta_1\beta)^{-2}\exp(\phi_1)}$$

where $t' = Fo^* C_r/\rho\epsilon = \frac{Dv\,Cr}{L_t^2\,\rho\epsilon}\, t.$

Therefore the time scales associated with the movement of the wet zone boundaries are given by:

$$\tau_{e0} = \frac{\rho\epsilon\theta(z_0,t)z_0^2}{D_v C_r} \quad ; \quad \tau_{e1} = \frac{\rho\epsilon\theta(z_1,t)(1-z_1)^2}{D_v C_r}$$

As stated earlier in this section, the validity of this quasi-steady assumption depends on the ratio of τ_d to τ_e (here we assume $\tau_c \simeq \tau_d$ since Sc $\simeq$ 1). The previous analysis then requires:

$$\begin{aligned} \frac{\tau_{e0}}{\tau_{d0}} &= \frac{\rho\epsilon\theta z_o^2 \,/\, D_v C_r}{z_o^2 \,/\, D_v} = \rho\epsilon\theta(z_0,t) \,/\, C_r \gg 1 \\ \frac{\tau_{e1}}{\tau_{d0}} &= \frac{\rho\epsilon\theta(1-z_1)^2 \,/\, D_v C_r}{(1-z_1)^2 \,/\, D_v} = \rho\epsilon\theta(z_1,t) \,/\, C_r \gg 1 \end{aligned} \qquad (15)$$

The above conditions are satisified for water (ρ/Cr > 1000) at liquid contents greater than .01. Therefore the quasi-steady analysis is valid for practical liquid content values that would be experienced in fiberglass insulation.

In the numerical scheme used to simulate the behavior of this transient phenomenon, the required time step must satisfy the following condition:

$$\tau_d \ll \tau_{\text{time step}} \ll \tau_e$$

The time step is reevaluated at each step to be:

$$\tau_{\text{time step}} = \sqrt{\tau_d \, \tau_e}$$

Section 2.4.3 contains solutions to cases for which the quasi-steady analysis is valid and demonstrates the error imposed if the time constant requirement is not satisfied.

2.4.2 NUMERICAL SOLUTION OF THE SPATIALLY UNSTEADY PROBLEM

As in the spatially steady problem, the advantages of a numerical solution over an analytic solution that is based on simplifying assumptions are increased accuracy and flexibility in allowing variations in the physical properties, such as thermal capacitance and conductivity, as a function of liquid content. An additional goal of the numerical solution presented here is to verify the quasi-steady analytic solution presented in section 2.4.1. As in the analytic solution the variations in physical properties are neglected in this formulation.

The numerical scheme proceeds by considering finite difference elements. In dry zones the time dependent heat and mass balances yield:

$$\partial T/\partial t = \alpha \, \partial^2 T/\partial x^2 \qquad (16)$$

$$\partial C/\partial t = Dv \, \partial^2 C/\partial x^2 \qquad (17)$$

In the wet zone the effects of phase change must be considered. Hence:

$$\partial T/\partial t = \alpha \, \partial^2 T/\partial x^2 + \frac{h_{fg} \, Dv}{\rho C_p} \, \partial^2 C/\partial x^2 - \frac{h_{fg} \, Dv}{\rho C_p} \, \partial C/\partial t \qquad (18)$$

The coupling of the transient changes in temperature and concentration is clear from eq.(18). Decoupling is achieved by the following expression for $\partial C/\partial t$:

$$\partial C/\partial t = dC/dT \times \partial T/\partial t \qquad (19)$$

Introducing eq. (19) into (18) yields:

$$\partial T/\partial t \left(1+\frac{h_{fg}}{\rho}\frac{D_v}{c_p} dC/dT\right) = \alpha\partial^2 T/\partial x^2 + \frac{h_{fg} D_v}{\rho c_p}\partial^2 C/\partial x^2 \qquad (20)$$

Because of the high degree of nonlinearity in eq.(20) an explicit finite difference algorithm is chosen. This algorithm determines the temperature and concentration at each node at time step k+1 based only on the temperature and concentration profiles at step k. Eqs.(16) and (17) are discretized as follows:

$$\Delta T(i)^k = \Delta t\ \alpha\ \frac{T(i+1)^k - 2T(i)^k + T(i-1)^k}{\Delta z^2} \qquad (21)$$

$$\Delta C(i)^k = \Delta t\ Dv\ \frac{C(i+1)^k - 2C(i)^k + C(i-1)^k}{\Delta z^2} \qquad (22)$$

$$T(i)^{k+1} = T(i)^k + \Delta T(i)^k$$

$$C(i)^{k+1} = C(i)^k + \Delta C(i)^k$$

In the wet zone eq.(20) becomes:

$$\Delta T(i) = \frac{\Delta time}{\left(1+\frac{h_{fg}}{\rho c_p}\frac{dC}{dT}\right)}\left[\alpha\left[\frac{T(i+1)^k - 2T(i)^k + T(i-1)^k}{\Delta z^2}\right] + \frac{h_{fg} D_v}{\rho c_p}\left[\frac{C(i+1)^k - 2C(i)^k + C(i-1)^k}{\Delta z^2}\right]\right]$$

$$T(i)^{k+1} = T(i)^{k} + \Delta T(i)^{k}$$

$$C(i)^{k+1} = C_{sat}(T(i)^{k+1}))$$

where dC/dT is obtained from saturation data.

Therefore, in the wet zone the coupling of the temperature and concentration as a result of the saturation conditions, requires the solution of only $\tilde{O}T$. $\tilde{O}C$ is determined from saturation data.

Had eq.(20) been linear the stability criterion for an explicit finite difference method would require:

$$\alpha\ \Delta\text{time} / \Delta z^2 < .5 \left[1+\frac{h_{fg}}{\rho c_p} \frac{dC}{dT} \right]$$

and

$$Dv\ \Delta\text{time} / \Delta z^2 < .5 \left[1+\frac{h_{fg}}{\rho c_p} \frac{dC}{dT} \right]$$

As an illustrative example, with

$\Delta z = .02$ m

Th = 305 K Tc=274K

hh = .9 hc = .9

$\rho = 1$ kg/m^3 $c_p = 1000$ J/kgK

$h_{fg} = 2.4E6$ J/kg

dC/dT = .001 kg/m^{3}K

Δtime $\sim$ 30 seconds

In practice the nonlinearity imposed by the coupling of the temperature and concentration fields makes the time constant much smaller then 30 seconds. By way of a trial and error

procedure it was determined that Δtime had to be less than 0.1 seconds to avoid numerical oscillation. Since many of the applications of interest such as the drying of a wet insulation sample are expected to take hours, this numerical technique is of limited value. It is possible to increase the grid size and thus increase the minimum step size. However when analysing a typical insulation section of 50 cm., a modest number of five nodes would require a spatial step size of .01 m, a value smaller than the Δz used in the example. In spite of theses drawbacks the numerical technique has been used to validate the quasi-steady assumption made in the analytical solution. The following section compares the two solutions.

2.4.3 COMPARISON OF ANALYTICAL AND NUMERICAL SOLUTIONS TO THE SPATIALLY UNSTEADY PROBLEM

In this section two methods for predicting the transient behavior of heat and mass transfer through porous media with phase change are compared. These methods are the analytical solution described in section 2.4.1, and the numerical solution described in section 2.4.2. Two cases are examined here which are illustrative examples of the drying of a slab of a porous medium given an initial liquid distribution. The two cases are identical except for the amount of liquid initially present in the wet zone. The first case demonstrates an example in which the quasi-steady analytic solution is valid, whereas the second case shows the discrepancy between the models when the quasi-steady assumption does not apply.

EXAMPLE A:

In this example a slab of a porous medium is dried. The boundary conditions are:

Th = 305 K	Tc = 274 K
hh = 10 %	hc = 10 %

The initial liquid content is uniformly distributed in wet zone whose position is:

$$z_0(t=0) = .16 \qquad z_1(t=0) = .97$$

$$\theta(x,t=0) = \begin{cases} 0.05 & .16 < x < .97 \\ 0 & \text{elsewhere} \end{cases}$$

The criteria for the quasi-steady analysis to be valid is given in eq.(14):

$$\frac{\tau_e}{\tau_d} = \rho\epsilon\theta(z_0,t) \;/\; C_r \gg 1$$

In this example $Cr = C_{sat}(Tr) = C_{sat}(289.5) = .011$ kg/m^3, therefore $\frac{\tau_e}{\tau_d} = 4545$ so the quasi-steady assumption should be valid.

Figure 10 shows the time history of the wet zone boundaries. The smooth curve is the analytical solution and the data points are from the numerical method. Both techniques agree very well on the movement of the wet zone as the drying process proceeds. As expected the movement of the boundaries is quickest when the boundaries are nearest the edges of the slab.

Figure 11 represents the time history of the heat fluxes into and out of the slabs as predicted by the quasi-steady model and the numerical model. Again the agreement between the two solutions is excellent. Initially the heat fluxes from both the hot and cold reservoir are into the slab. This can be explained by the evaporative cooling occurring at the edges of the wet zone. Thus the temperature is at its minimum at the cold wet/dry interface. As drying proceeds, the wet zone edges move away from the slab

COMPARISON OF NUMERICAL AND ANALYTICAL SOLUTIONS FOR

WET ZONE BOUNDARY POSITION VS. TIME

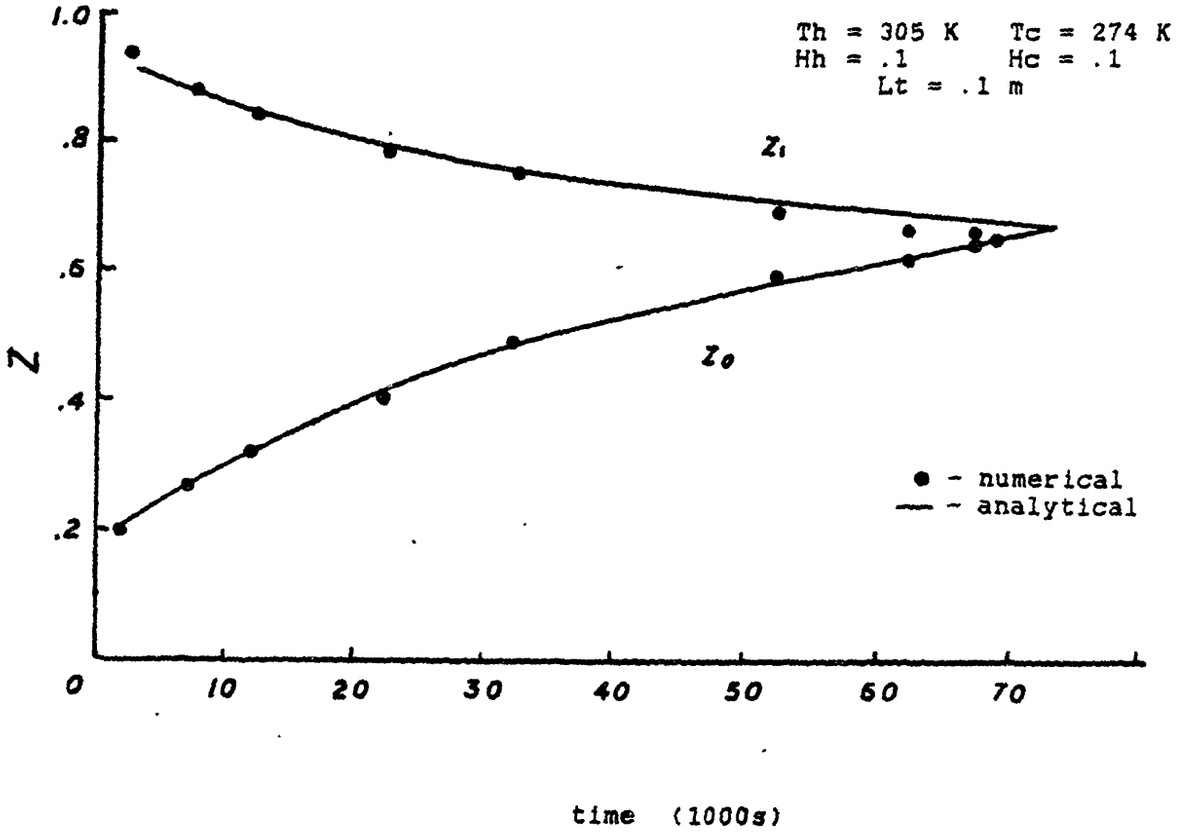

FIG 10

COMPARISON OF NUMERICAL AND ANALYTICAL SOLUTIONS FOR HEAT FLUX VS. TIME

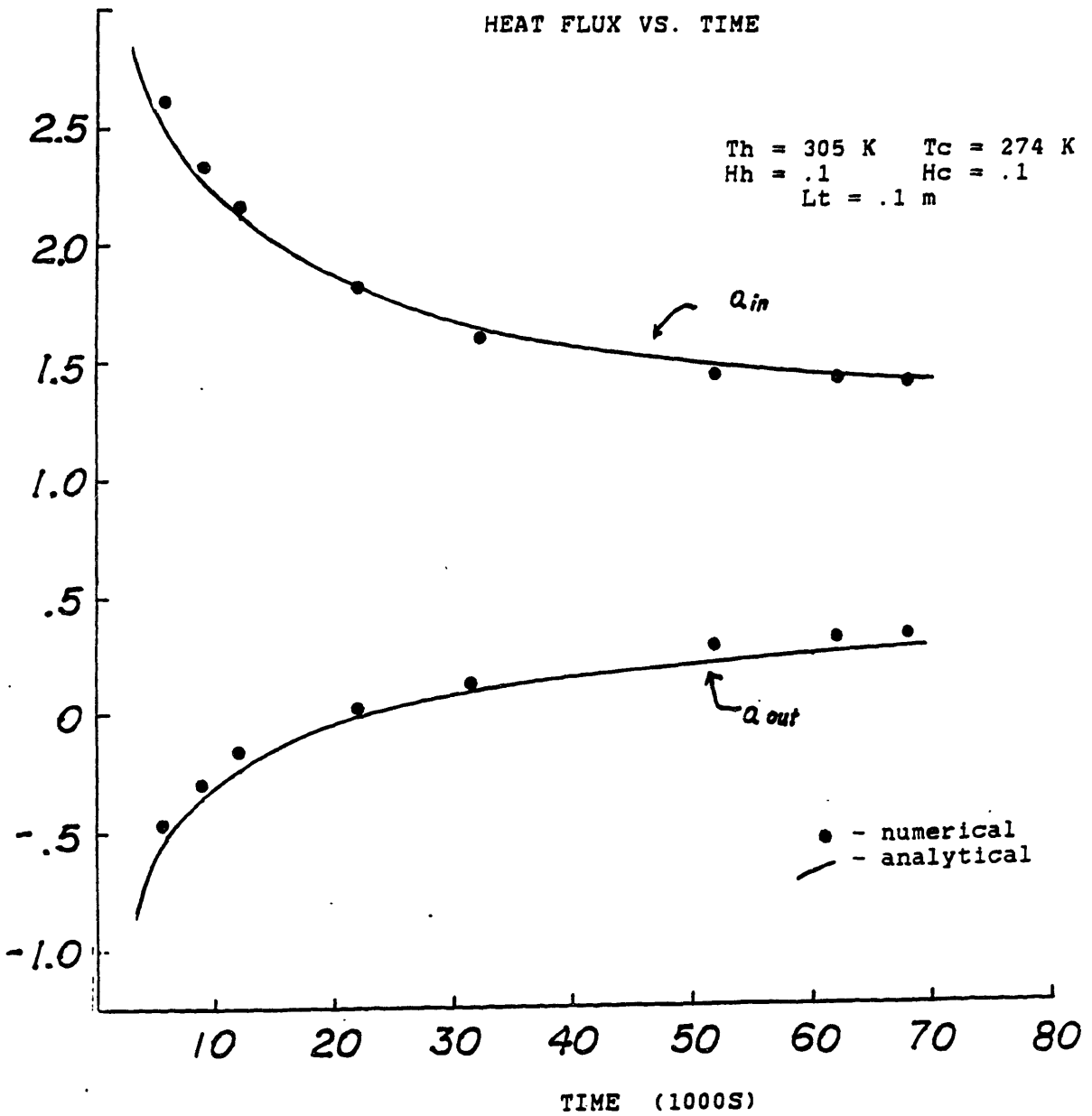

FIG 11

boundaries, and the rate of evaporation decreases. Eventually the cold side of the wet zone receives enough heat from the hot side to match the evaporation requirements at the interface. From that point on, the heat flux out of the slab at the cold edge is positive.

Note that the heat fluxes do not converge to values that they would experience in a dry sample until after all the moisture has evaporated. This can be explained by the fact that the rate of evaporation is governed by the thickness of the dry zone separating each reservoir from its corresponding wet/dry interface, rather than the thickness of the wet zone itself. As long as there is some liquid to be evaporated, there will be more heat entering the slab than leaving it. In section 2.4.1 it was shown that the heat fluxes at any instant are determined by the values of T_h, T_c, H_h, H_c, z_0, and z_1. Therefore the heat flux is independent of the amount of liquid present. The dependence of the heat fluxes on the wet zone boundary positions can be seen from figures 10 and 11. Note that the rate of change of Qin and Qout are closely related to the rate of change of z_0 and z_1. Once the water in the wet zone is evaporated, the interior of the slab will be warmed until the steady-state linear temperature profile is reached. However this last warming stage while appear as as step change to dry conditions in the transient model, due to the assumed linear temperature profile in the dry region.

Figures 12 - 15 show the temperature and vapor concentration profiles at various times for the same example depicted in figures 10 and 11. These profiles were determined by the numerical method. The quasi-steady assumption is verified by the linear profiles in the dry regions. It is precisely these linear profiles in the dry region that enable the quasi-steady analysis to effectively model this transient problem.

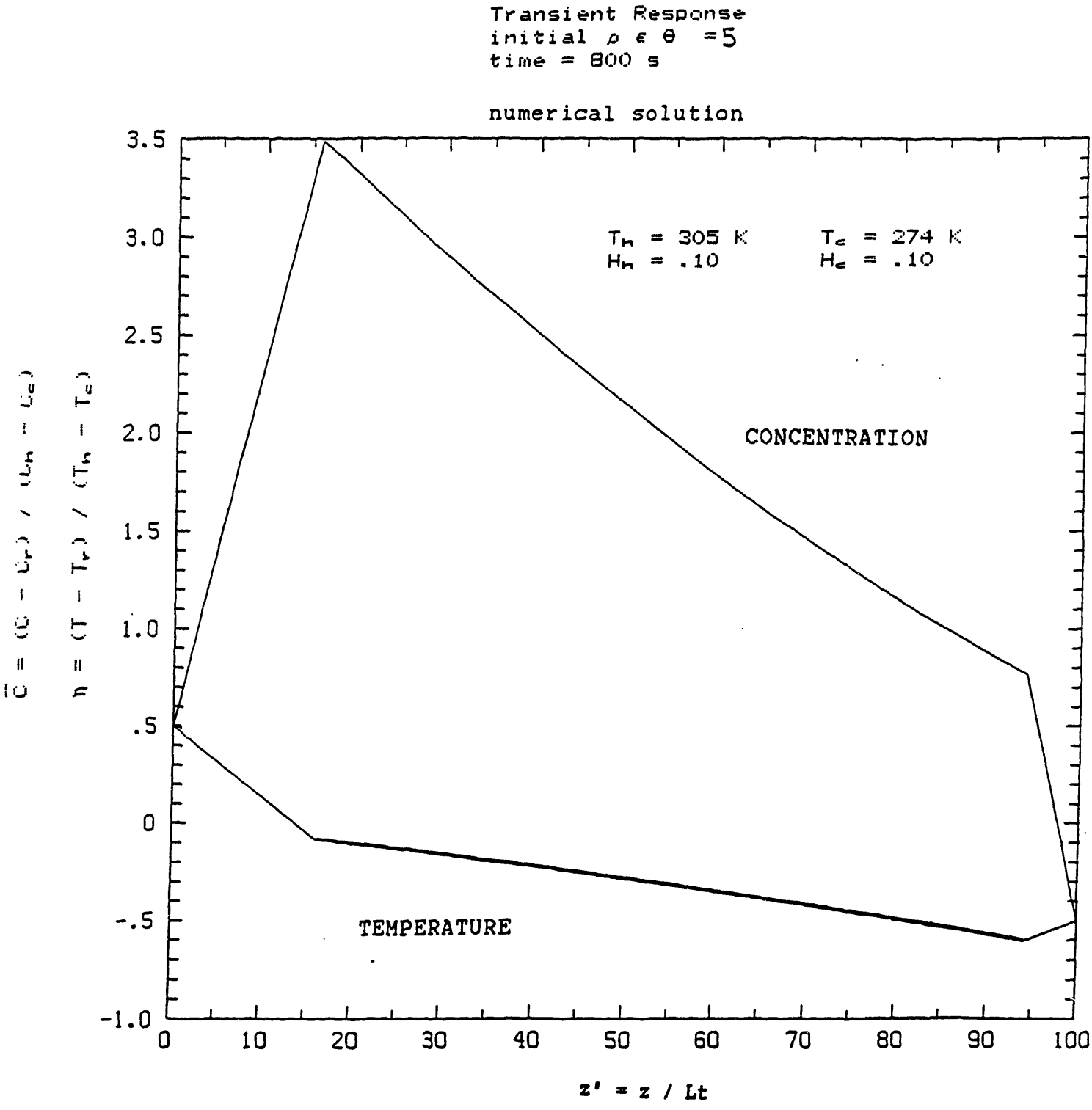
Transient Response
initial ρ ε θ =5
time = 800 s
numerical solution
T_h = 305 K
H_h = .10
T_c = 274 K
H_c = .10
CONCENTRATION
TEMPERATURE
3.5
3.0
2.5
2.0
1.5
1.0
.5
0
-.5
-1.0
0
10
20
30
40
50
60
70
80
90
100
z' = z / Lt

FIG 12

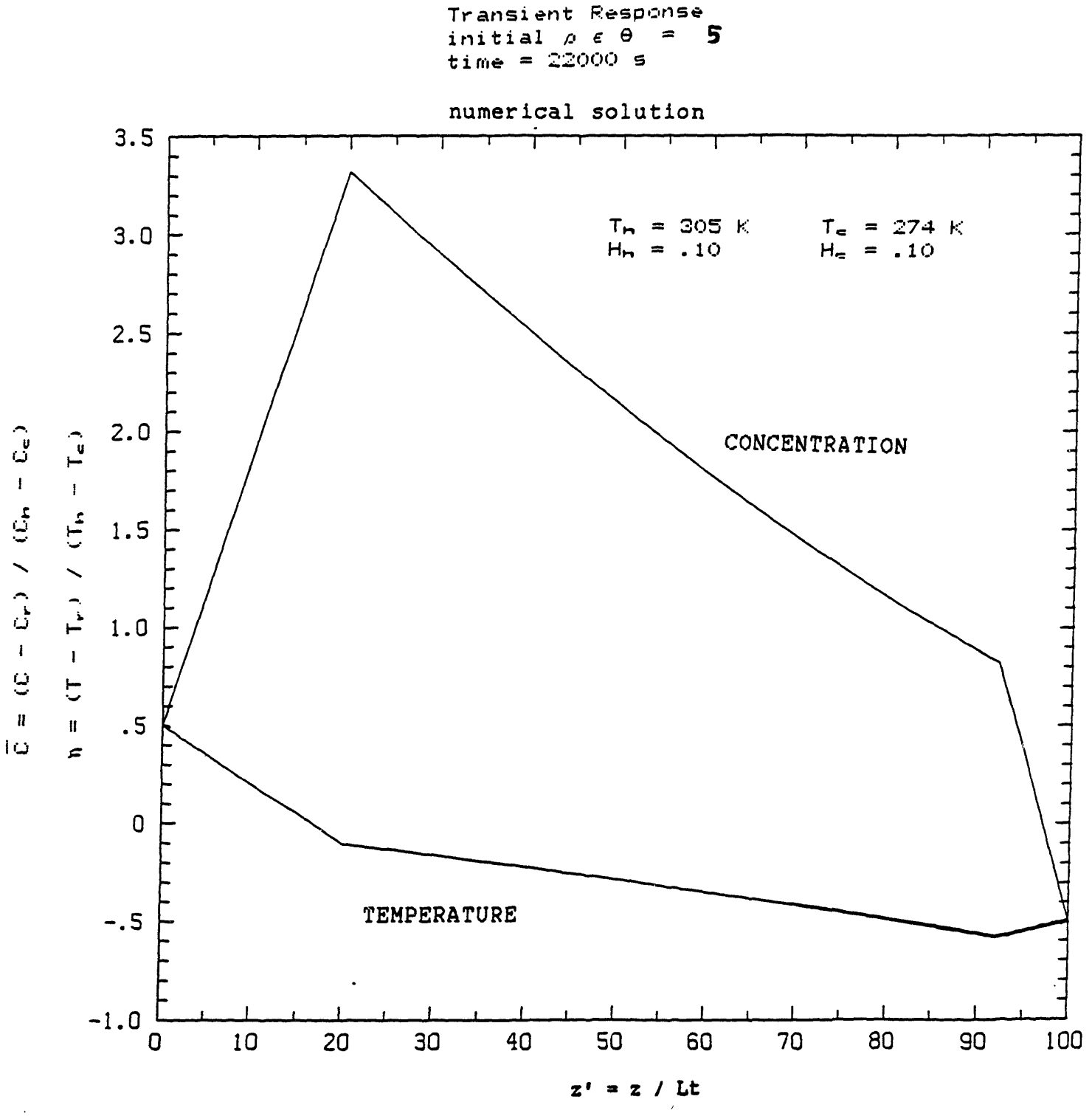
Transient Response
initial ρ ε θ = 5
time = 22000 s
numerical solution
T_h = 305 K
H_h = .10
T_c = 274 K
H_c = .10
CONCENTRATION
TEMPERATURE
$\bar{C} = (C - C_c) / (C_h - C_c)$
$h = (T - T_c) / (T_h - T_c)$
$z' = z / Lt$
3.5
3.0
2.5
2.0
1.5
1.0
.5
0
-.5
-1.0
0
10
20
30
40
50
60
70
80
90
100

FIG 13

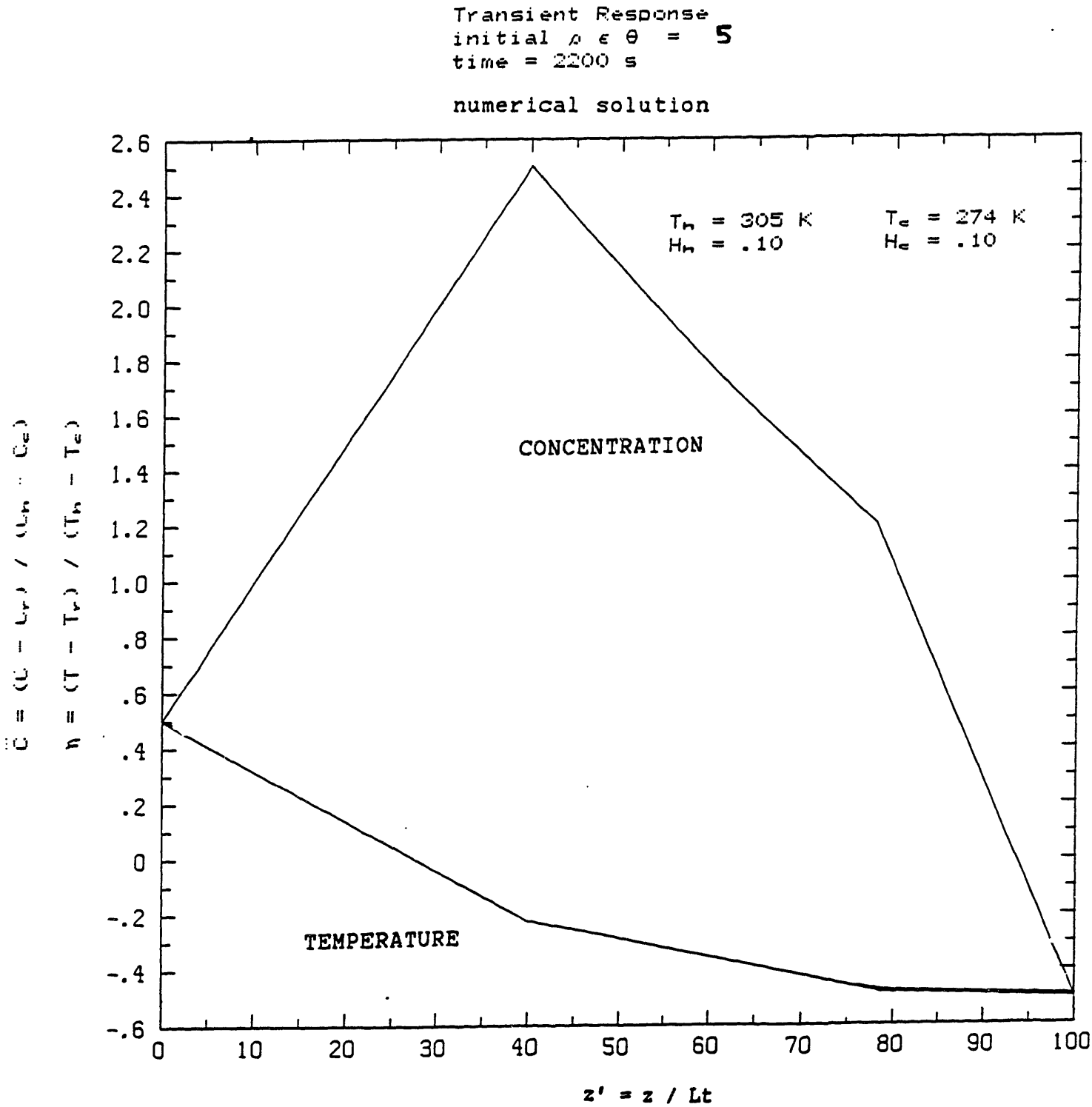
Transient Response
initial ρ ε θ = 5
time = 2200 s
numerical solution
T_h = 305 K
H_h = .10
T_c = 274 K
H_c = .10
CONCENTRATION
TEMPERATURE
2.6
2.4
2.2
2.0
1.8
1.6
1.4
1.2
1.0
.8
.6
.4
.2
0
-.2
-.4
-.6
0
10
20
30
40
50
60
70
80
90
100
z' = z / Lt

FIG 14

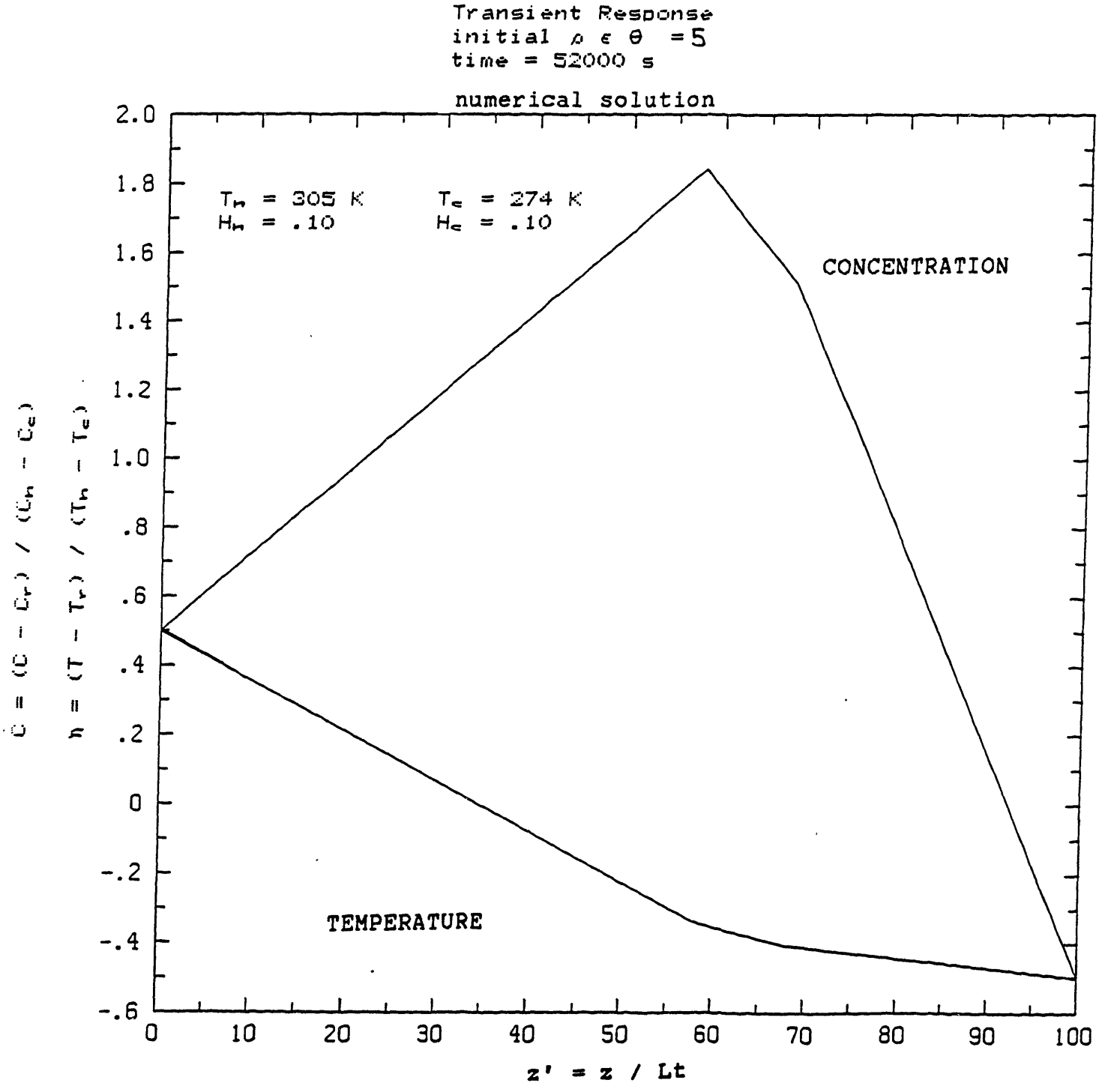
Transient Response
initial ρ ε θ =5
time = 52000 s
numerical solution
T_h = 305 K
H_h = .10
T_c = 274 K
H_c = .10
CONCENTRATION
TEMPERATURE
C = (C - C_r) / (C_h - C_c)
h = (T - T_r) / (T_h - T_c)
2.0
1.8
1.6
1.4
1.2
1.0
.8
.6
.4
.2
0
-.2
-.4
-.6
0
10
20
30
40
50
60
70
80
90
100
z' = z / Lt

FIG 15

EXAMPLE B:

In this example a slab of a porous medium is dried, however the initial liquid content is much less than in example A. The boundary conditions are:

Th = 305 K Tc = 274 K

hh = 10 % hc = 10 %

The initial liquid content is uniformly distributed in wet zone whose position is:

$z_0(t=0) = .16$ $z_1(t=0) = .97$

$$\theta(x,t=0) = \begin{cases} 5\ E\text{-}6 & .16 < x < .97 \\ 0 & \text{elsewhere} \end{cases}$$

The criteria for the quasi-steady analysis to be valid is:

$$\frac{\tau_e}{\tau_d} = \rho\epsilon\theta(z0,t) \ / \ Cr \ >> 1$$

In this case $\frac{\tau_e}{\tau_d} = .454$ so the quasi-steady criterion is not met. This example is solved by the numerical method. Figures 16 - 18 give the temperature and concentration distribution at various times. Note the nonlinear temperature and concentration in the dry zones. In this example the liquid content is so small that the rate of wet zone boudary movement is of the same order as the conduction and diffusion rates through the dry zone.

In comparing the analytic model with the numerical model, it has been shown that there is excellent agreement for cases in which the quasi-steady criterion in eq.(15) is satisfied. In applications involving condensation of water in insulation this criterion is met in all cases of practical interest. The deciding factor on which method to use is based solely on computational time. With a mesh of twenty nodes in the numerical method, the computation time required to simulate 5 hours of drying in example A, was approximately 12 hours. In contrast, the computation time needed for the quasi-steady solution was only 30 minutes. Hence the quasi-steady analysis is both fast and accurate, whereas the numerical technique developed in this work is impractical when used to model the drying of significant amounts of water.

TRANSIENT RESPONSE
initial $\rho\epsilon\theta$ = 0.005
time = 100 s

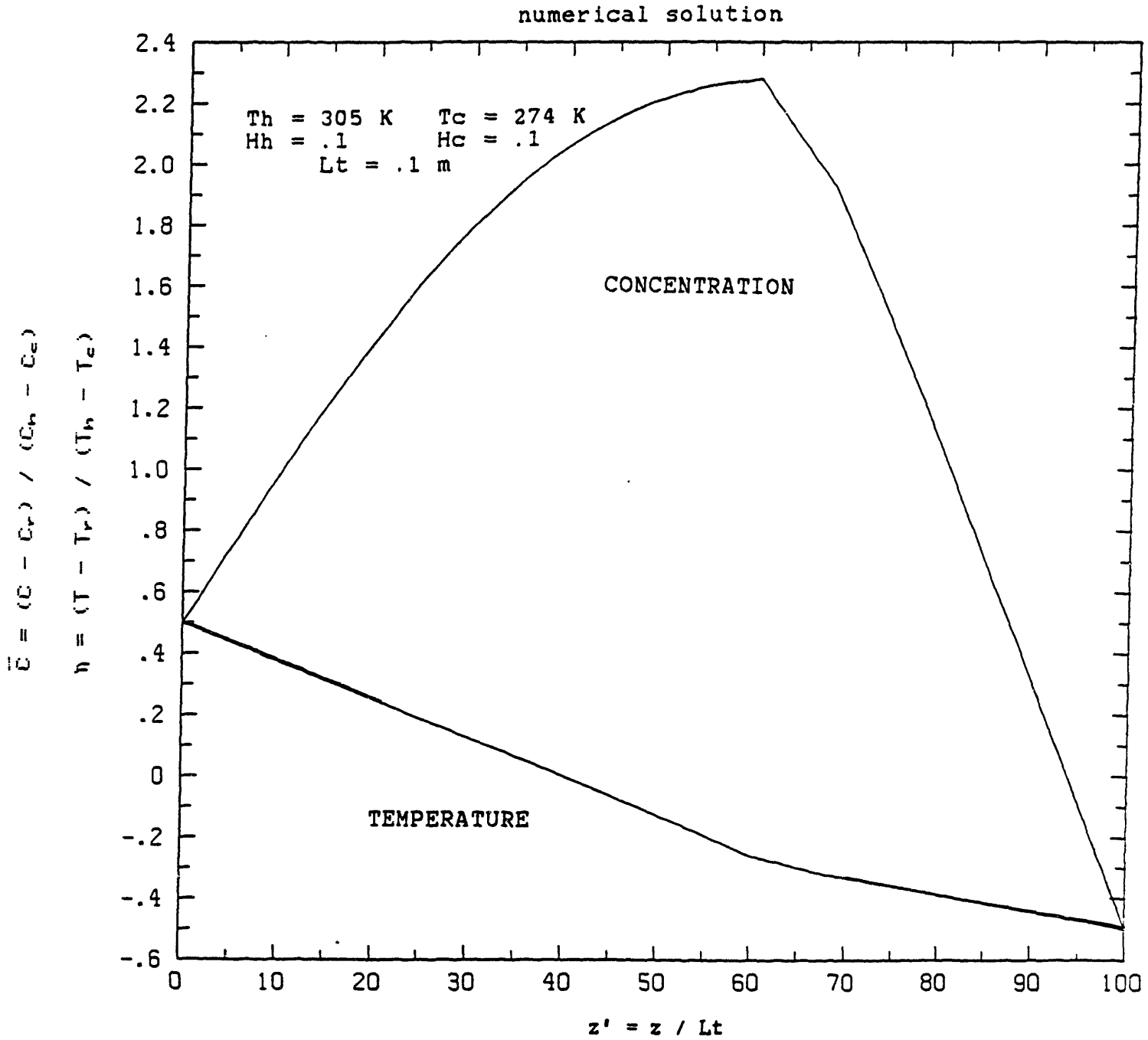

FIG 16

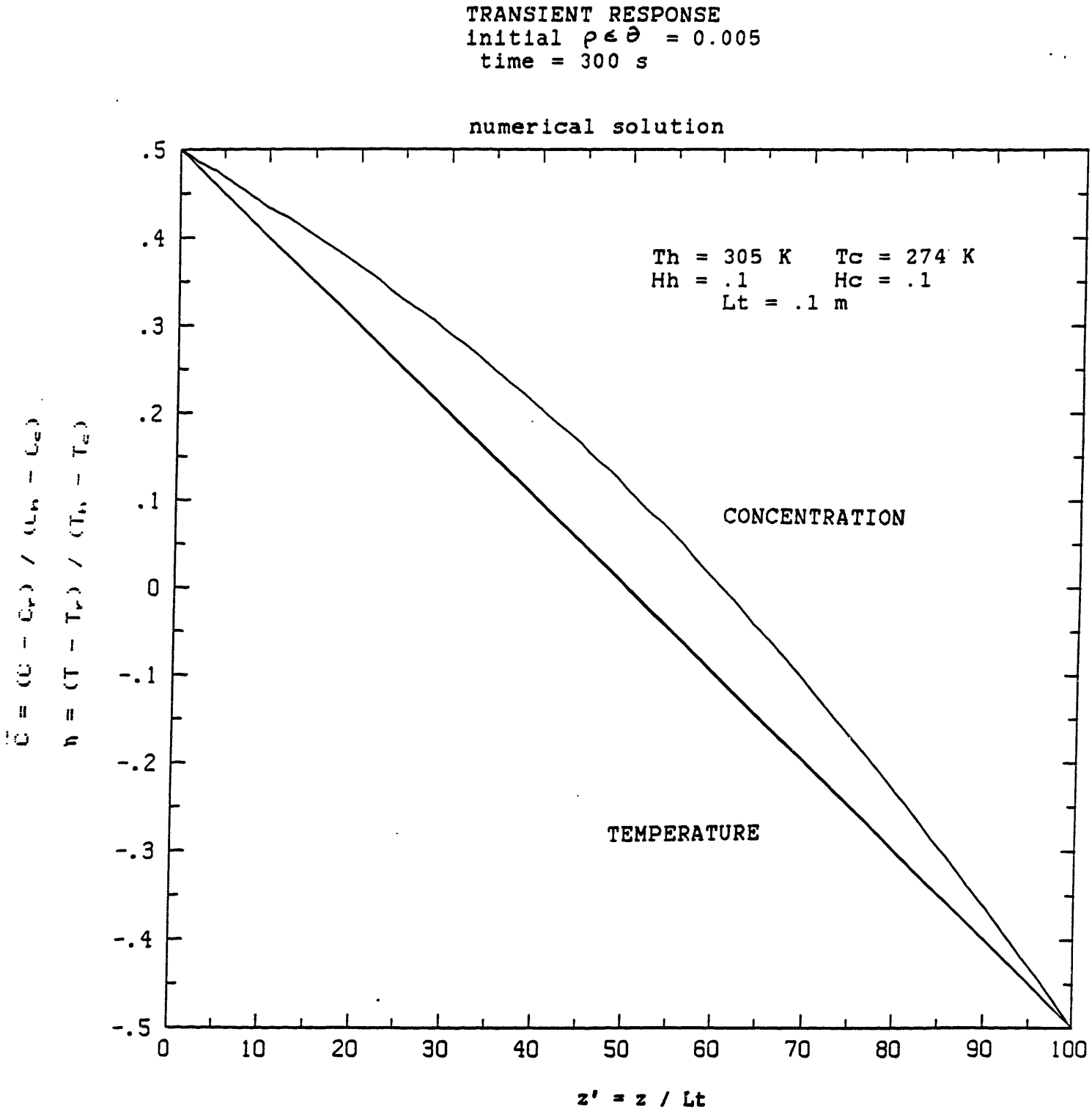
TRANSIENT RESPONSE
initial ρ∈∂ = 0.005
time = 300 s
numerical solution
Th = 305 K Tc = 274 K
Hh = .1 Hc = .1
Lt = .1 m
CONCENTRATION
TEMPERATURE
.5
.4
.3
.2
.1
0
-.1
-.2
-.3
-.4
-.5
0
10
20
30
40
50
60
70
80
90
100
z' = z / Lt

FIG 17

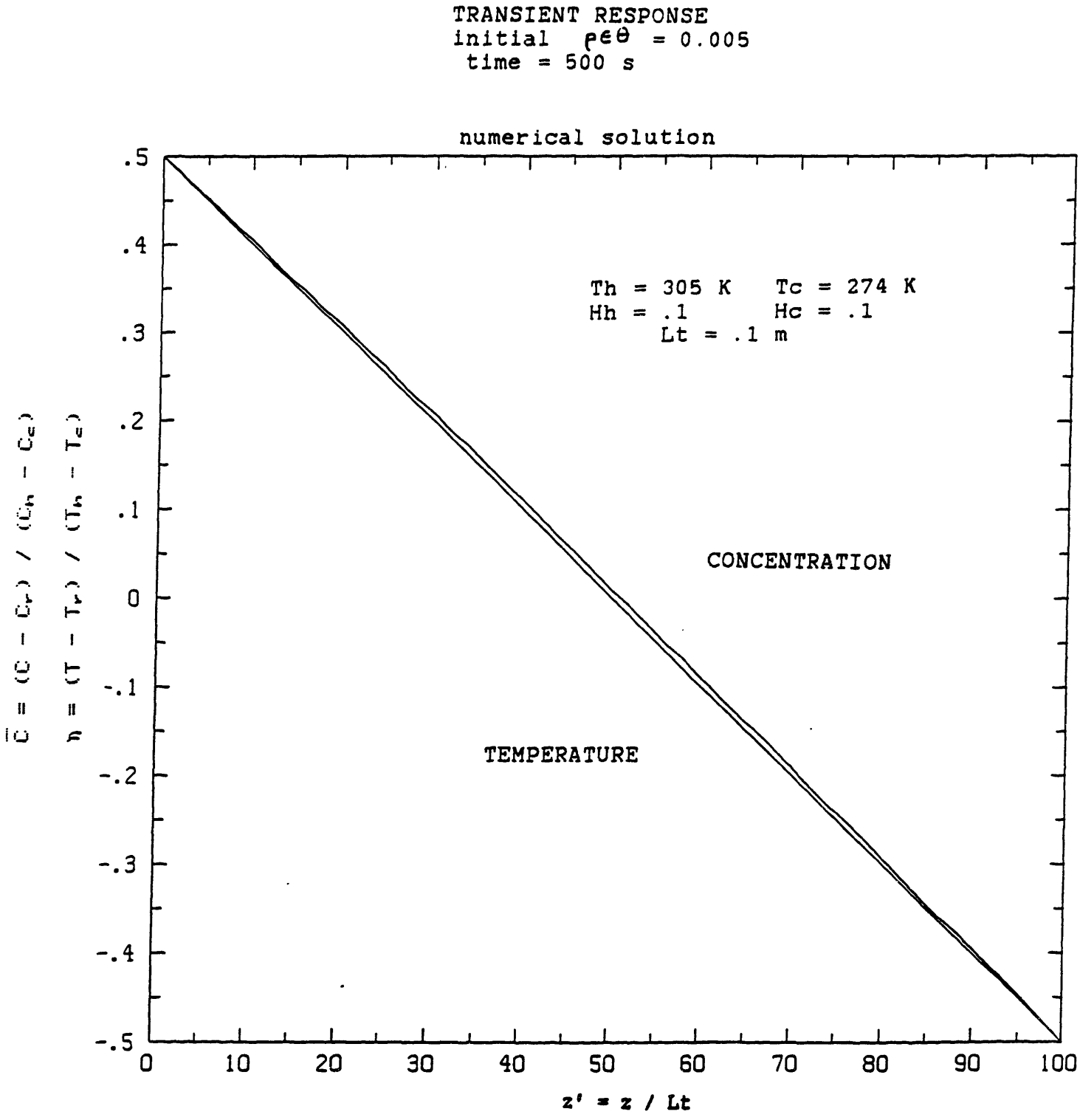
TRANSIENT RESPONSE
initial ρεθ = 0.005
time = 500 s
numerical solution
Th = 305 K Tc = 274 K
Hh = .1 Hc = .1
Lt = .1 m
CONCENTRATION
TEMPERATURE
z' = z / Lt
.5
.4
.3
.2
.1
0
-.1
-.2
-.3
-.4
-.5
0
10
20
30
40
50
60
70
80
90
100

FIG 18

2.5. TREATMENT OF VAPOR BARRIERS

In many applications involving heat and mass transport through a porous slab, one or both sides of the slab may be in contact with a membrane which is impermeable to mass flux, but conductive of heat. In a thermal insulation application, such a membrane is called a vapor barrier. This section examines the modifications necessary in the unsteady analytic formulation required to model the effect of a vapor barrier.

Consider the cases discussed in section 2, with the modification that a vapor barrier is placed at the cold side. Constant temperature is assumed at the slab boundaries and a constant humidity is imposed at the hot side. At the vapor barrier, for the case of no condensation at the barrier, the zero mass flux condition requires:

$$dC/dz = 0 \qquad \text{at } z = 1 \qquad (23)$$

If no condensation occurs in the slab, then the steady-state mass flux is governed by diffusion with no sources or sinks. Hence,

$$m = D_v \, dC/dz \qquad (24)$$

and m, the vapor flux rate, is constant throughout the slab. The boundary condition at z=1 given by eq.(23) indicates the C is constant, and equal to C_h, across the slab and there is no mass flux.

Since the temperature is linear across the slab with no condensation, the relative humidity increases monotonically

from the hot side to the cold side. Therefore as T_c is lowered, or C_h increased, the relative humidity at the cold side will approach 100 per cent, and condensation will begin at the vapor barrier. Under these conditions there will be no spatially steady position of the wet zone. Condensation will accumulate at the cold side and migrate towards the hot side as time proceeds.

The preceeding discussion indicates that the occurrence of condensation in a slab of a porous medium with a vapor barrier on the cold side can be determined solely from the values of T_h,T_c and C_h. If C_h is greater than the saturation concentration of T_c, condensation will occur. With condensation the zero mass flux condition at the vapor barrier becomes:

$$\Gamma(z=1) = -D_v \, dC/dz \qquad (25)$$

where Γ is the condensation rate at the vapor barrier. Hence if C_h is greater than the saturation concentration of T_c, there will be mass flux into the slab.

Under conditions of high concentration gradients in the slab, it is possible for condensation to occur in a finite region adjacent to the vapor barrier as well as at the vapor barrier itself. Two cases are illustrated in fig 19. In case I the concentration gradient is such that all condensation occurs at z=1, the vapor barrier. In case II, the concentration gradient is steep enough with respect to the temperature gradient to produce a region of condensation.

Vapor Concentration Profile

with Vapor Barrier at $\bar{z} = 1$

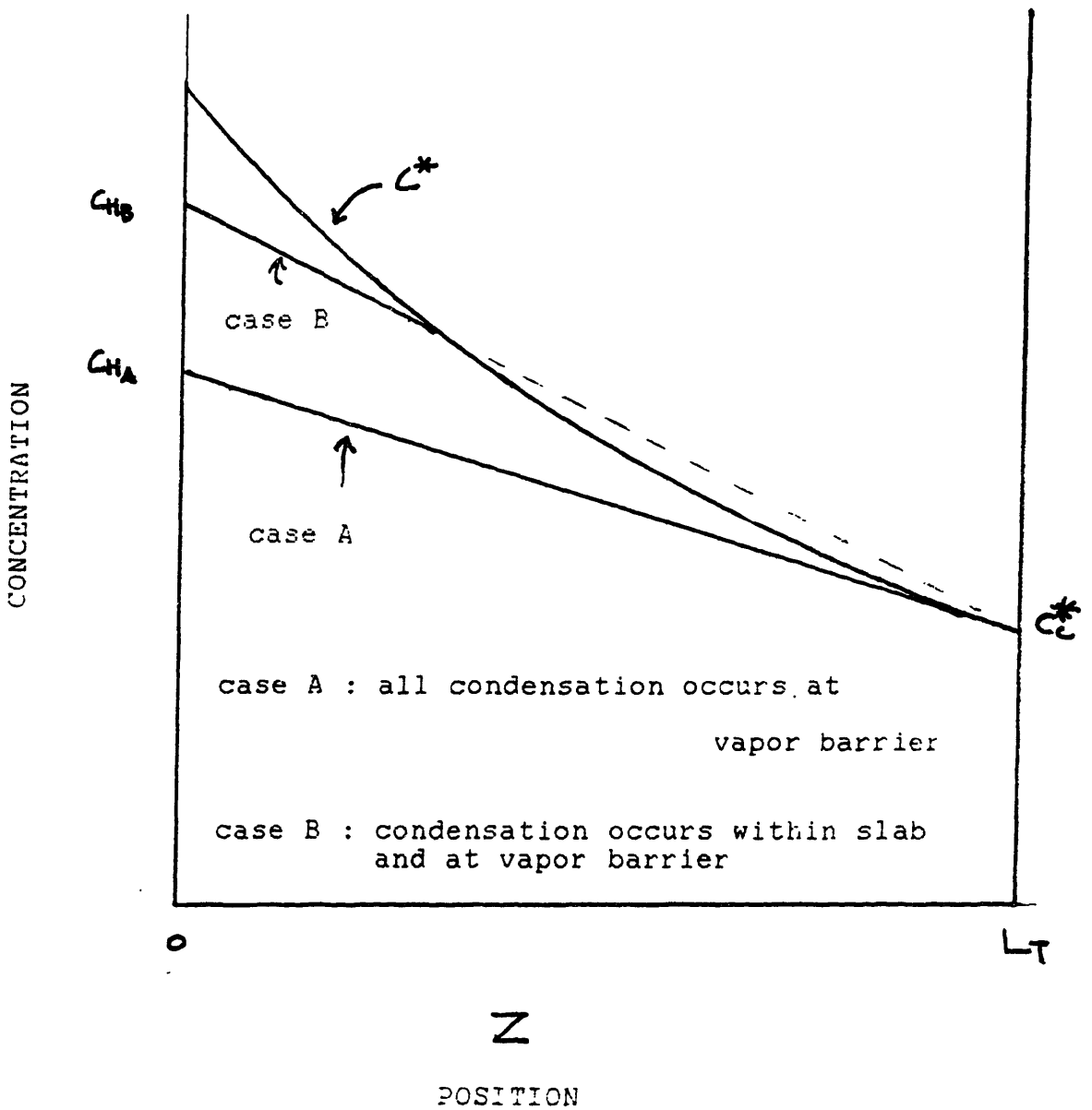

FIG 19

Assuming there is condensation at the vapor barrier, the criterion for the existence of a finite region of condensate is:

$$\frac{Ch - Cc}{Lt} > \frac{Th - Tc}{Lt} \left.\frac{dC^*}{dT}\right|_{T_c} \qquad (26)$$

The C^* curve in figure 19 is the plot of the saturation concentration corresponding to the linear temperature profile. The right hand side of eq.(26) is the slope of C^* under conditions of condensation occurring only at the vapor barrier. Hence the occurrence of a condensate region within the slab can be determined from the relative values of Th,Tc, and Ch.

If the inequality in eq.(26) is satisfied, the region of condensation is determined via the analysis of section 2.2.2. for the case of immobile condensate. Here, however z1 is known a priori to be 1. In most typical cases the rate of condensation in the interior of the slab is much smaller than the amount of condensation at the vapor barrier on the cold side. Figure 20 shows the cumulative condensation rate across the slab.

The previous analysis of the effect of a vapor barrier can be incorporated into the transient model. The movement of the cold side of the wet region can be understood by recalling eq.(14b) from section 2.4.1.

$$\theta(z1,t)\, d(1-z1)^2/dt =$$

$$\frac{2\, \exp(\phi 1) - hc\exp(\phi c) - (1+\eta 1\beta)^{-2}\exp(\phi 1)(\eta 1 - \eta c)}{1 + \Omega\, \gamma/Le\ (1+\eta 1\beta)^{-2}\exp(\phi 1)}$$

If the cold side of the condensate region is at the vapor barrier, the right hand side of eq.(14b) is clearly zero, so the cold side of the wet zone will remain at the vapor barrier until the region dries out completely. If on the other hand the wet region ends at $z_1 < 1$, the right hand side of eq.(14b) is negative, so the wet region moves towards the vapor barrier.

In the computer program the condensate at the vapor barrier is assumed to become uniformly distributed in a thin element of the slab (~ .05 L_t thick). In transient problems this liquid content can quickly grow and become unreasonably high. Hence a model of the growing condensate film needs to be incorporated which takes into account the mobility of condensate due to gravity and liquid diffusion.

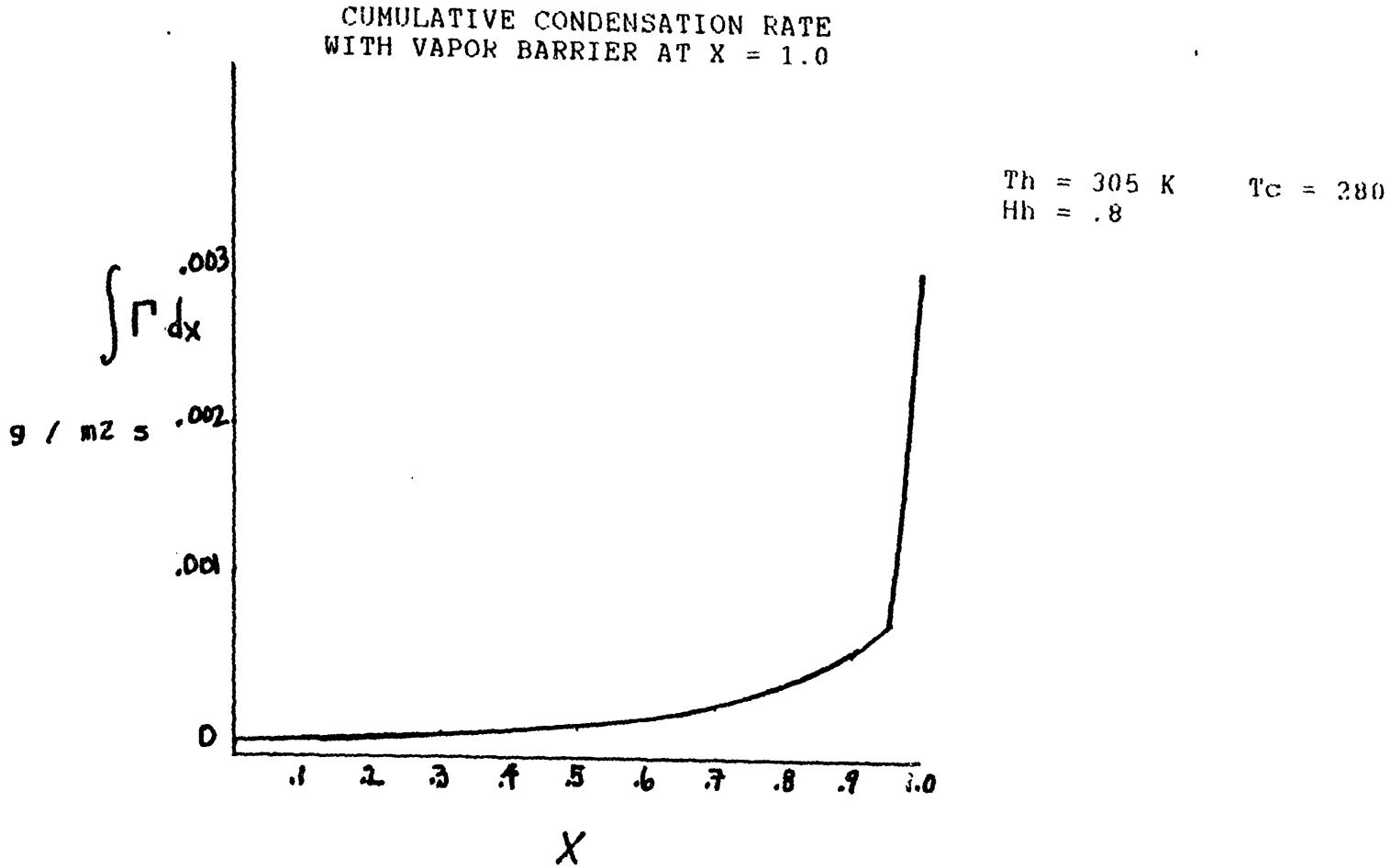
CUMULATIVE CONDENSATION RATE
WITH VAPOR BARRIER AT X = 1.0
Th = 305 K
Tc = 280
Hh = .8
$\int \Gamma dx$
g / m2 s
.003
.002
.001
0
.1
.2
.3
.4
.5
.6
.7
.8
.9
1.0
X

FIG 20

3. COMPARISON OF THE QUASI-STEADY MODEL WITH AN EXISTING MODEL AND DATA

The results of section 2 indicate that the analytic solution presented is well suited for modelling the transient heat and mass behavior of a reasonable amount of condensate in a slab of porous insulation.

The transport of heat and mass through a medium density wetted insulation sample has been studied by Thomas et al[2]. Their investigation provides data with which the analytic model presented here is compared.

Thomas et al also modelled the behavior of heat and mass transfer through wet insulation. They derived a series of differential equations that govern the heat and mass transport in the insulation sample. The main differences between the analytic solution presented in this work and the model developed by Thomas are:

1) The Thomas formulation accounts for heat transferred by diffusing air and vapor, whereas this analysis assumes that conduction is the dominant mechanism of heat transfer.

2) The Thomas model accounts for the variation in heat capacitance due to liquid content, while this model ignores such variations.

3) The Thomas solution requires an explicit solution of six coupled differential equations and is therefore restricted to a very coarse spatial grid to enable reasonable computation time. The analysis presented here is discretized in time, but not in space.

In short the analysis presented in this work has made several simplifying assumptions which enable an analytic solution for the temperature and concentration profiles to be formulated. In addition to the ease of using the analytic model over an explicit technique, the advantage of an analytic solution over a set of differential equations that must be integrated simultaneously is the insight into the governing parameters that the analytic solution offers. In section 2.2 the parameter λ, which is based on the physical properties and the boundary temperatures and humidity, was shown to be the variable controlling the rate of condensation in the wet zone and the net heat and mass flux through the insulation.

The experiment conducted by Thomas et al.[2] consisted of uniformly wetting six layers of insulation and stacking them together to form one specimen. The specimen was then heat-sealed in plastic film. The test section was inserted in a guarded hot plate device and subjected to a temperature gradient. Transient temperature measurements were made with inserted thermocouples and transient liquid content measurements were made periodically by removing the specimen from the testing device, removing the insulation from the plastic film, and weighing the individual layers to determine moisture content. After each measurement the specimen was reassembled, resealed in plastic film, and reinserted into the testing chamber.

The resulting data give the temperature profile and liquid content distribution as a function of time. The temperature data are plotted in figure 21a, along with the Thomas model prediction and the prediction based on the quasi-steady model presented here. Clearly both models track the data very closely. Hence it can be inferred that the simplifying assumptions inherent in this analysis introduce no significant loss of accuracy. On the contrary, the smoothness of the analytic solution enables a higher degree of certainty when predicting the motion of the wet zone.

Tables 3 and 4 and figures 21B and 21C present the liquid content distribution data for two experiments. In the first experiment the initial value of θ was .025, and in the second experiment the initial θ was .051. Though the data are sparse, it appears that the quasi-steady analysis is better than the explicit solution at predicting the movement of moisture in the slab. This improvement must be attributed to the fact that the error imposed by the explicit solution of the series of differential equations in the Thomas model outweighs the error imposed by the assumptions in the quasi-steady model. Both models tend to overpredict the rate of movement of the wet region towards the cold side. This may be attributed to the role that gravity plays in pulling the condensate towards the hot side and the effect of liquid diffusion, which was shown in section 2.3.2.3 to cause the wet zone to spread out. Both

the Thomas model and the quasi-steady model presented here ignore the effects of gravity and liquid diffusion. It is clear that both theorectical models are much worse at predicting the liquid content distribution in the case in which the initial θ was .051. This would be expected if liquid motion was occurring, since the degree of liquid mobility increases with total liquid content.

COMPARISON OF TEMPERATURE DATA WITH TRANSIENT MODELS

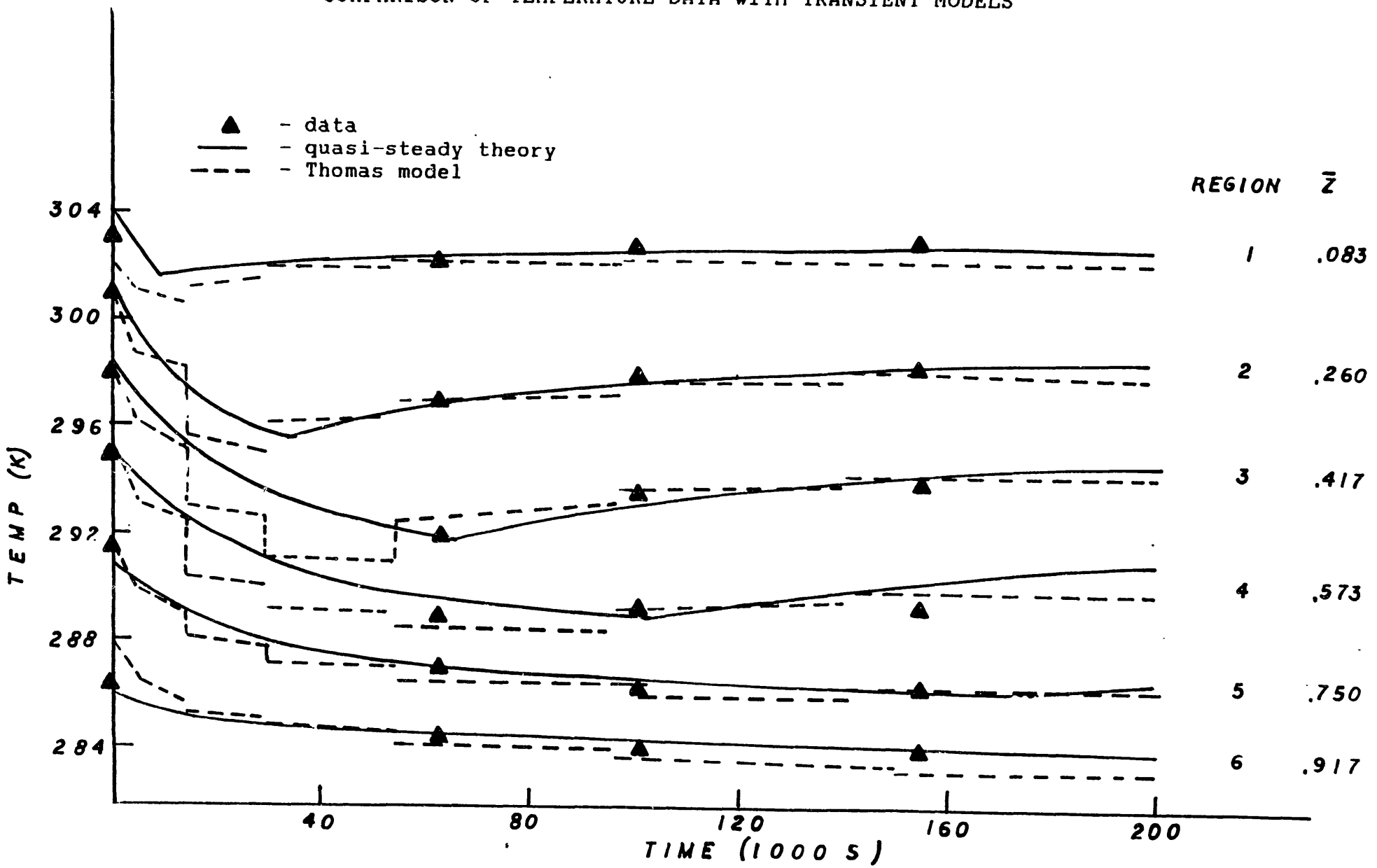

FIG 21a

TABLE 3

COMPARISON OF MODEL PREDICTIONS AND MEASURED MOISTURE DISTRIBUTIONS
Initial moisture distribution θ = .024

elapsed time, h	value	MOISTURE DISTRIBUTION $[\rho\epsilon\theta\ (z,t)]$ (kg/m^3) Region 1	2	3	4	5	6
	measured	23.5	23.0	22.6	26.4	26.4	24.5
0	analytic	24.0	24.0	24.0	24.0	24.0	24.0
	explicit	24.0	24.0	24.0	24.0	24.0	24.0
	measured	0.0	0.0	0.0	8.16	36.0	98.4
43	analytic	0.0	0.0	0.0	0.0	32.8	111.2
	explicit	0.0	0.0	0.0	0.0	0.0	144.0

Test conditions: L=40.56mm T_h=31.7 T_c=9.7
Data from Thomas et al[2]

TABLE 4

COMPARISON OF MODEL PREDICTIONS AND MEASURED MOISTURE DISTRIBUTIONS
Initial moisture distribution θ = .051

elapsed time, h	value	MOISTURE DISTRIBUTION $[\rho\epsilon\theta\ (z,t)]$ kg/m^3 Region 1	2	3	4	5
	measured	51.0	51.0	52.4	54.8	52.0
0	analytic	51.0	51.0	51.0	51.0	51.0
	explicit	51.0	51.0	51.0	51.0	51.0
	measured	0.0	17.8	65.4	75.5	89.0
43	analytic	0.0	0.0	0.0	64.5	190.0
	explicit	0.0	0.0	0.0	41.4	213.6
	measured	0.0	0.5	39.0	81.8	97.7
120	analytic	0.0	0.0	0.0	0.0	255.0
	explicit	0.0	0.0	0.0	0.0	255.0

Test conditions: L=35.38mm T_h=31.1 T_c=9.8
Data from Thomas et al[2]

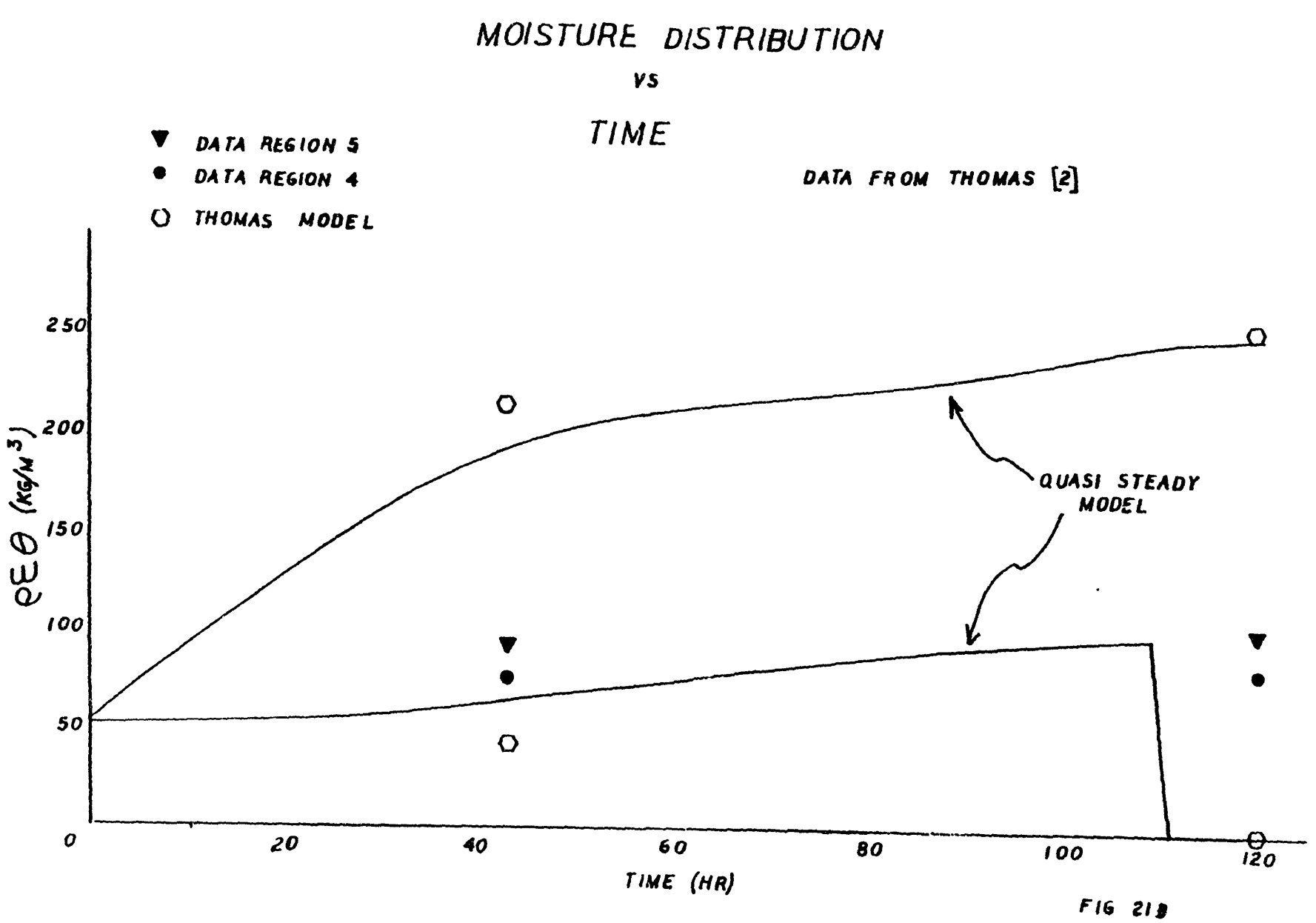
MOISTURE DISTRIBUTION
VS
TIME
DATA REGION 5
DATA REGION 4
THOMAS MODEL
DATA FROM THOMAS [2]
250
200
150
100
50
0
ρεθ (KG/M³)
QUASI STEADY MODEL
20
40
60
80
100
120
TIME (HR)

FIG 21

MOISTURE DISTRIBUTION

VS

TIME

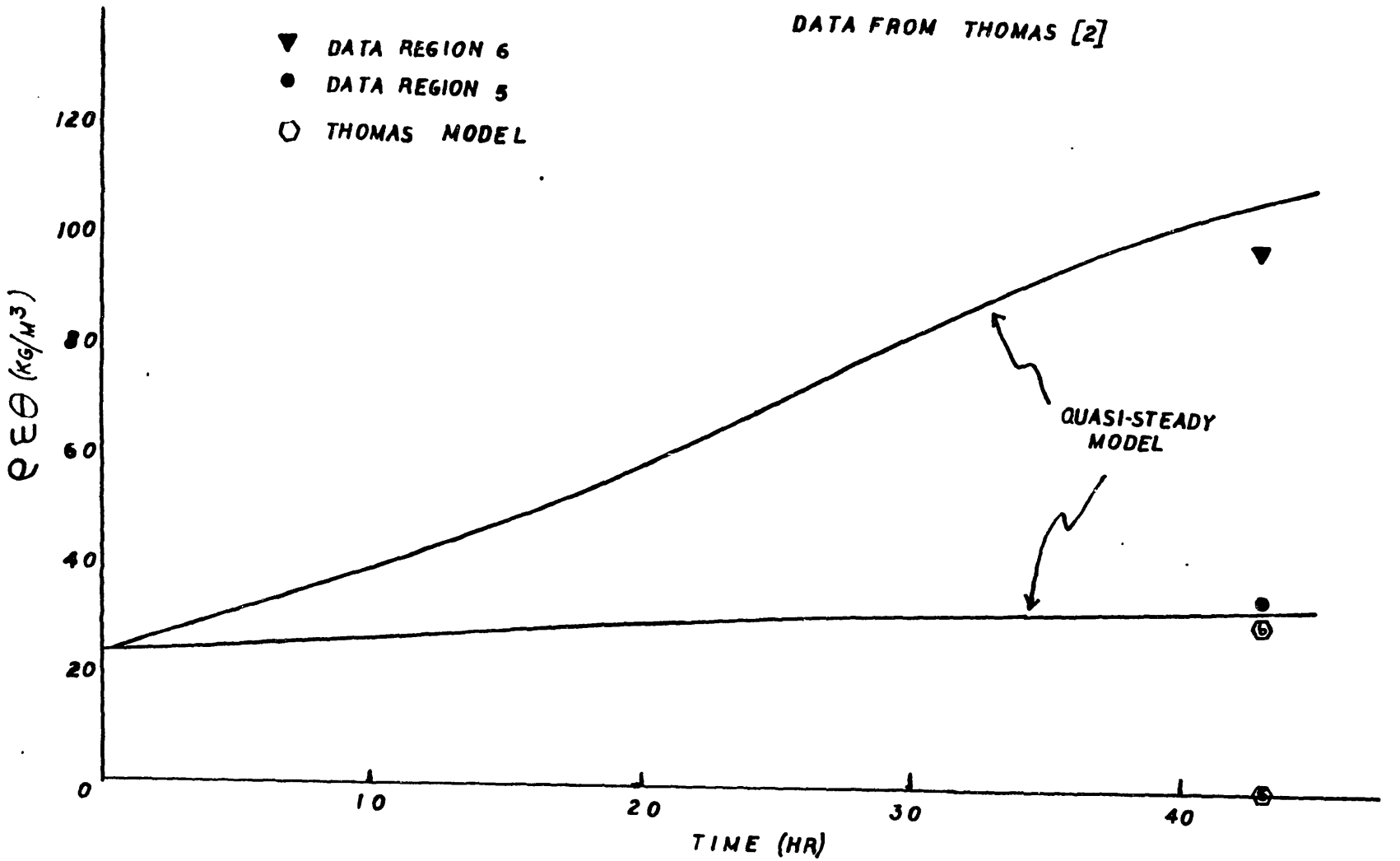

FIG 21c

4. Experiments

4.1. Apparatus

The purpose of the experimental apparatus was to maintain a wide range of uniform temperature and humidity conditions on two sides of a horizontal test section of porous insulation. A schematic of the apparatus is given in figure 22. The apparatus consists of two chambers; the top chamber is referred to as the cold box and the bottom chamber is the hot box.

4.1.1. Hot Box

The interior dimensions of the hot box are 17" x 17" x 24". The walls are constructed of Dexicon steel framing, polyethlyene vapor barrier, plywood sheeting and guard heaters sandwiched between two panels of R-8 extruded polystrene insulation.

The hot box contains a fan and heating coil to maintain the desired homogeneous temperature and humidity conditions on the hot side of the test section. The humidity level is controlled by bubbling air through a salt solution. Lithium chloride and sodium chloride were used in the following experiments. The relative humidity over a saturated lithium chloride solution varies from 11.2 % at 0 ^{o}F to 17 % at 87

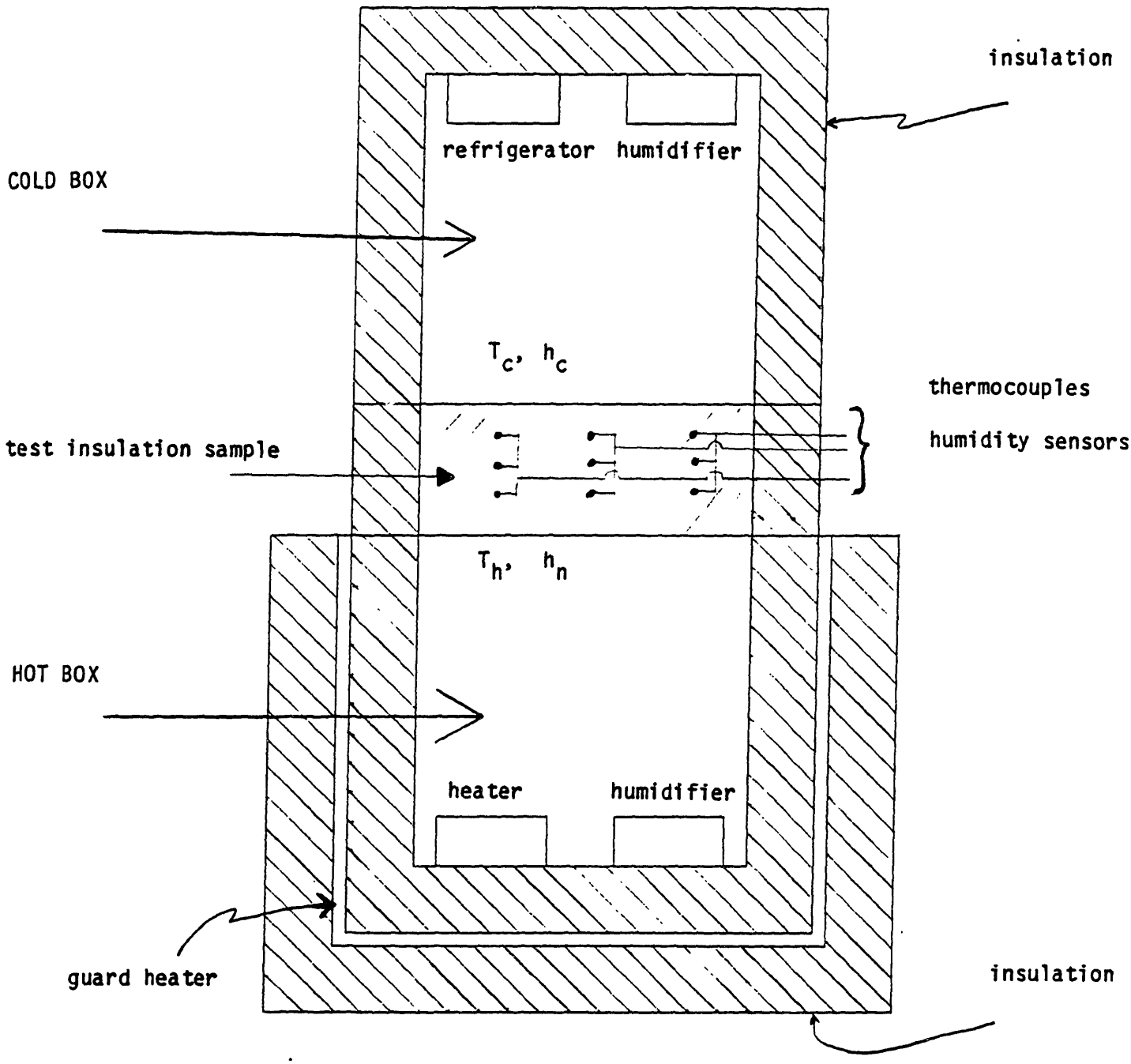

EXPERIMENTAL APPARATUS

FIG 22 A

^{o}F. For sodium chloride, the relative humidity varies from 73 % to 75 % over the range of 32 ^{o}F to 212 ^{o}F [6]. By diluting these salt solution relative humidities can be achieved up to 100 %.

Guard heaters were used on the five exterior sides of the hot box. The guard heaters are constructed of electric resistance heat tape bonded to 1/8" aluminum sheet metal. The voltage applied to the electric heat tape is controlled to keep the aluminum plate at the same temperature as the adjacent interior surface of the hot box. This in effect prevents heat from being conducted out of the hot box walls. Hence all of the energy supplied to the fan and heater must be conducted, through the test section, into the cold box. Thus the guard heater enables the heat flux through a test sample to be determined directly from the energy supplied to the hot box. This is verified in experiment 1.

4.1.2 Cold Box

The interior dimensions of the cold box are 17" x 17" x 24". The walls are constructed of Dexicon steel framing, polyethlyene vapor barrier, plywood sheeting and R-16 extruded polystyrene insulation.

The cold box temperature is controlled by circulating chilled propylene glycol / water solution through a coil of copper tubing. A fan continually blows the interior air over the cooling coil to maintain the required homogeneous

Detail of Test Section Installed in Apparatus

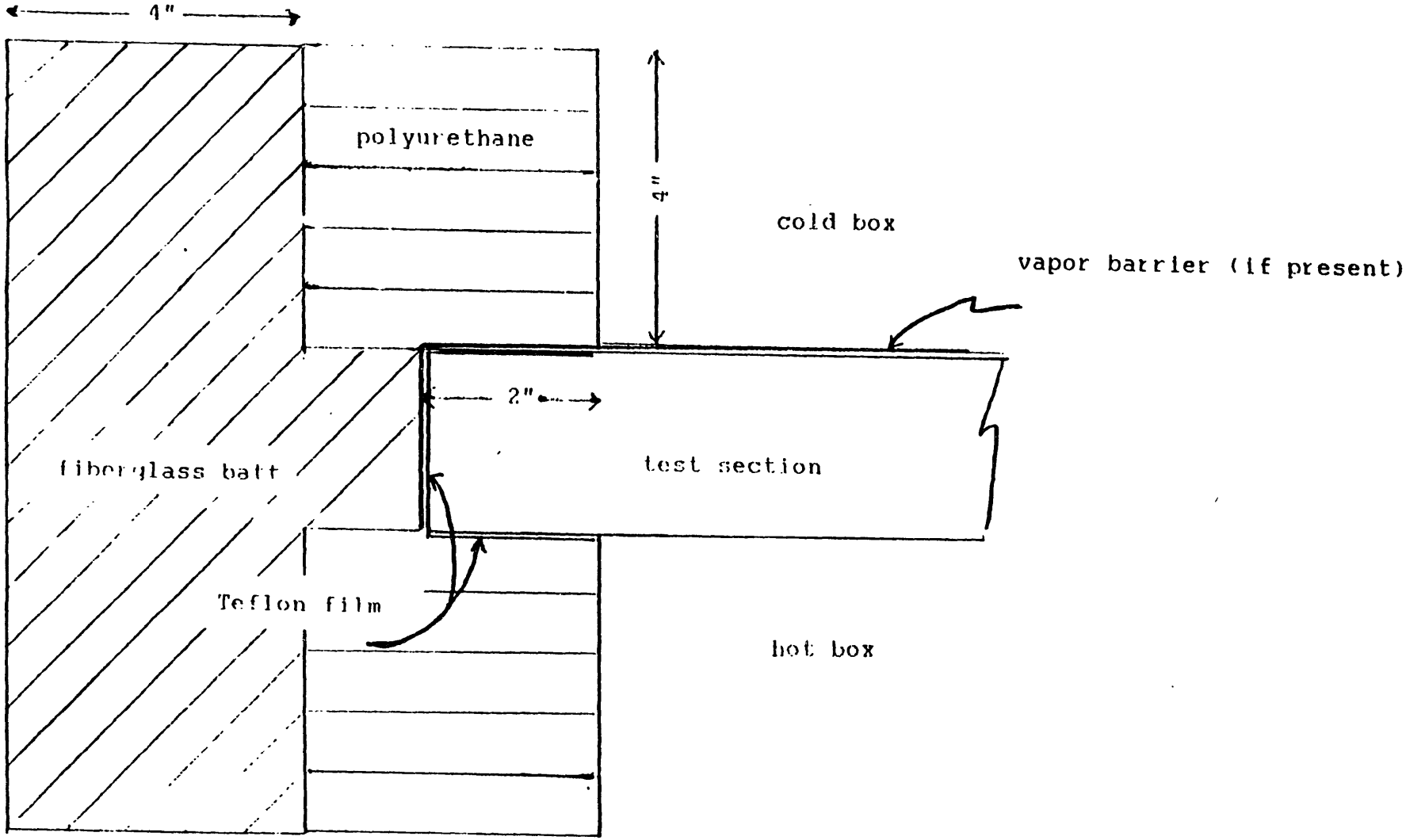

FIG 22 B

Cooling Loop Schematic

FIG 22 C

conditions. This cooling loop is depicted in figure 22C. As in the hot box, the humidity level is controlled by bubbling air through a salt solution.

4.1.3 Test Section and Probe Placement

The test section were 17" X 17" X 2" samples of rigid fiberglass board with a nominal density of three pounds per cubic foot. Figure 22B indicates how the test section was held in place in between the hot and cold boxes. The edges of the test section are covered with Teflon film to prevent capillary migration of condensate along the test section / apparatus interface. The Teflon film was fixed to the edges by taping it to the horizontal surfaces of the test section which were in contact with the polyurethane insulation (fig 22B)

The instrumentation probes consist of a humidity transducer and a thermocouple. Each probe is inserted into the test section from the edge. The probe positioning is illustrated in figure 23. An incision approximately two centimeters wide and fifteen centimeters deep is made horizontally in the sample at the desired position of the probe (fig 23). Two thin copper strips are inserted into the incision and then the probe is pushed between the copper strips to a depth of nearly fifteen centimeters. The metal

PROBE PLACEMENT IN TEST SECTION

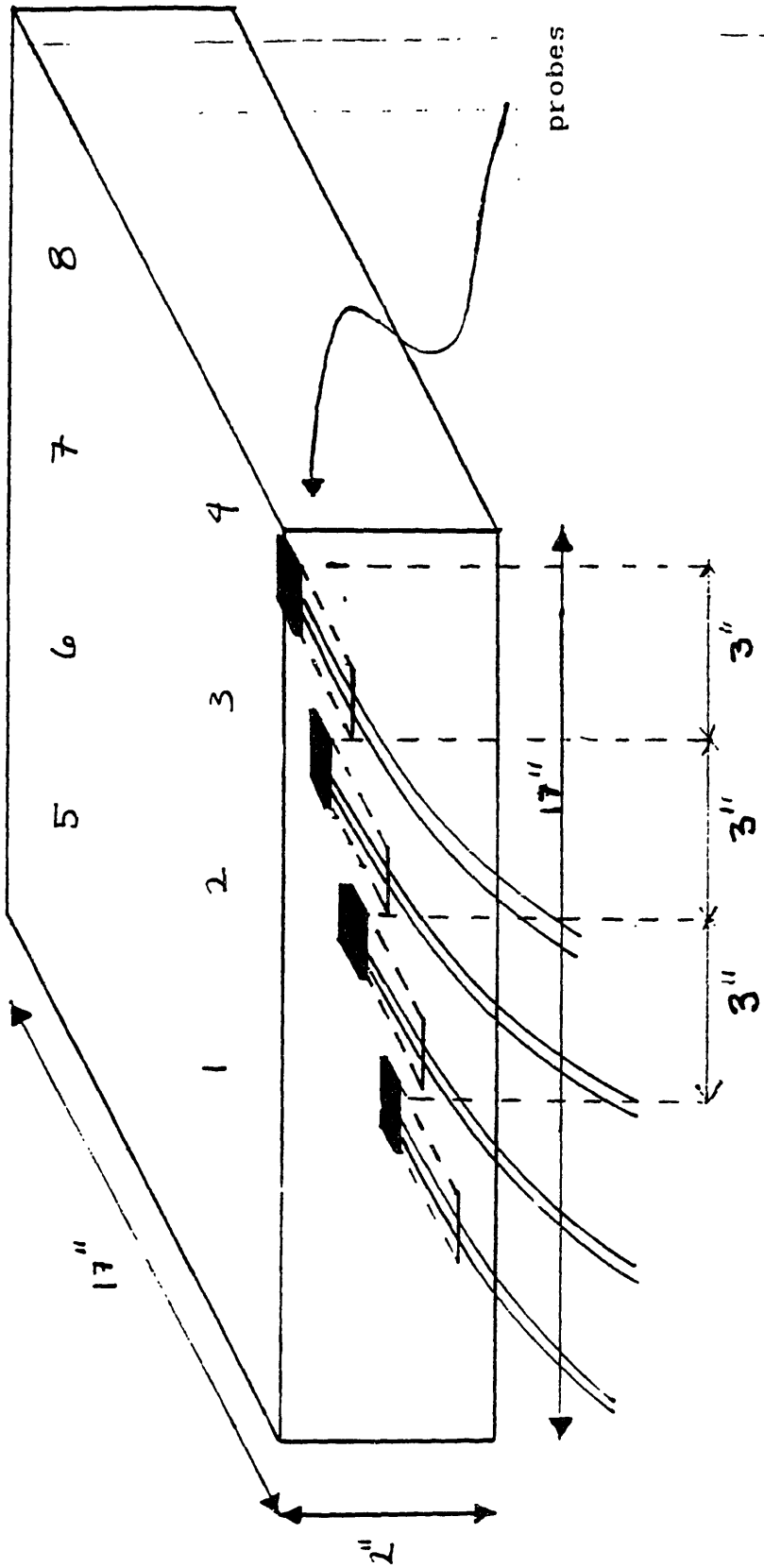

FIG 23

strips are subsequently removed, and the probe wires are taped to the test section to immobilze the probe.

4.1.4. Temperature and Humidity Measurements

Each probe consists of a type-K thermocouple (28 ga.) and a PCRC-55 humidity transducer. The humidity transducers, manufactured by Phys-Chemical Research Corporation, were coated with a special polymer film to protect the transducer from liquid water.

The impedance of the humidity transducer is sensitive to the relative humidity of the surrounding air. The impedance varies over three orders of magnitude from approximately 10 mega-ohms at 30% relative humidity to 100 kilo-ohms at 90% relative humidity. The impedance of each sensor was determined using a voltage divider circuit illustrated in figure 24. Since the transducers are subject to polarization from a DC current, a 600 Hz 10 volt signal is applied across the circuit. With a known reference impedance of 1 mega-ohms, the impedance of the transducer is determined by the following formula:

$$Z_{probe} = Z_{ref} \left[1 / (V_{in}/V_{probe} - 1)\right]$$

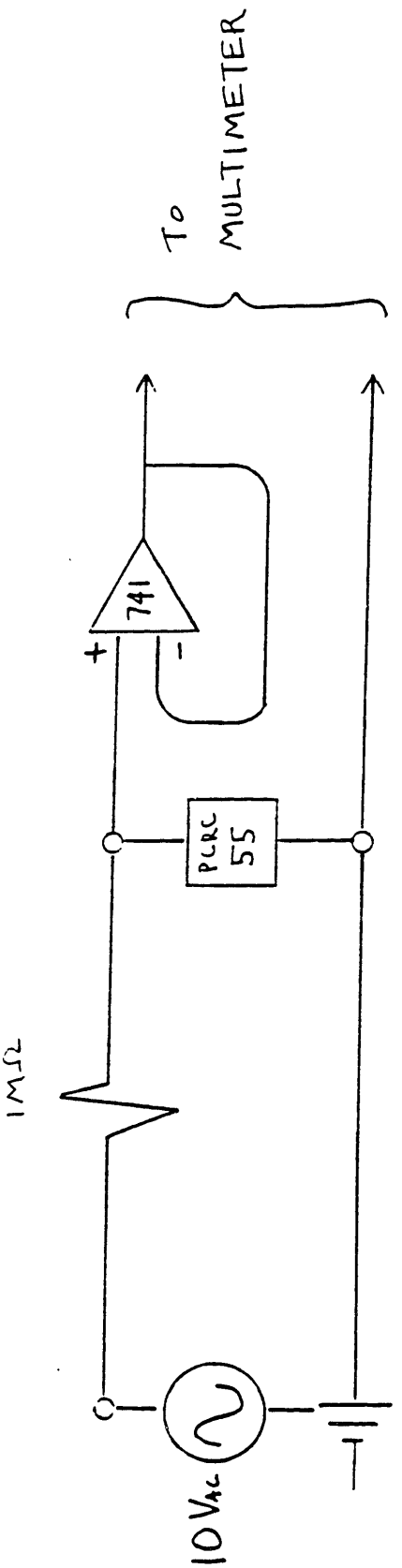

Voltage Divider Circuit

FIG 24

4.1.5 Humidity Transducer Calibration

Each humidity transducer was calibrated in a chamber in which the true relative humidity was determined by the equilibrium vapor pressure of various saturated salt solutions. The relative humidity was verified with a EG&G dew point hygrometer. Great care was taken to prevent the transducers from becoming wet with condensate in the calibration tests. The data from the calibration tests were fit to a curve of the form:

$$\ln(Z) = a\,(RH) + b\,/\,(RH) + c.$$

The calibration curves and calibration data for each humidity transducer at 25^{o}C are included in Appendix A. In general, the calibration curves are within 5 % of the manufacturer's specifications. Though variation among the ten humidity transducers's calibration curves is small, it is shown in experiment 1 that there is significant hysterisis effects experienced after the transducers become wet with condensate. The transducers are slightly temperature sensitive, such that the actual humidity is determined by adding 0.36 % RH for each degree that the probe is below 25 ^{o}C to the value from the calibration curve.

4.1.6. Data Acquisition

The voltage across each thermocouple and each humidity transducer is measured using an HP 3478A Multimeter controlled by an HP 3497A Data Acquistion / Control Unit. Data is automatically stored on diskettes at programmed time intervals.

4.2 Experiment 1

Measurement of the Thermal Conductivity of a Sample of Insulation

The objective of this experiment was to verify the adiabatic behavior of the exterior walls of the hot box with the guard heaters in use. A three inch sample of expanded polystyrene was inserted between the hot and cold boxes. The conductivity of this sample was accurately determined from tests made at Dynatech Corporation, Cambridge, Ma, using a guarded hot plate device (R-Matic by Dynatech). With the cold box maintained at a constant temperature, a known amount of energy was supplied to the hot box by the electric fan. The temperature of the guard heaters was adjusted to match their respective interior wall temperatures. In theory, all of the energy input must leave the hot box by conduction through the insulation sample. By measuring the temperature drop across the insulation sample, its conductivity is determined by the follow formula:

$$k = Q\ L\ /\ A\ \ \Delta T$$

where

L = the sample thickness = 3"

A = the sample cross sectional area = 2.37 ft^2

Q = the energy input

ΔT = the temperature drop across the sample

The energy input, Q, was determined by measuring the voltage and current input signals to the fan on an oscilloscope.

$$Q = V_{rms}\ I_{rms}\ \cos(\phi)$$

where

ϕ is the phase angle between the voltage and current.

In this experiment Q was determined to be 8.93 Btu / hr. With a steady-state temperauture drop across the sample of 83 ^{o}F, the calculated thermal conductivity was determined to be .297 Btu-in/hr ft^2 ^{o}F. The reported value of the conductivity of this sample was .283 ± 5% Btu-in/hr ft^2 ^{o}F. Thus the experimental error was approximately 5 %, which is within the measured uncertainty. This excellent agreement between the measured and accepted value of conductivity indicates that the exterior walls of the hot box can be made nearly adiabatic by use of the guard heaters, and the flow of heat to the cold box is nearly one-dimensional.

4.3 Experiment 2
Temperature and Concentration Profile in a Dry Slab of Insulation

The purpose of this experiment was to verify that both the steady-state temperature and concentration profiles in the slab of dry insulation were linear, as expected from the analysis of section 2.1

As described in section 4.1.3, the probes were inserted approximately 15 centimeters into the test section from the edge. However the undulations of the glass fibers made it difficult to know exactly where each probe was finally positioned. If it were demonstrated that the temperature profile was in fact linear in a dry sample, then that linear profile could be used to accurately determine probe position. Once the position of the probes had been determined, it would then be possible to examine the vapor concentration profile using the humidity sensors.

This experiment consisted of inserting eight probes containing humidity sensors and thermocouples into the test section and exposing the section to a steady-state temperature gradient in the hot box / cold box apparatus. The steady-state temperatures and humidities for each probe were recorded.

In the first run of this experiment, T_h = 50 ^oC and T_c = 15 ^oC. After steady-state conditions had been reached, the test section was removed from the apparatus and dissected to determine the actual position of the probes. If the temperature profile were linear, then the probe position could be determined as follows:

$$\bar{x}_{calc} = T_h - T \; / \; T_h - T_c$$

Figures 25 and 26 show the actual temperature and concentration profiles for this first run. The data are presented in Table 4.

TABLE 4

Experiment 2
Data for Run 1

Probe	Temp(^oC)	C(g/m^2)	$\bar{x}_{measured}$	$\bar{x}_{calc}$
1	50	54.1 ± 5%	0 ± .05	0 ± .05
2	48	48.0	0.10	0.06
3	42	45.1	0.20	0.23
4	37	31.0	0.41	0.37
5	25	20.7	0.67	0.71
6	22	18.6	0.74	0.80
7	17	12.9	0.94	0.90
8	15	10.2	1.0	1.0

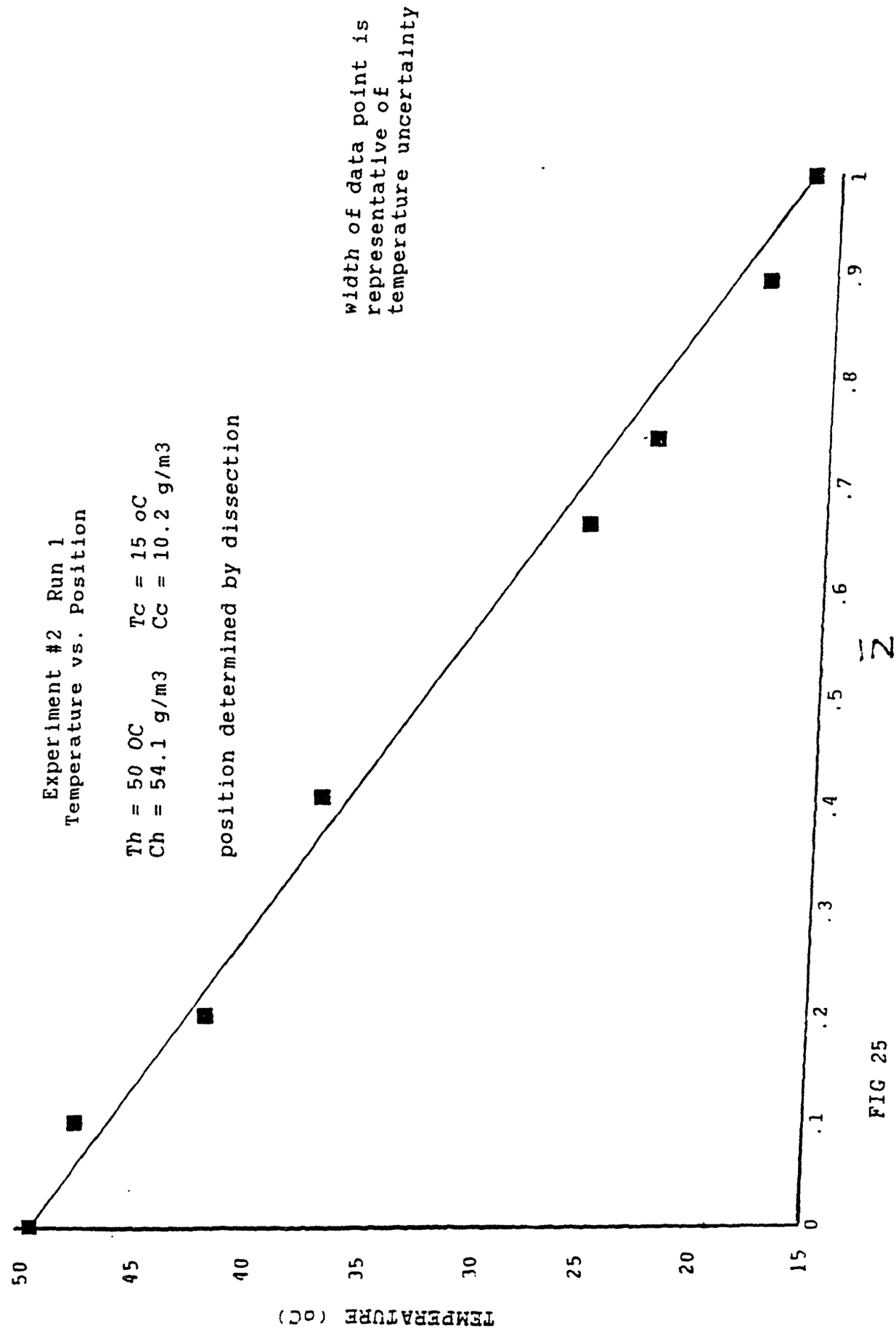
Experiment #2 Run 1
Temperature vs. Position
Th = 50 OC Tc = 15 oC
Ch = 54.1 g/m3 Cc = 10.2 g/m3
position determined by dissection
width of data point is representative of temperature uncertainty
TEMPERATURE (oC)
50
45
40
35
30
25
20
15
0
.1
.2
.3
.4
.5
.6
.7
.8
.9
1
Z

FIG 25

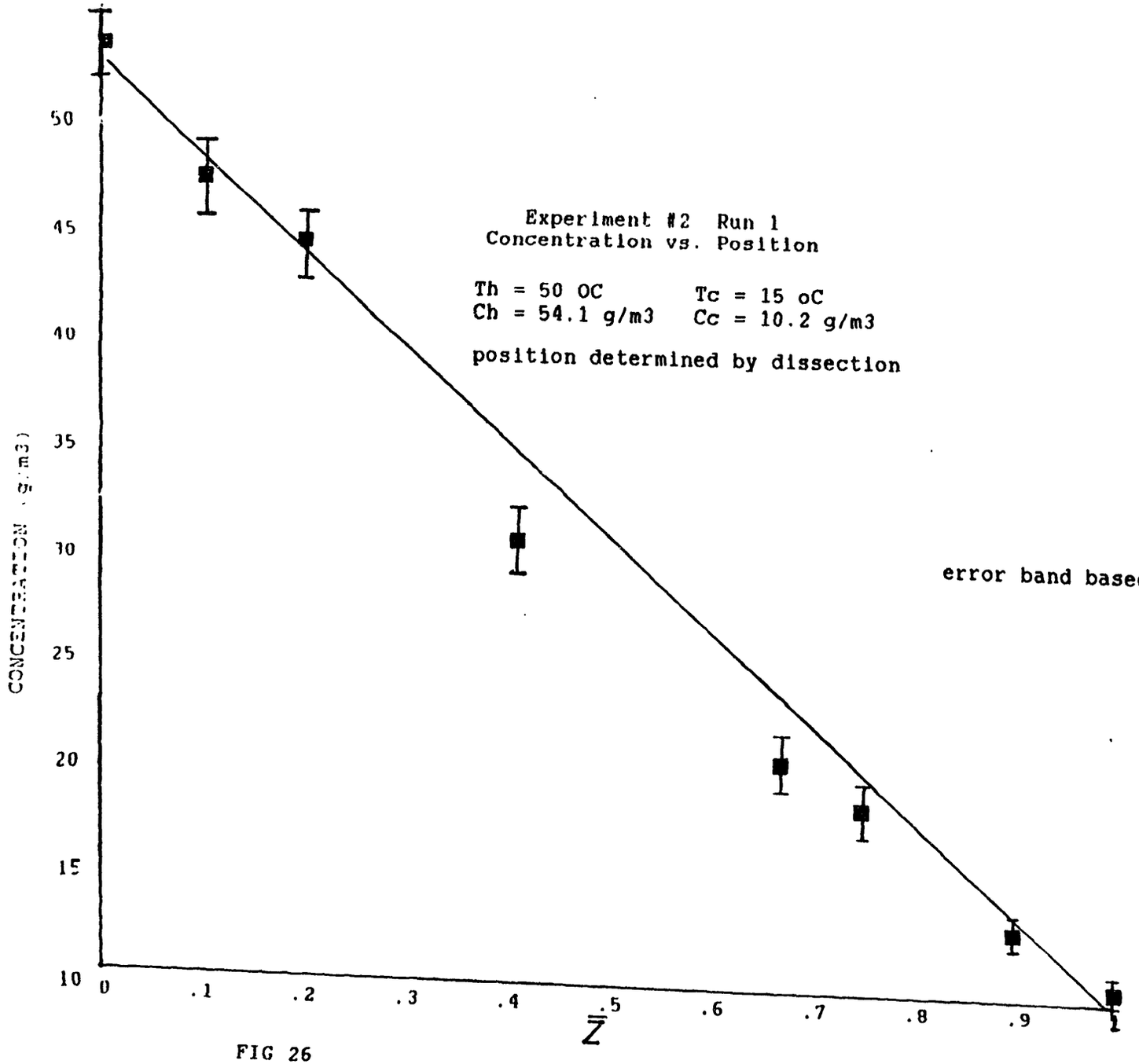
Experiment #2 Run 1
Concentration vs. Position
Th = 50 OC
Tc = 15 oC
Ch = 54.1 g/m3
Cc = 10.2 g/m3
position determined by dissection
error band based on ± 5% RH
CONCENTRATION (g/m3)
50
45
40
35
30
25
20
15
10
0
.1
.2
.3
.4
.5
.6
.7
.8
.9
1
Z

FIG 26

It is not clear whether the error in figures 25 and 26 is caused by dissecting the sample or by deviations from a linear profile. Since the discrepancy is relatively small, it is reasonable to assume that the temperature profile is linear and to determine the probe position accordingly. Note that the deviation from linearity in the concentration profile is much higher than in the temperature profile. This suggests that the humidity transducers are a less accurate measuring device than the thermocouples.

This experiment was conducted a second time. However in Run 2 the test section had been wet initially. The aim of the second run was to verify that that humidity sensors would return to their calibration curves after being subjected to liquid water. Approximately ten hours after the probes indicated that the section had dried completely and had reached steady-state conditions, the same procedure as in Run 1 was used for determining temperature and concentration profiles. The humidities in both reservoirs in this case were less than those in Run 1. Figures 27 and 28 show the temperature and concentration profiles for this case and table 5 presents the data.

Figures 27 and 28 indicate that although the thermocouples are unaffected by exposure to liquid water, the humidity sensors do not return to their original calibration curves. After a ten hour exposure to a dessicant environment, it was observed that the probes would

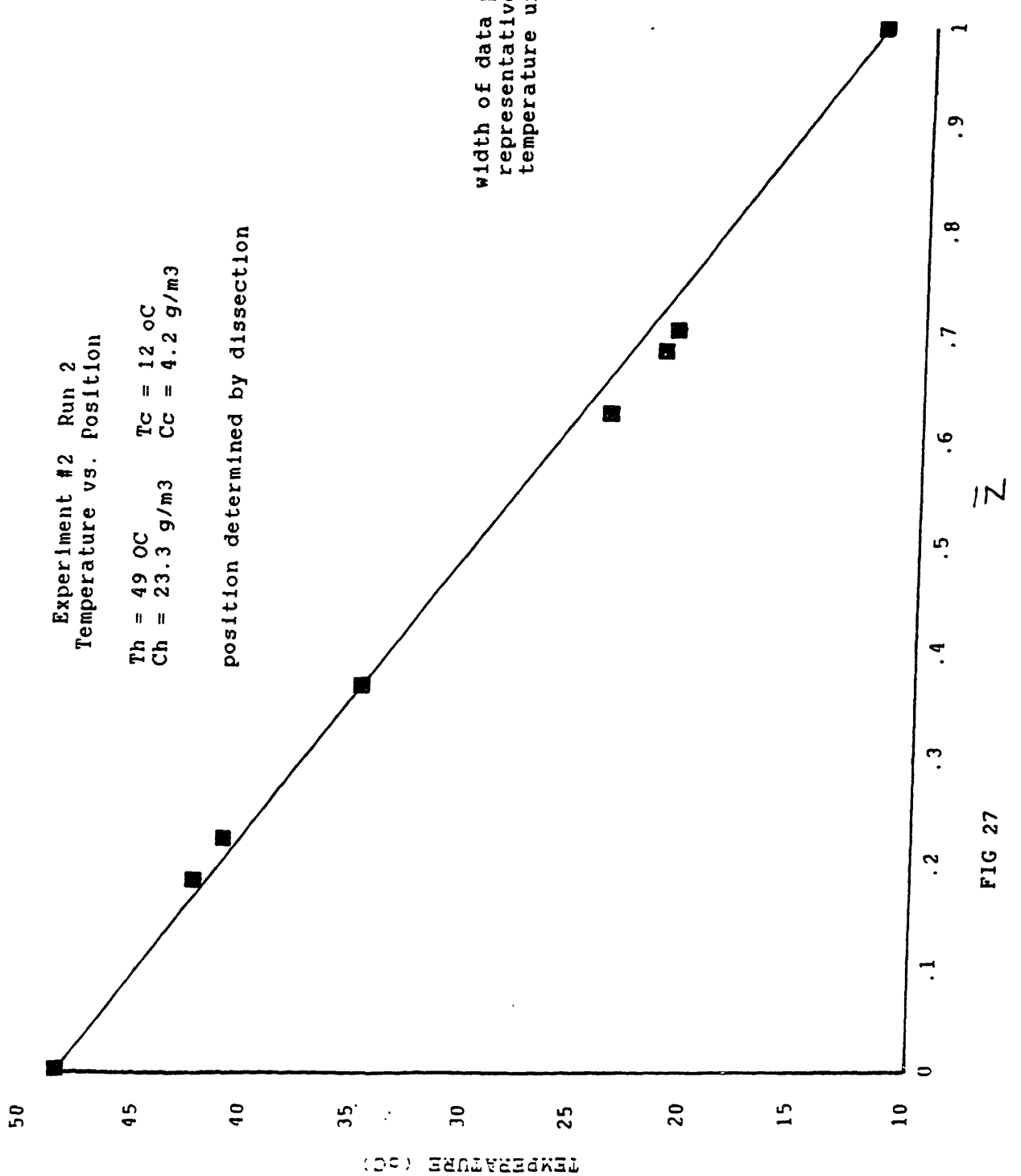
Experiment #2 Run 2
Temperature vs. Position
Th = 49 OC Tc = 12 oC
Ch = 23.3 g/m3 Cc = 4.2 g/m3
position determined by dissection
width of data point is
representative of
temperature uncertainty
TEMPERATURE (oC)
50
45
40
35
30
25
20
15
10
0
.1
.2
.3
.4
.5
.6
.7
.8
.9
1
Z

FIG 27

Experiment #2 Run 2
Concentration vs. Position

Th = 49 OC Tc = 12 oC
Ch = 23.3 g/m3 Cc = 4.2 g/m3

position determined by dissection

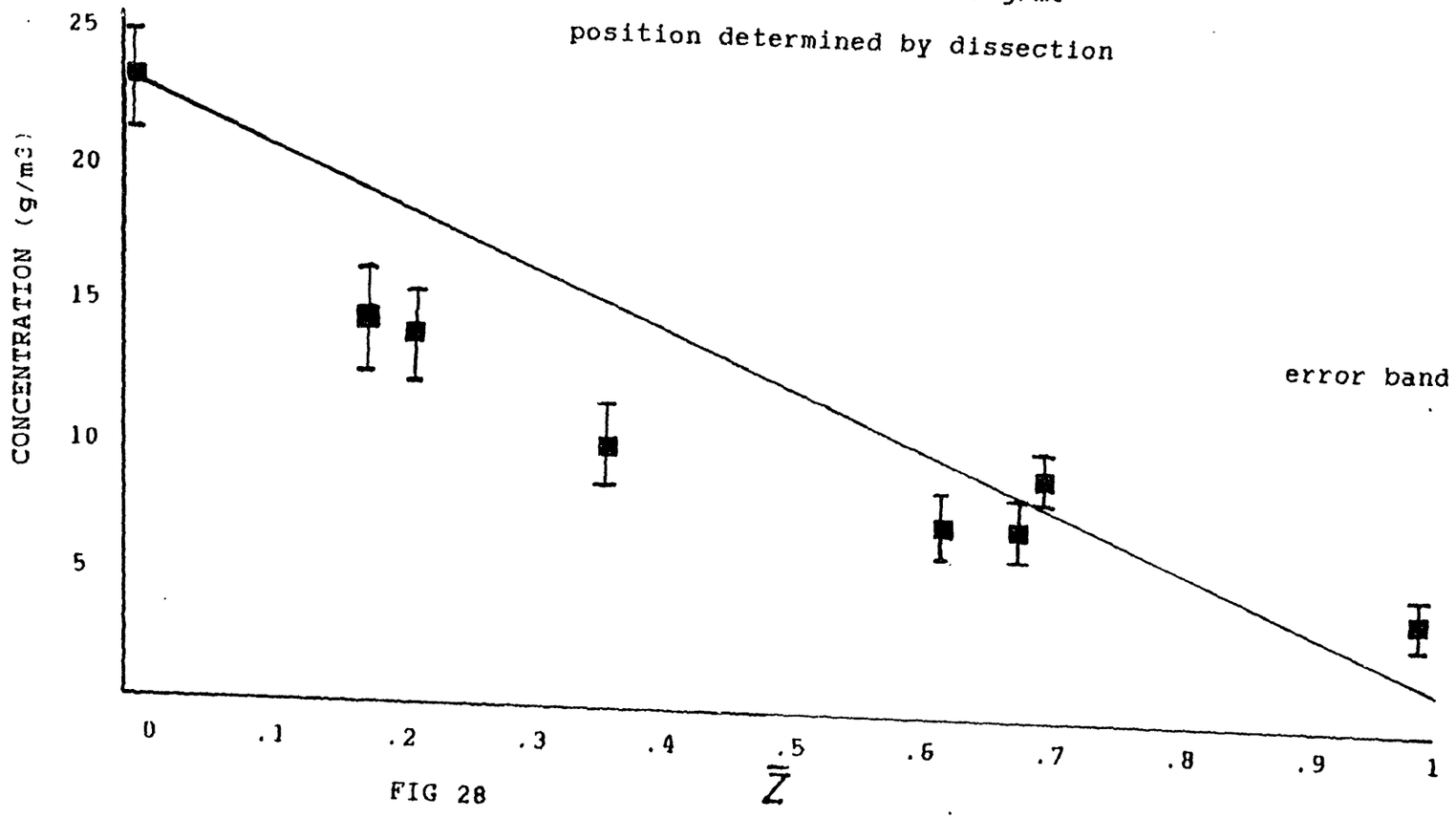

error band based on ±5% RH

FIG 28

return to their calibration curves. This demonstrates a major problem in measuring the vapor concentration profile in a test section with condensation, since it is impossible to extract the probes to expose them to dessicant while an experiment is being run This problem is discussed in section 6.

The results of Experiment 2 showed that the probe position can be accurately determined by assuming a linear temperature profile in a dry specimen. This method of determining probe position is employed in the following experiments. Unfortunately the humidity sensor readings are unreliable after the sensors have been exposed to condensate.

TABLE 5
Experiment 2
Data for Run 2

Probe	Temp(^{o}C)	C(g/m^2)	$x_{measured}$	$\bar{x}_{calc}$
1	49	23.3 ± 5%	0 ± .05	0 ± .05
2	43	14.5	0.18	0.17
3	41	14.0	0.22	0.20
4	35	10.0	0.37	0.37
5	24	7.3	0.63	0.67
6	22	7.3	0.69	0.74
7	21	9.1	0.71	0.75
8	12	4.2	1.0	1.0

4.4 Experiment 3

Heat and Mass Transport Through Porous Media With a Vapor Barrier

In this experiment a test section with an initial liquid content was placed in the hot box / cold box apparatus with a vapor barrier between the cold side of the specimen and the cold box reservoir. The hot box was maintained at approximately 46.5 ^{o}C, 35 % relative humidity, and the cold box temperature was 17 ^{o}C. As discussed in section 3, the effect of the vapor barrier on the cold side of the test section should be to move the condensate towards the vapor barrier. Experiment 3 was conducted to examine this theory and to compare the temperature profile data with the quasi-steady model prediction.

4.4.1 Initial Liquid Content

The initial liquid content was introduced into the test section by submerging the test section in a water bath. An identical control section, cut from the same board of fiberglass as the test section, was also placed in the bath. In this experiment the test section and the control section were completely submerged in water for six hours. The samples were then set to drip dry in the horizontal position at room temperature for 24 hours.

The control section was cut into halves and each half was sliced into four specimens as illustrated in figure 29. The

wet and dry weights of each specimen are presented in Table 6. The parameter θ in table 6 is the ratio of liquid volume to air volume in the specimen. θ is determined by the following equation:

$$\theta = \frac{\text{wet weight - dry weight}}{\rho_w \quad \epsilon \quad \text{Volume}}$$

The average value of θ for each region was used in the simulation. The distribution of the average values and the data for θ are plotted in figure 30. The amount of liquid in the region closest to the hot side is extremely large and thus would be expected to move via liquid diffusion and possibly gravity. However the model assumes that the condensate is immobile.

TABLE 6
Experiment 3
Initial Liquid Content Data

Region	Specimen	Wet Wt.	Dry Wt.	Volume	θ	θ_{ave}
0<x<.25	11	42.2g	2.7g	69 cm^3	.78	
	12	83.7	3.8	103	.80	.79
.25<x<.5	21	9.5	2.6	69	.10	
	22	18.1	3.1	103	.15	.13
.5<x<.75	31	2.6	2.5	69	.0014	
	32	3.7	3.5	103	.0020	.0017
.75<x<1	41	2.9	2.5	69	.006	
	42	4.8	4.2	103	.006	.006

CONTROL SECTION

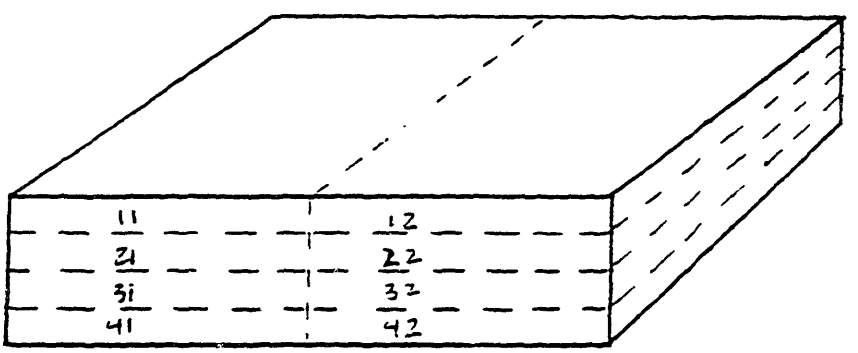

SPECIMENS

FIG 29

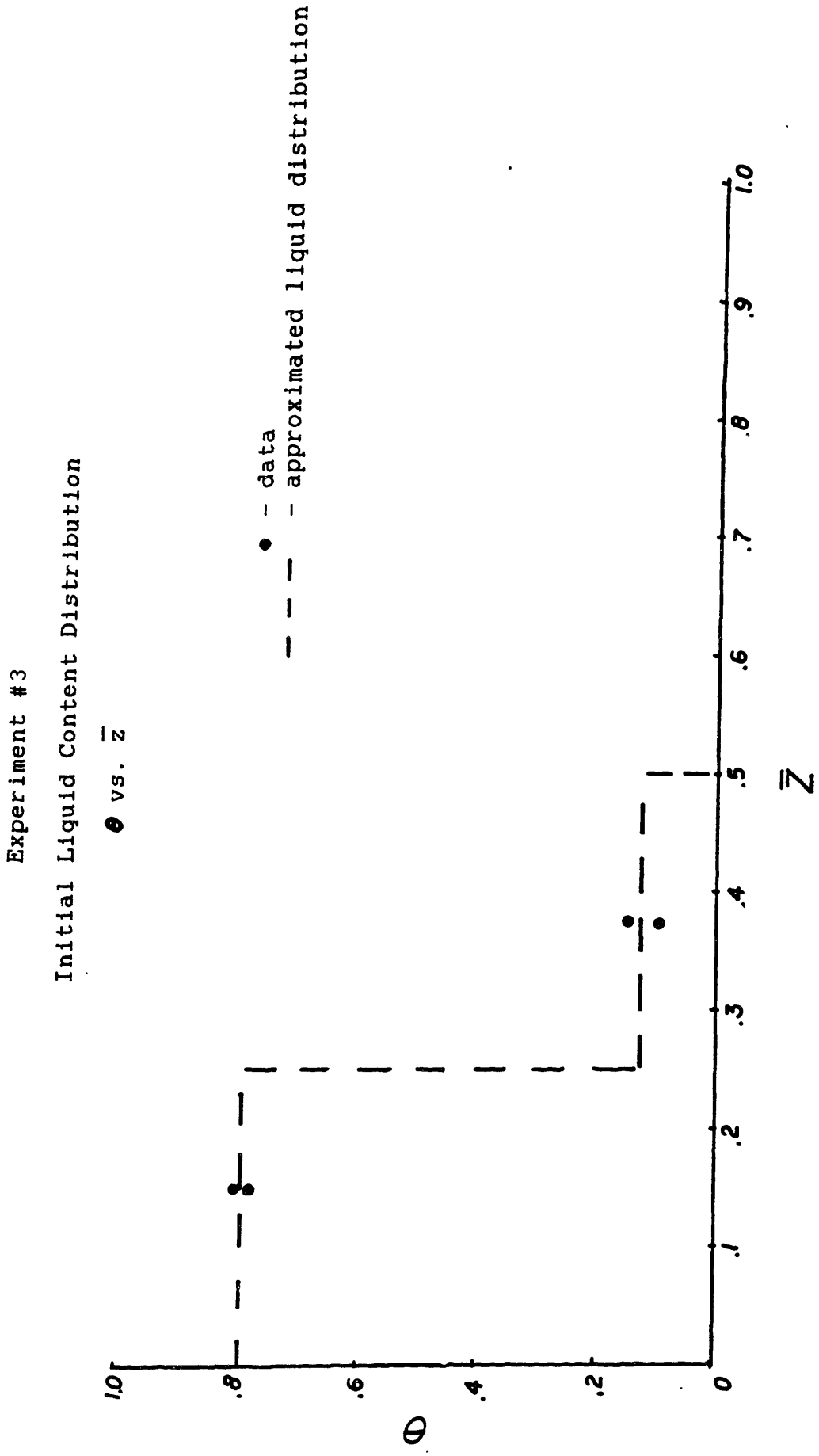
Experiment #3
Initial Liquid Content Distribution
θ vs. z̄
● - data
– – – - approximated liquid distribution
θ
z̄
0
.2
.4
.6
.8
1.0
.1
.3
.5
.7
.9

FIG 30

4.4.2 Comparison of Data and Theory

The temperature data in Table 7 indicate that steady-state conditions in the hot and cold reservoirs (probes 1 and 8 respectively) are reached in approximately three hours (10500 secs). Figures 31 and 33 are plots of the temperature profiles at 23000 and 100000 seconds after the test section was inserted into the apparatus. Figure 32 is a plot of the deviation between data and theory as a function of position. The temperature profile predicted by the quasi-steady model is indicated by the line in the figures, and the data are represented by the points. In the quasi-steady model, the solution to the temperature profile in the wet zone is based on eq. (11), while the wet zone boundary motion is governed by eq. (14). Figure 33 presents the deviation between data and theory for the temperature profile at 100,000 seconds. It is apparent that there is much better agreement between the data and the model at the hot side of the section than at the cold side. This is because the high liquid contents at the vapor barrier induce liquid motion, which the model does not take into account. Both the model and data indicate an abrupt change in the temperature gradient near the hot side of the section. The location of this change corresponds to the wet zone boundary according the the quasi-steady model. The data support the model's prediction of the wet zone boundary location.

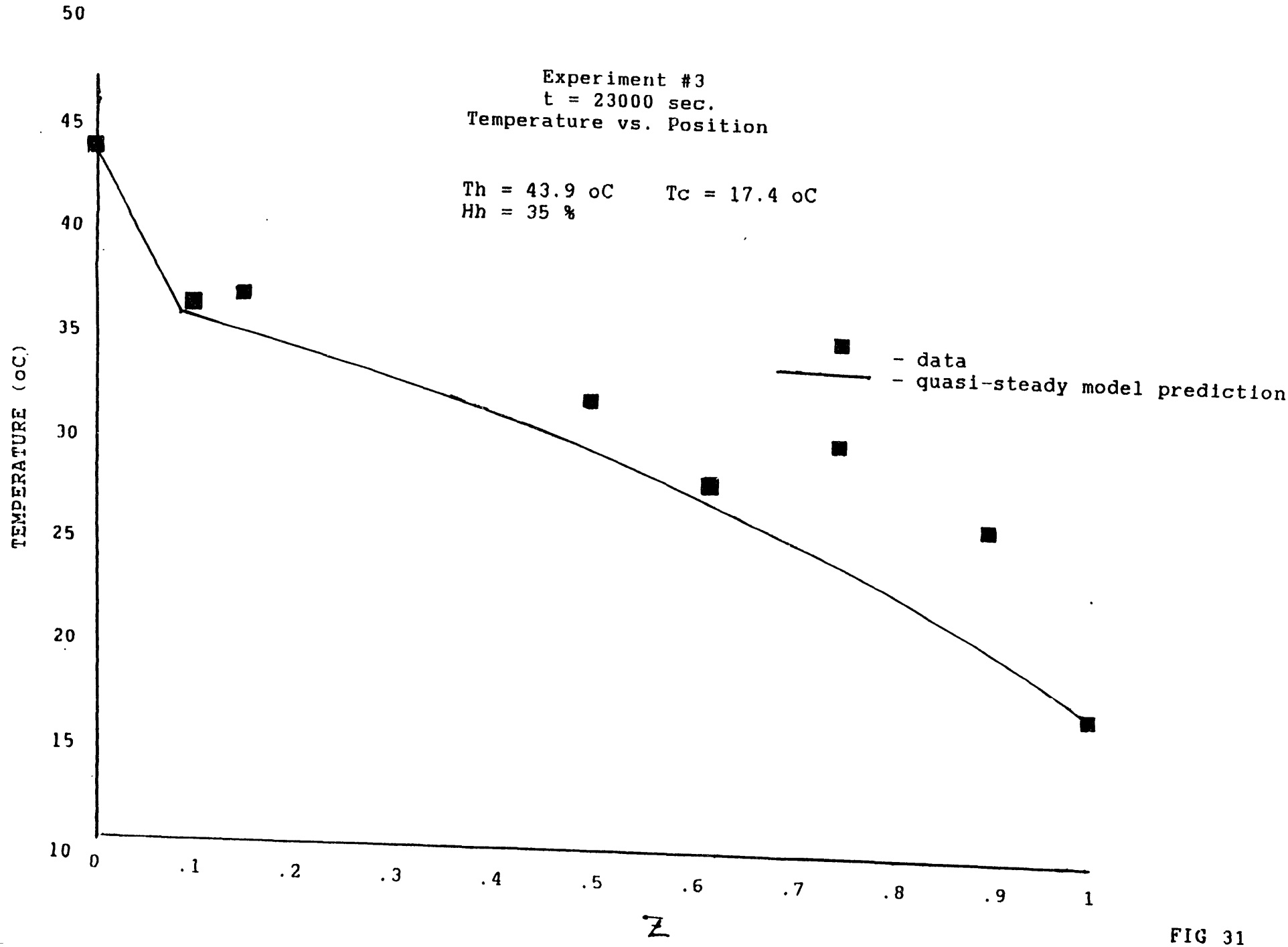
Experiment #3
t = 23000 sec.
Temperature vs. Position
Th = 43.9 oC
Hh = 35 %
Tc = 17.4 oC
- data
- quasi-steady model prediction
TEMPERATURE (oC)
50
45
40
35
30
25
20
15
10
0
.1
.2
.3
.4
.5
.6
.7
.8
.9
1
Z

FIG 31

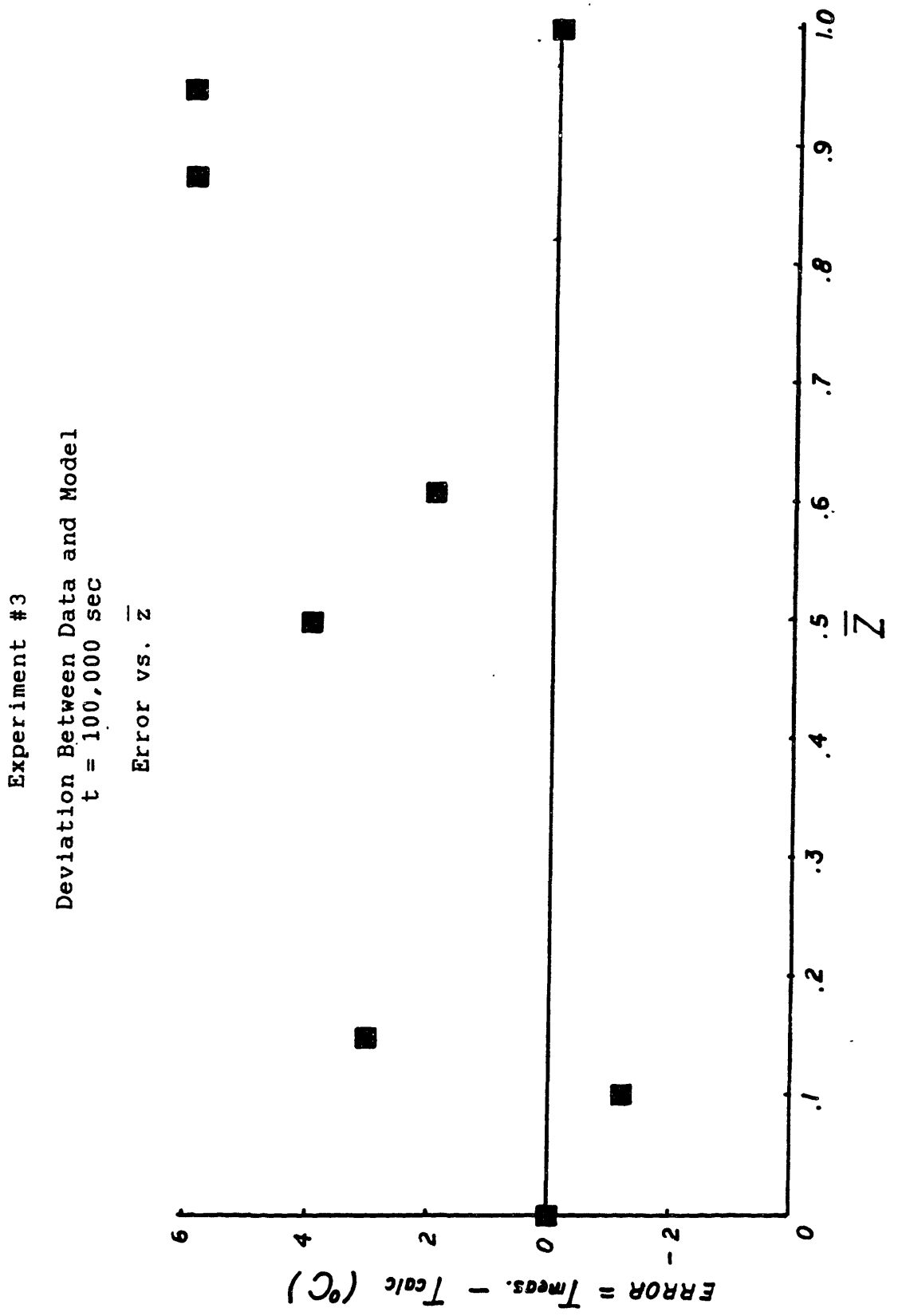
Experiment #3
Deviation Between Data and Model
t = 100,000 sec
Error vs. $\bar{z}$
ERROR = $T_{meas.} - T_{calc}$ (°C)
6
4
2
0
-2
0
.1
.2
.3
.4
.5
.6
.7
.8
.9
1.0
$\bar{Z}$

FIG 32

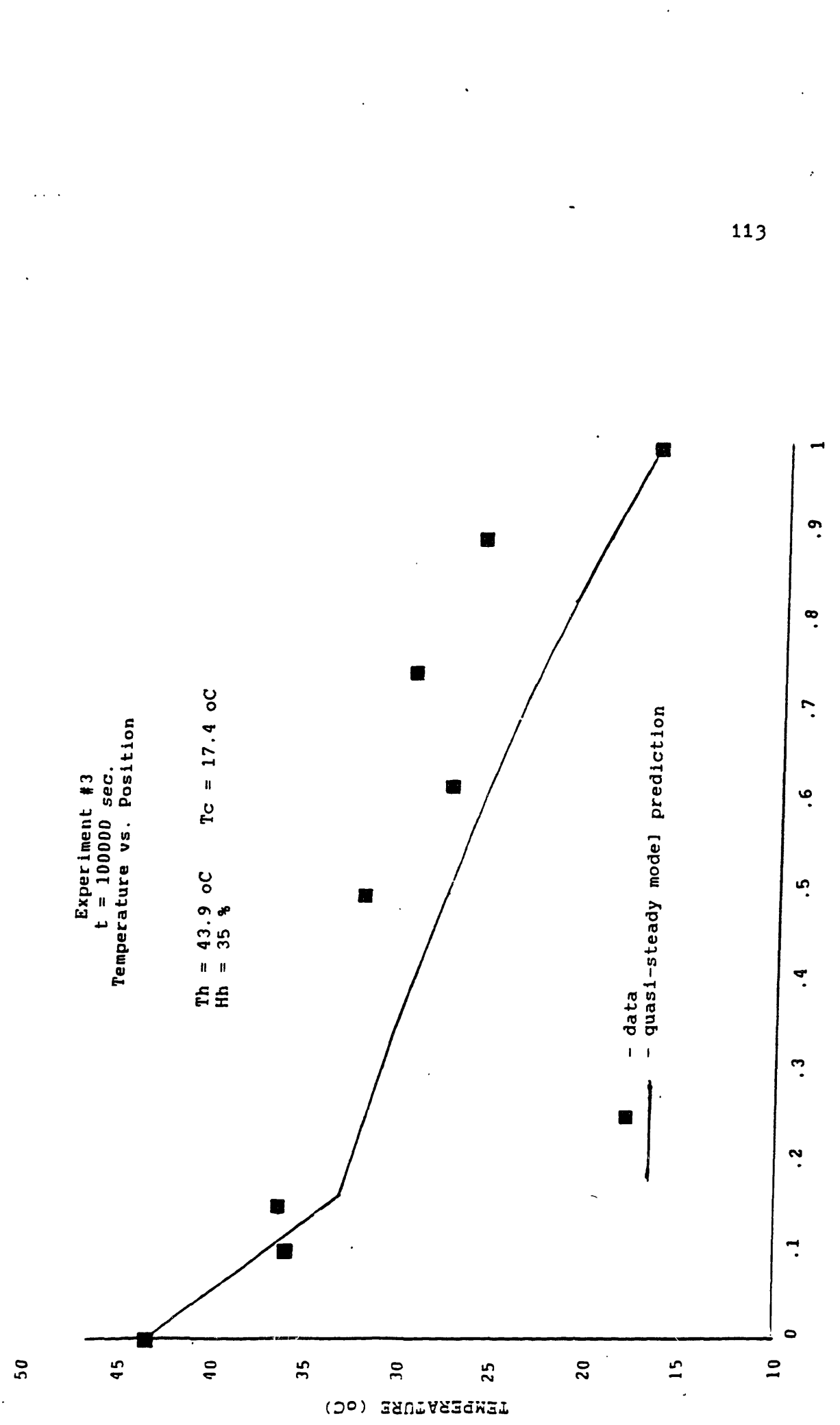
Experiment #3
t = 100000 sec.
Temperature vs. Position
Th = 43.9 oC
Hh = 35 %
Tc = 17.4 oC
- data
- quasi-steady model prediction
TEMPERATURE (oC)
Z
50
45
40
35
30
25
20
15
10
0
.1
.2
.3
.4
.5
.6
.7
.8
.9
1

FIG 33

At the discontinuity in temperature gradient near the hot side, the data indicate that there is a local minimum temperature. This is not expected by the quasi-steady theory. It has been shown in section 2.2 (eq. (11)) that in any one dimensional wet zone, the temperature gradient is always negative as long as the parameter λ is positive. Thus it can be argued that this minimum temperature in the slab cannot be explained simply by variations in physical properites, such as conductivity and diffusivity, due to the prensence of liquid. Rather this local minimum temperature must be due to a two-dimensional moisture distribution. Perhaps there is moisture in the region between probe 3 and the hot side that is actually dry for probe 2. Under close examination of the insulation, patches of encrusted glass fibers are observed that could explain how moisture gets trapped in isolated sites. If there were such a patch of insulation located between probe 3 and the hot side, the water on the cold side of the patch would not be able to diffuse towards the hot box. This moisture would increase the thermal conductivity between the hot side and probe 3, and would explain the higher temperature measured at probe 3.

TABLE 7

Experiment 3
Temperature (^{o}C) Data

probe	1	2	3	4	5	6	7	8
time (sec)	$\bar{z}$ = 0.0	.10	.15	.50	.62	.75	.90	1.0
4700	37.0	29.2	30.2	28.7	27.3	26.1	25.3	22.6
10500	39.1	32.2	32.8	29.5	27.6	25.6	24.7	18.0
15200	39.7	32.6	33.1	29.3	27.2	25.2	24.3	15.6
20000	40.1	32.8	33.4	29.3	27.2	25.0	24.1	16.0
23000	40.3	33.0	33.6	29.4	27.2	25.0	24.0	17.3
90000	43.9	36.5	37.1	32.4	30.1	27.9	26.5	17.4
100000	43.9	36.6	37.1	32.5	30.2	28.1	26.7	17.6

The anomolous data near the cold side may be explained by the development of isolated regions of condensate near the vapor barrier. The photograph shows a typical wet patch that was observed in a similar experiment. Though the mechanism for producing these patches of condensate is not obvious, it may be attributed to irregularities in both the fiberglass and the vapor barrier / fiberglass interface, and the surface tension of the condensate. These patches have been observed in cases of high liquid content, which would be expected at the vapor barrier (see figure 20, section 2.5).

If the temperatures at these anomolous points near the cold side are attributed to an irregular liquid distribution, it is clear that the model will fail to predict these data.

Another possible reason for the elevated temperatures near the cold side is the formation of a somewhat impermeable layer of condensate near the vapor barrier. The theory expects there to be a high liquid content level near the vapor barrier. If this is the case, it may be that the vapor that would have been expected to diffuse to the vpaor barrier cannot permeate the high liquid content layer, and thus condenses within the slab. Given this scenario, the released latent heat would have to be conducted out of the slab, and hence the temperatures near the cold side would be elevated.

Ignoring the data closest to the cold side, there appears to be excellent agreement between the quasi-steady model and the data. Table 8 shows the normalized heat fluxes entering and leaving the slab at the times corresponding to the profiles given in figures 31 and 32. In this table the data closest to the cold side are ignored.

There is excellent agreement between data and theory on the overall heat transfer entering and leaving the slab. However it must be noted that the model is not valid in the region of high liquid content that may occur at the vapor barrier, because this liquid is prone to diffusion and gravity as well as irregular distribution. Though the quasi-

steady model predicts the approximate location of the wet / dry interface, a small discrepancy in wet zone boundary location will yield a large deviation in predicted temperatures closer to the cold side. This high sensitivity of temperature profile on wet zone boundary location can also explain the relatively large deviations between theory and data near the cold side. Since there is good agreement on the general shape of the temperature profile in the wet zone, the error in the model lies in its method for determining wet zone boundary movement. This may be attributed to its assumption of immobile condensate.

After approximately 30 hours the test section was removed from the apparatus and dissected to determine the shape of the final moisture distribution. These data are given in table 9. A plot of the final liquid distribution with the prediction of the quasi-steady model is given in figure 34.

TABLE 8
Heat Fluxes Entering and Leaving Test Section

time (sec)	$\bar{Q}_{in}$ measured	$\bar{Q}_{in}$ theory	$\bar{Q}_{out}$ measured	$\bar{Q}_{out}$ theory	$\bar{Q}_{in} / \bar{Q}_{out}$ measured	$\bar{Q}_{in} / \bar{Q}_{out}$ theory
23 000	2.96	3.36	1.07	1.17	2.8	3.0
100 000	2.83	2.72	1.04	0.98	2.7	2.8

note: 1) $\bar{Q} = Q / Q_{dry\ sample}$
2) data of probe 6 & 7 neglected

TABLE 9
Final Liquid Distribution

Region	θ_{ave}
$0 < \bar{x} < .25$	.047
$.25 < \bar{x} < .50$	.022
$.50 < \bar{x} < .75$	.034
$.75 < \bar{x} < 1.0$	.214

Experiment #3

Final Liquid Content Distribution
experimental and theorectical

θ_{ave} vs. $\bar{z}$

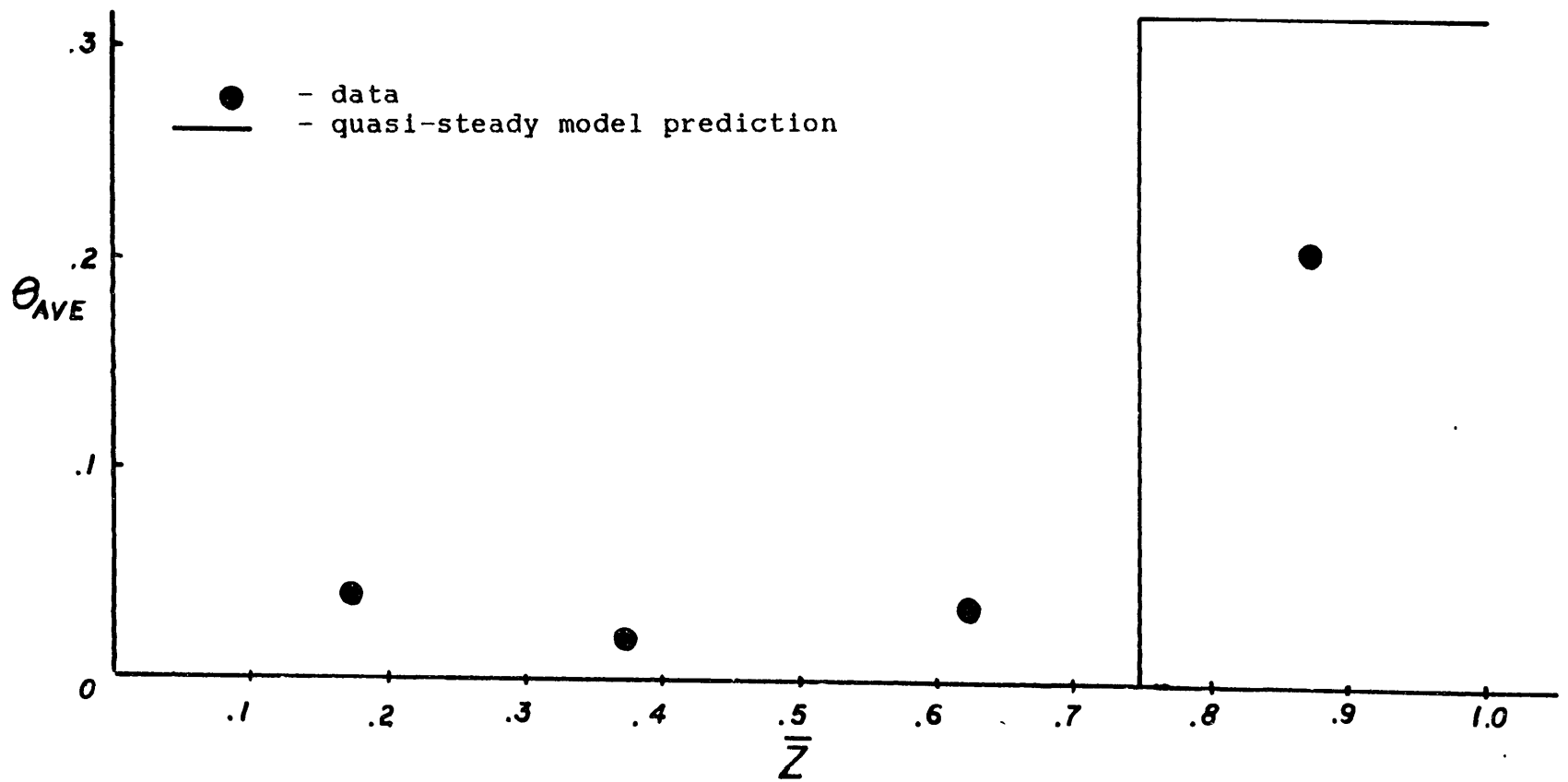

FIG 34

As expected from the analysis in section 2.5 the majority of the condensate in the sample was found in the region closest to the vapor barrier. Recall that the initial liquid content was concentrated on the hot side. The final liquid distribution data indicate that the quasi-steady model does a good job of predicting the movement of moisture in fiberglass insulation

4.5. Experiment 4
Drying of a Wet Sample of Insulation

In this experiment a test section of fiberglass with an initial liquid distribution was subjected to boundary conditions that caused the water to evaporate completely over a period of approximately 10 hours. The temperature profile data were recorded and compared to the quasi-steady model developed in section 2.

4.5.1 Initial Liquid Content

An initial liquid content was introduced into the test section by partial submersion in a water bath as in experiment 3. The depth of the water bath was approximately one third of the thickness of the section, providing distinct regions of wet and dry conditions. An identical control section from the same piece of insulation, was also placed in the bath. After five hours, both the test section and the control section were removed from the bath and placed on a rack to drip dry in a horizontal position for twelve hours. By carefully examining the control section, it was determined that the penetration depth of the liquid was nearly uniform. Visual inspection also indicated that the liquid was distributed evenly in the wet zone. This observation combined with the difficulty in actually

measuring the liquid content profile led to the approximation that the liquid was uniformly distibuted in the two centimeter section that was apparently wet. Subsequent measurements of the weights of various control specimens from the apparent dry region confirmed that the moisture content was negligible.

The control sample was cut into several pieces which were weighed wet. After drying each piece, the initial liquid content was determined by subtracting the dry weight of each specimen from its corresponding wet weight. The parameter θ was calculated be the formula given in section 4.3. Table 10 presents the data for the initial liquid content. This liquid distribution is plotted in figure 35.

TABLE 10

Experiment 4
Initial Liquid Content Data

Specimen	Wet Wt	Dry Wt	Volume	θ
1	15.0 g	5.5 g	199.5 cm^3	.049
2	10.3	3.9	124.6	.053
3	10.7	4.2	127.5	.053
4	6.9	3.0	87.1	.046

$\theta_{ave} = .050$

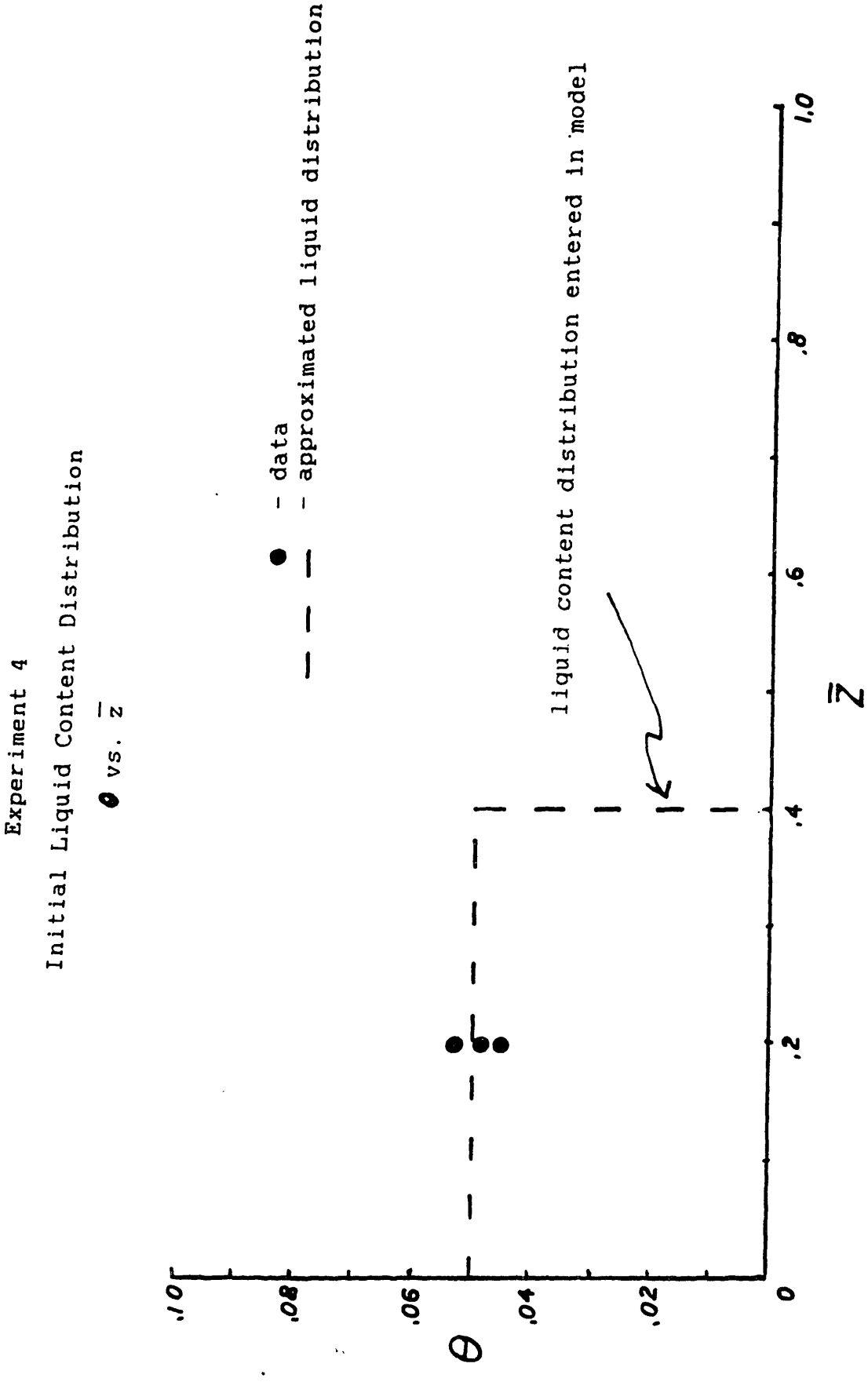
Experiment 4
Initial Liquid Content Distribution
θ vs. z̄
● - data
— — — - approximated liquid distribution
liquid content distribution entered in model
θ
z̄
.10
.08
.06
.04
.02
0
.2
.4
.6
.8
1.0

FIG 35

4.5.2 Experimental Conditions

Following the drip drying period the test section was inserted into the hot box / cold box apparatus. The steady-state conditions in the hot box were maintained at 43 ± 2 ^{o}C and .34 ± .04 relative humidity. The cold box temperature was 9.5 ± 2 ^{o}C and the humidity was .90 ± .04.

The high humidity in the cold box resulted from vapor diffusing into the cold reservoir faster than it could be removed by the salt solution method of humidity regulation. This high humidity on the cold side of the sample was not desirable since this experiment was examining the drying process. This humidity control problem is addressed in section 6.

The wet side of the test section was placed adjacent to to the hot reservoir. The low relative humidity in the hot box caused the liquid to evaporate and diffuse towards both reservoirs. Temperature data were collected at eight points in the slab approximately every fifteen minutes for ten hours.

4.5.3 Comparison of Data and Theory

The resulting temperature data of probes 1 and 8 indicate that steady-state conditions in the hot and cold boxes were reached in approximately three hours (Table 11). Typical

temperature profiles are shown in figures 36 and 37 at 20,000 and 30,0000 seconds after insertion of the test section into the apparatus. The line on the figures gives the temperature profile predicted by the quasi-steady model.

The deviation between data and theory at 20,0000 seconds is shown on figure 38. Though the temperature data generally do not coincide with the theoretical prediction, it appears that both the data and theory agree on the effect of evaporating condensate on the heat transfer in a wet section of porous insulation. The measured heat fluxes, as calculated from the temperature gradient at the egdes at times of 20,000 and 30,000 seconds, and the predicted heat fluxes are compared in Table 12. Throughout the simulation the quasi-steady model overpredicts the rate of movement of the wet zone towards the cold side. As in experiment 3, the data and theory agree on the general shape of the temperature profile in the wet zone. However the high sensitivity of the absolute temperature profile on wet zone boundary position causes significant deviation between data and theory. Among the reasons for the discrepancy between data and theory, the most important appears to be the assumption that the condensate is immobile. It was shown in section 2 that the effect of mobile condensate in general is to spread out the wet zone. In this experiment the potential for mobile condensate is enhanced by the force of gravity pulling the condensate towards the hot side of the test section. Therefore it is plausible that the reason

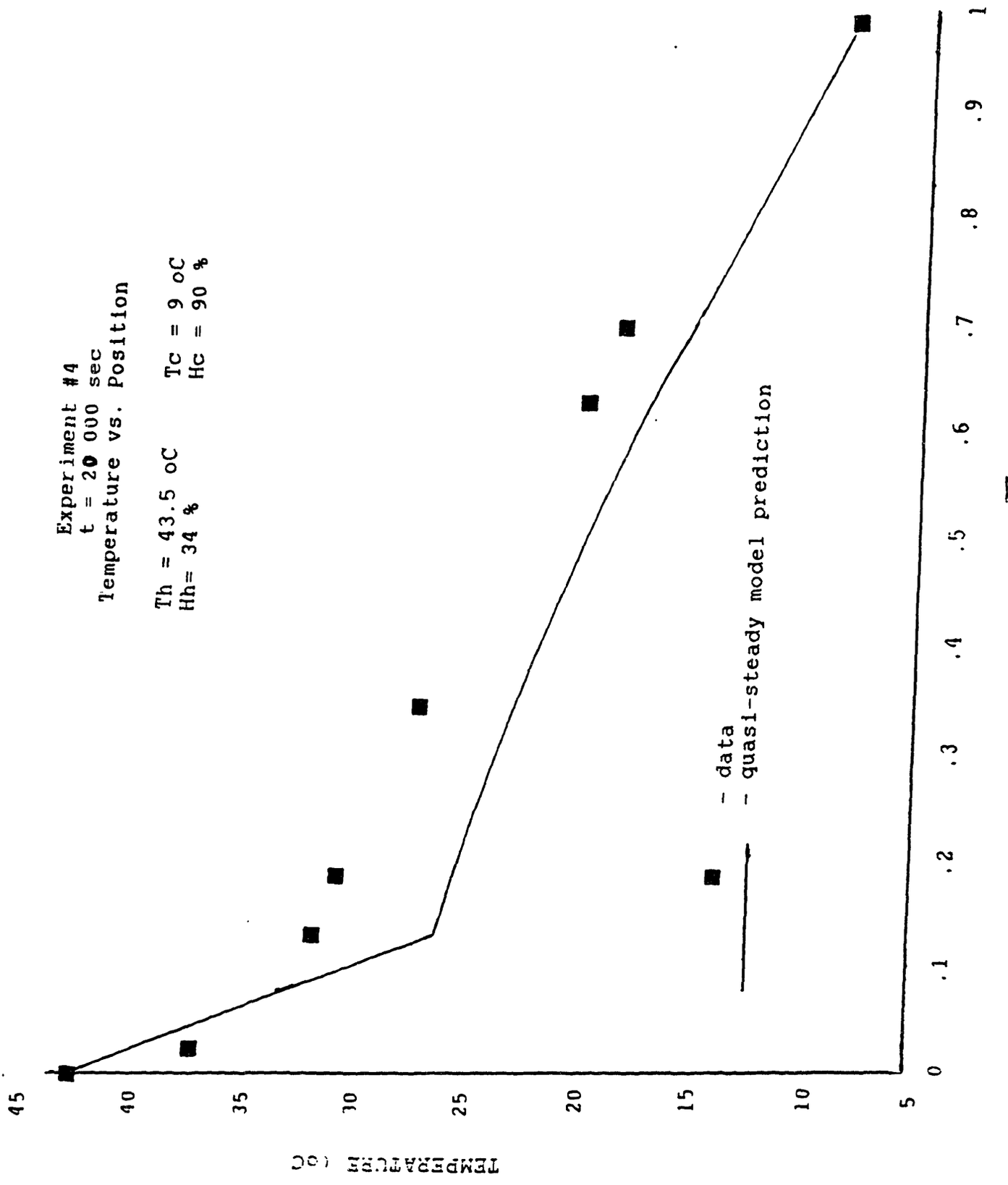
Experiment #4
t = 20 000 sec
Temperature vs. Position
Th = 43.5 oC
Hh= 34 %
Tc = 9 oC
Hc = 90 %
- data
- quasi-steady model prediction
TEMPERATURE (oC
45
40
35
30
25
20
15
10
5
0
.1
.2
.3
.4
.5
.6
.7
.8
.9
1
Z

FIG 36

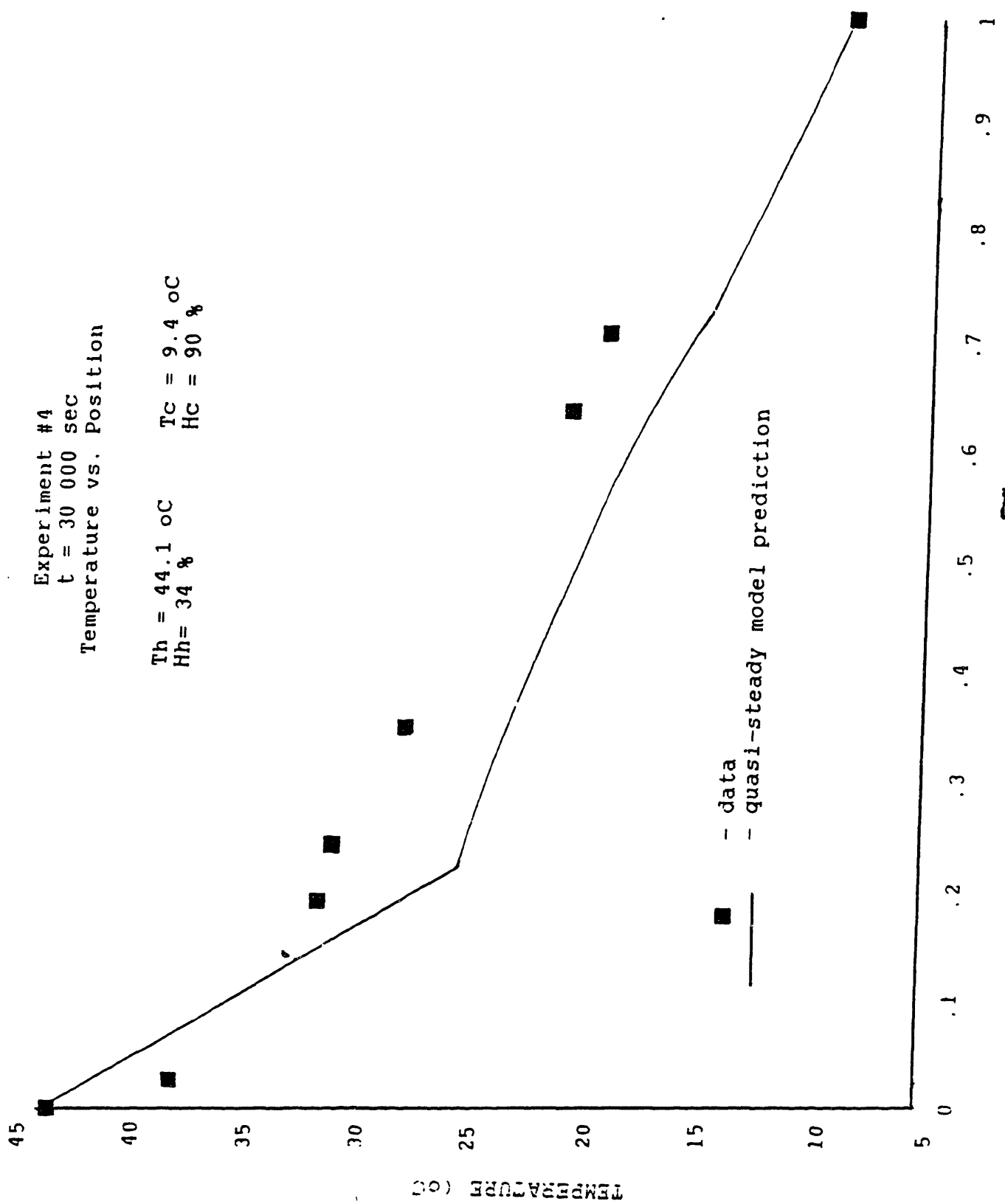
Experiment #4
t = 30 000 sec
Temperature vs. Position
Th = 44.1 oC
Hh= 34 %
Tc = 9.4 oC
Hc = 90 %
- data
- quasi-steady model prediction
TEMPERATURE (oC)
Z
45
40
35
30
25
20
15
10
5
0
.1
.2
.3
.4
.5
.6
.7
.8
.9
1

FIG 37

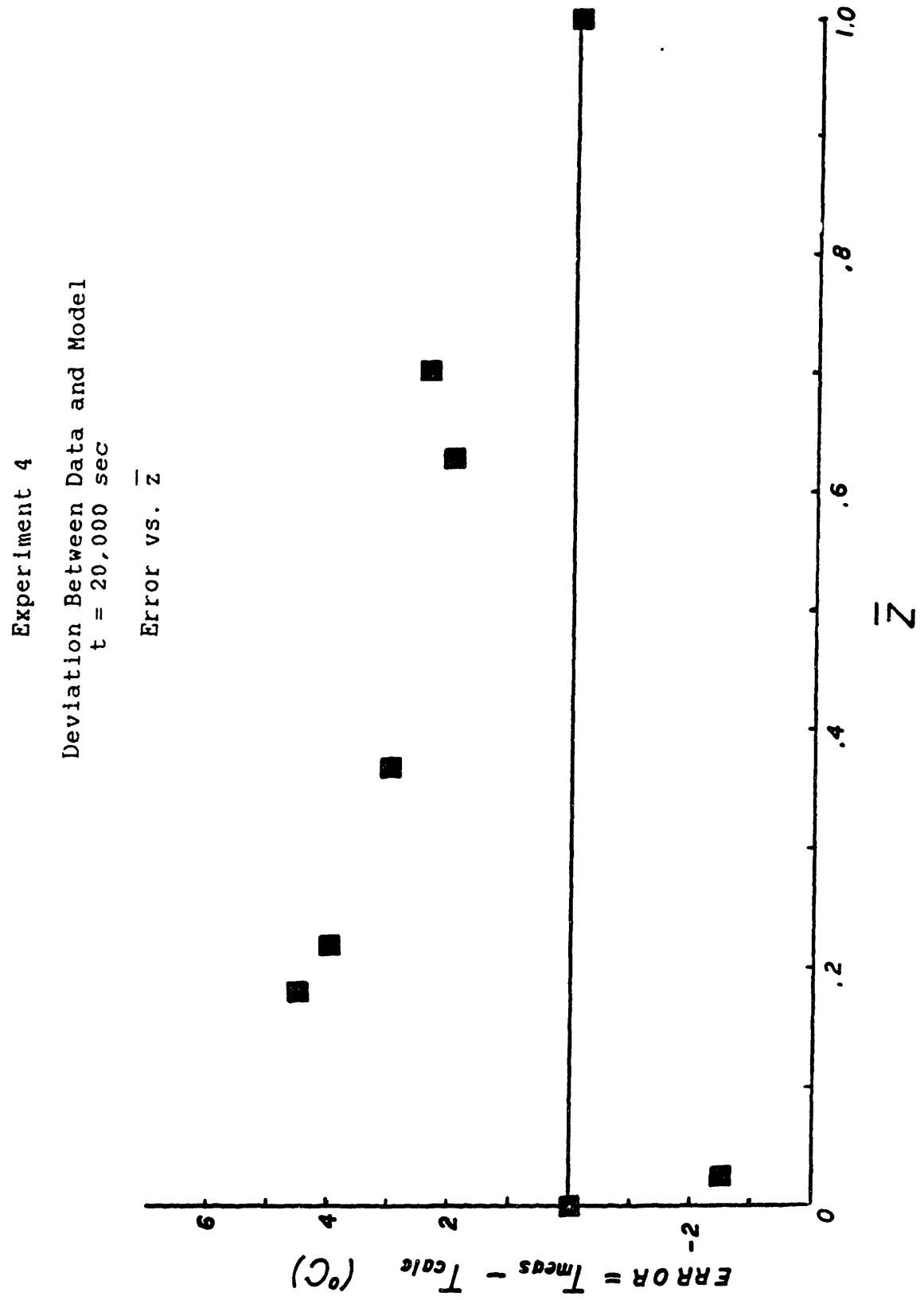
Experiment 4
Deviation Between Data and Model
t = 20,000 sec
Error vs. $\bar{z}$
ERROR = $T_{meas} - T_{calc}$ (°C)
6
4
2
-2
0
.2
.4
.6
.8
1.0
$\bar{z}$

FIG 38

for the model predicting a faster migration of the wet zone towards the cold side is the immobile condensate assumption inherent in the present model.

Overall both the data and the theory indicate a significant variation between the heat entering the slab and the heat leaving. The net accumulation of energy in the section is responsible for the evaporation of the liquid.

The results show that the effective insulating value of a section of a wet porous medium if viewed from the hot side, is greatly reduced by the evaporation of the liquid, even if the actual conductivity of the medium is assumed to be unaffected by liquid content. However, the insulating value of the same medium with respect to the cold reservoir is actually improved. This phenomenon is caused by the evaporative cooling within the insulation that increases the temperature gradient near the hot side and reduces the gradient at the cold side.

The implications of this experiment indicate that care must be exercised when evaluating the heat transfer behavior of damp insulation. The insulating value of the insulation will be very different when determined from both the hot side of the sample and the cold side.

TABLE 11

Experiment 4
Temperature Data

Probe		1	2	3	4	5	6	7	8
time (sec)	$\bar{z}$ =	0	.025	.18	.22	.37	.63	.71	1.0
5000		40.9	35.2	30.5	29.8	27.3	22.8	22.7	13.8
10000		41.9	36.2	31.4	30.6	27.6	21.8	21.5	10.4
15000		42.3	36.6	31.5	30.6	27.0	20.5	20.3	8.9
20000		43.0	37.3	32.0	31.2	27.4	20.5	20.1	8.5
25000		43.5	37.9	32.4	31.6	27.9	20.9	20.4	8.9
30000		44.1	38.4	32.9	32.1	28.5	21.5	20.9	9.4
35000		44.6	38.9	33.2	32.2	28.6	21.7	21.2	9.8
40000		45.6	42.8	35.9	32.8	27.9	21.6	21.3	10.3

TABLE 12

Experiment 4
Comparison of Measured and Predicted
Heat Fluxes

time (sec)	$\bar{Q}_{in}$		$\bar{Q}_{out}$		$\bar{Q}_{in} / \bar{Q}_{out}$	
	measured	theory	measured	theory	measured	theory
20 000	6.6	4.11	1.16	.77	5.7	5.3
30 000	6.6	2.68	1.14	.57	5.8	4.7

note:1) $\bar{Q} = Q / Q_{\text{dry sample}}$

5. Conclusions and Summary

The experiments by Thomas et al and those presented in Chapter 4 have verified that the process of simultaneous heat and mass transfer in porous media, as it is applied to roof insulation, can be simulated using the quasi-steady model developed in chapter 2. Experimental data have shown that the quasi-steady model can accurately predict transient temperature profiles, heat transfer rates, and moisture movement through insulation for cases in which the assumptions inherent in the model are valid. These assumptions include immobile liquid, and constant properties such as thermal conductivity and mass diffusivity.

For the case of horizontal fiberglass insulation these assumptions are appropriate in general. It has been shown [3] that the condensate in horizontal fiberglass insulation remains immobile at liquid content levels up to approximately 70 % by volume. The comparison of the quasi-steady model and the Thomas model has shown that the effects of property variations due to liquid levels in practical cases of interest, is negligible.

When examining simultaneous heat and mass transfer through porous media other than horizontal fibergalss, the validity of these assumptions must be determined on an individual basis. For example, Motakef [3] has determined that for vertically oriented fiberglass, mobility of liquid begins at a liquid content level of 5%, which is cosiderably less than

the 70% critical liquid content level for horizontal fiberglass.

In cases in which the assumptions of the quasi-steady model are not valid a different model must be used. If it were determined that the variations in properties due to liquid content are significant, a numerical approach, such as the finite difference algorithm developed in chapter 2 would be required. Since the algorithm presented in this work proved to be too slow for practical problems, it would have to be amended. The required changes would involve an implicit numerical technique and a coarser spatial grid.

If it were determined that liquid mobility would b a significant factor, the present quasi-steady model must be amended to incorporate a model for liquid diffusion.

It is possible improve the quasi-steady model by accounting for liquid mobility. However such improvements will not account for the two-dimensional behavior of condensate and the irregularities of the insulating medium that were observed in experiments 3 and 4 in chapter 4.

In spite of two-dimensional affects, the experiments in Chapter 4 demonstrate the ability of the model to predict the predominant trends of heat and moisture transfer in fiberglass insulation. The differences in heat fluxes entering and leaving the insulation in the presence of a wet region were accurately predicted in experiments 3 and 4. The model also predicted the motion of the wet zone which is essential when determining what environmental conditions

will cause a wet insulation sample to dry out. The results of experiments 3 and 4 indicate that the quasi-steady model can be expected to predict the transient moisture distribution to within 25 % and heat fluxes to within 15%.

In short, the present work offers a relatively simple model that can predict the transient behavior of heat and liquid transfer through insulation. The next step in formulating a model of a roofing system is to account for its composite structure. This should amount to cascading several slabs together, each characterized by a thermal conductivity, vapor diffusivity and liquid water diffusivity. The treatment of vapor barriers described in chapter 3 will also be applied to the composite roof.

6. Experimental Problems and Suggested Revisions

Several difficulties were encountered in the preceeding experiments that inhibited the full utilization of the hot box / cold box apparatus. Foremost is the prblem of measuring humidity. This difficulty was demonstrated in experiment 2. The humidity sensors seemed to experience extensive hysteresis after coming in contact with condensate. Although the sensors could return to their calibration curves after being placed in a dessicator for several hours, the sensors would not be calibrated while within the test section. Since all of the experiments of interest in this work involve liquid water in the test section, the use of the PCRC-55 humidity transducers is severely limited.

Until suitable humidity sensors are developed, it is suggested that future experiments avoid the complication of measuring relative humidity within the sample and concentrate on accurate temperaure measurements.

Another recurring problem was that of condensate dripping from the cooling coil of the cold box onto the test section. This problem was solved temporarily by placing absorbent sponges beneath the coil to catch the condensate. However this method has the disadvantage of accumulating large amount of liquid water within the cold box. This liquid acts as a source of vapor which competes against the salt solution in controlling the humidity. This was seen in

experiment 4, where the steady-state relative humidity in the cold box could not be maintained below 90 %. It was desired to keep the cold box drier, but the technique of bubbling air through the salt solution was not effective enough.

Future use of this apparatus should therefore be preceded by the design of a condensate drain placed under the cooling coil to remove the condensate from the cold box. Additionally, a more effective technique of humidity control in both the hot and cold boxes should be designed. Much higher air flow rates through the salt solution combined with a condensate removal system should provide greater humidity control.

Greater control of the cold box temperature is also desirable. Though the circulation of the antifreeze solution through the coiling coil could bring the cold box down to 5 ^{o}C for a limited time, the steady-state temperature could not be maintained below 15 ^{o}C. A colder cold box would enable larger temperature and concentraiton gradients to be imposed on the test section. This would reduce the required accuracy of the temperature and, more importantly, the humidity sensing devices.

The limiting factor in the temperature control of the cold box was the steady-state cooling capacity of the freezer. The rate of heat rejected at the condensor could not meet the demands of the cooling load of the cold box. Some of the heat from the overworked freezer condensor was

conducted back into the interior of the freezer, in effect short circuiting the cooling loop.

There are two alternative methods for solving this problem. First, a secondary cooling loop could be fixed to the condensor of the freezer and thus improve the maximum heat rejection rate that the freezer could maintain.

Secondly, and perhaps more effective, the freezer could be replaced by a properly sized compressor and refrigerant system. The antifreeze loop would be eliminated and the cold box would be controlled by a thermostat connected to the compressor. If the refrgieration loop is applied directly to the cold box, the sizing of the compressor would be critical in this application. An oversized compressor would be short cycled at a frequency that could render the cooling cycle inoperable, and an undersized compressor would not be able to meet the cooling load.

The nominal heat removal rate for this apparatus is of the order of 100 Btu/hr or 0.01 tons of refrigeration. The Carnot efficiency for a refrigeration cycle is given by:

$$\beta = T_l \; / \; T_h - T_l$$

For this application T_l = 273 K and T_h = 330, β = 4.7. Thus the horsepower the the compressor should be approximately:

$$HP = ton \; \frac{1}{4} \; 4.715 \; / \; \beta = .01$$

A refrigeration compressor of 0.01 HP is not a standard size, therefore this compressor may have to be custom manufactured.

If a larger compressor were used it would have to be in conjunction with a heat storage system. In this configuration a secondary loop like the one presently used would be employed.

BIBLIOGRAPHY

1. Hillel, D. (1982) Introduction to Soil Physics, Academic Press Inc., Orlando, Florida.

2. Thomas, W.C., Bal, G.P., and Onega,R.J. (1983) "Heat and Moisture Transfer in Glass Fiber Roof-Insulating Material", ASTM STP 789, pp 582-601.

3. Motakef, S. (1984) "Simultaneous Heat and Mass Transport with Phase Change in Insulated Structures", Ph.D. Thesis, Dept. of Mechanical Engineering, Massachusettes Institute Of Technology, Cambridge, MA.

4. Katsenelenbogen, S.S. (1978) "Experimental Study of Water Vapor Transmission Through a Porous Insulation", M.S.M.E. Thesis, Dept. of Mechanical Engineering, Massachusettes Institute Of Technology, Cambridge, MA.

5. Bomberg, M. and Shirtliffe, C.J. (1978) "Influence of Moisture and Moisture Gradients on Heat Transfer Through Porous Building Materials", ASTM STP 660 pp.221-233.

6. Wexler, A. (1965) "Humidity and Moisture Measurements and Control ien Science", Reinhold Publishing Corp., N.Y.,N.Y.

7. Strang, G. (1986) Introduction to Applied Mathematics, Wellesley C
ambridge Press, Wellesley, MA.

8. List, R.J. (1966) Smithsonian Meteorological Tables, 6th rev. ed., Smithsonian Institution, Washington, D.C.

9. Vinieratos, E.R. and Verschoor, D.D.,(10/78) "Influence of Insulation Deficiencies on Heat Loss In Walls and Ceilings",Proc. U.S. D.O.E./ASTM Thermal Insulation Conference, Tampa, FL

10. Tsongas, G.A., Odell, G.I. and Thompson, J.C.,(12/79) "A Field Study of Moisture Damage in Walls Insulated Without a Vapor Barrier", Proc. ASHRAE/DOE - ORNL Conference, Thermal Performance of the Exterior Envelopes of Buildings, Kissimmee, FL.

11. U.S. Dept. of Commerce, (1984) 1982 Census of Construction Industries, Bureau of The Census, CC82-I-18

12. Wong, Y.C. and Sauer, H.J. Jr., (1983), "Total Energy Costs of Building Construction and Operation", Thermal Insulation, Materials, and Systems for Energy Conservation in the '80s, ASTM STP 789, American Society for Testing and Materials, pp.149-160.

APPENDIX A

Humidity Sensor Calibration Data

HUMIDITY SENSOR CALIBRATION DATA
ln (Z) *vs.* RH (%)

RH%	41.4	66.1	69.2	72.8	75.0	87.3	92.5
Probe							
1	15.1	12.9	12.5	12.4	12.4	11.1	10.8
2	15.1	13.0	12.6	12.5	12.5	11.2	10.9
3	15.1	13.0	12.6	12.4	12.4	11.1	10.9
4	15.1	12.9	12.5	12.4	12.4	11.1	10.9
5	15.1	12.9	12.5	12.4	12.4	11.1	10.9
6	15.0	12.9	12.5	12.4	12.4	11.1	10.9
7	15.0	12.9	12.5	12.4	12.4	11.1	10.9
8	15.0	13.0	12.5	12.4	12.4	11.1	10.9
9	15.1	13.0	12.5	12.4	12.4	11.1	10.9
10	15.2	13.0	12.5	12.4	12.5	11.1	10.9

Data collected at 25 ^{0}C

PROBE # 1

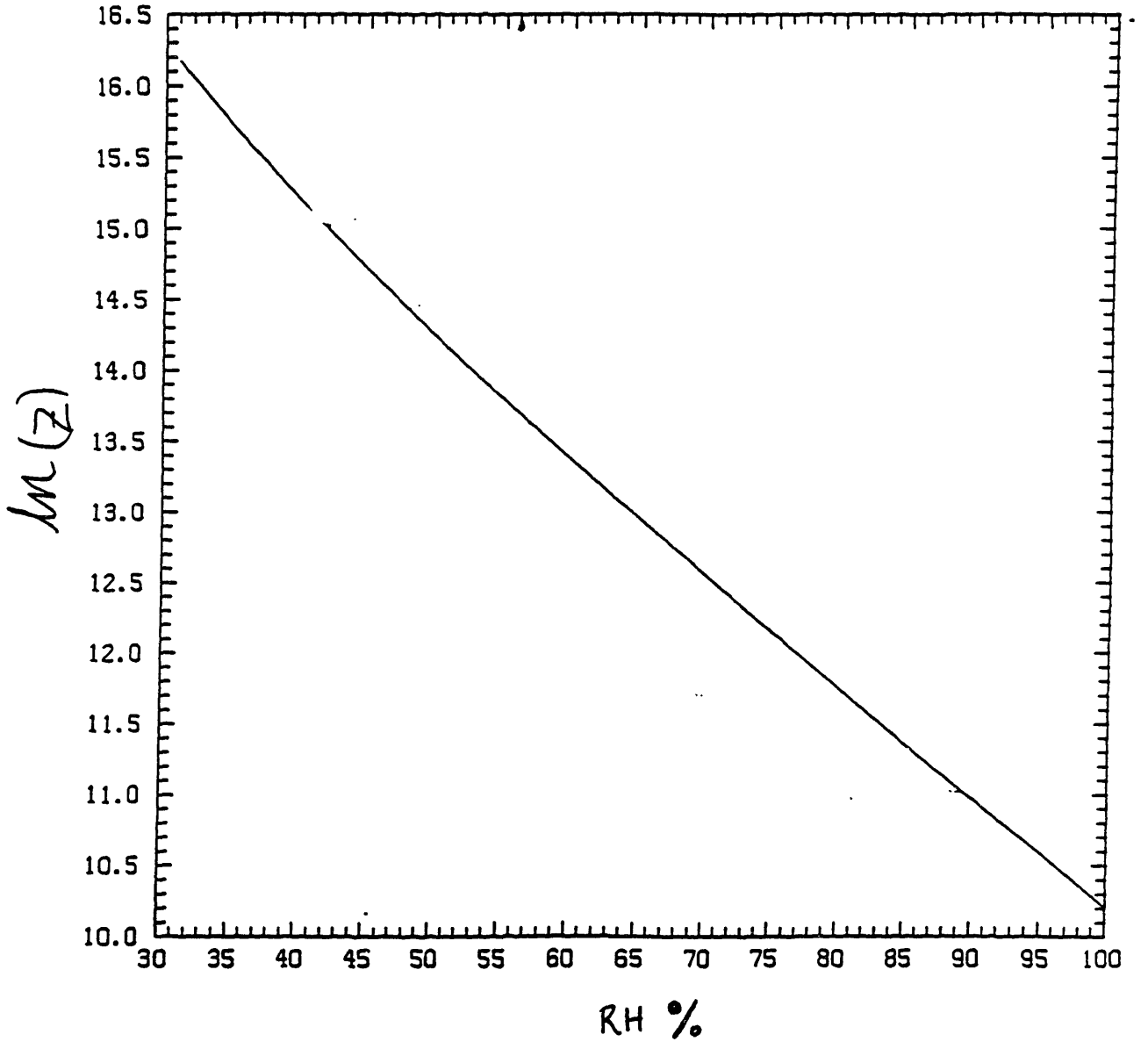
16.5
16.0
15.5
15.0
14.5
14.0
13.5
13.0
12.5
12.0
11.5
11.0
10.5
10.0
ln(Z)
30
35
40
45
50
55
60
65
70
75
80
85
90
95
100
RH %

PROBE # 2

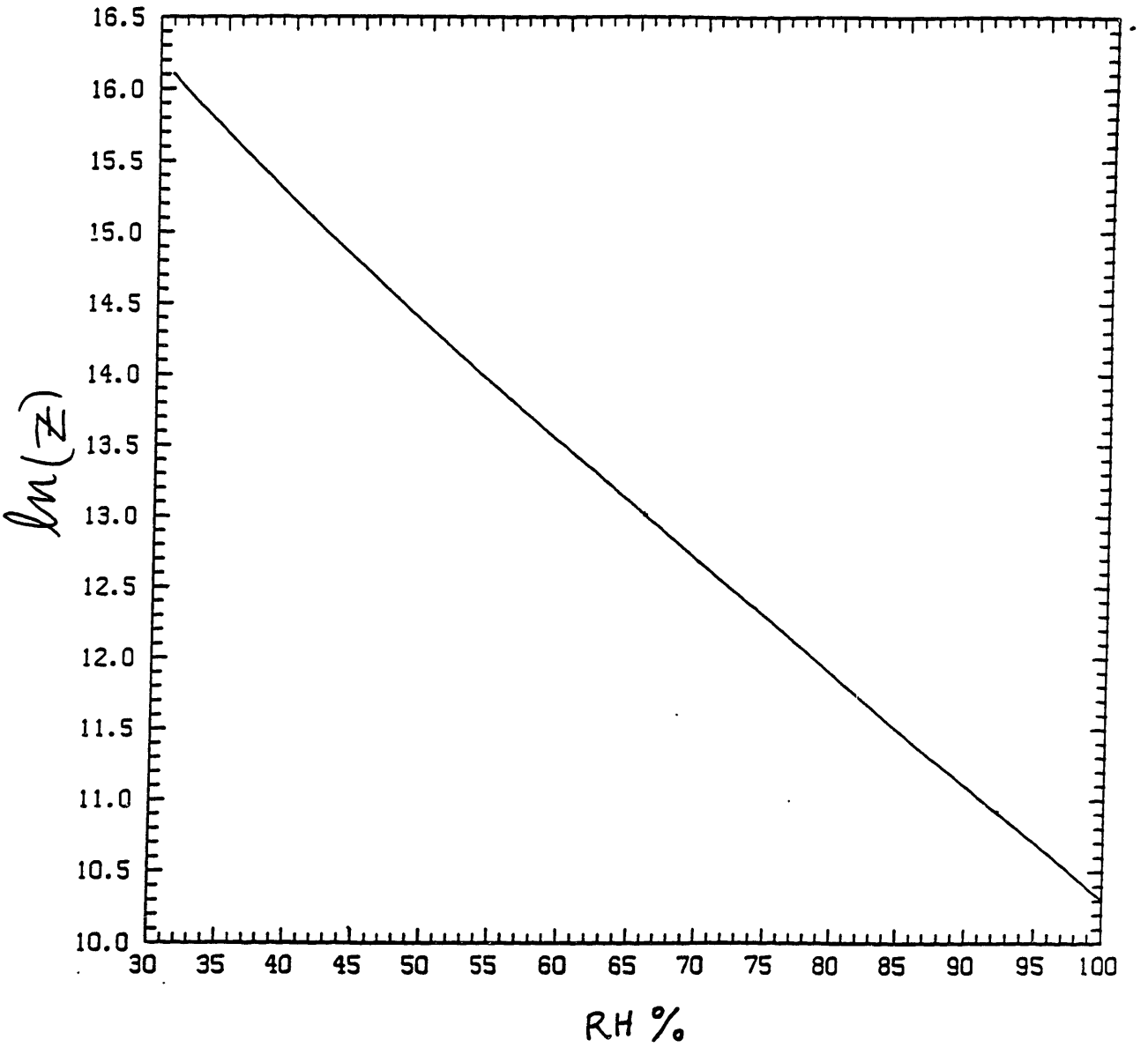
16.5
16.0
15.5
15.0
14.5
14.0
13.5
13.0
12.5
12.0
11.5
11.0
10.5
10.0
ln(Z)
30
35
40
45
50
55
60
65
70
75
80
85
90
95
100
RH %

PROBE # 3

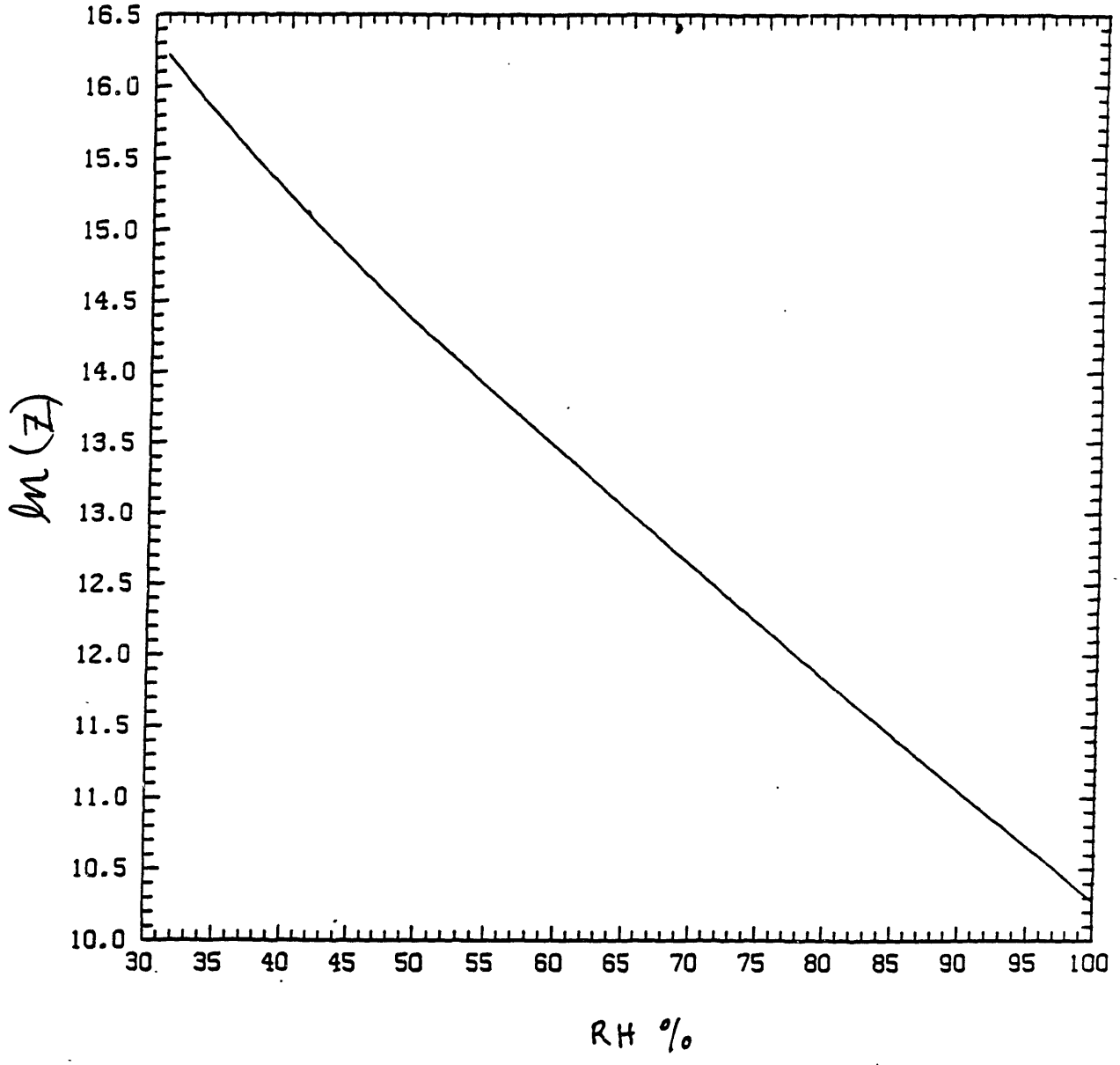
16.5
16.0
15.5
15.0
14.5
14.0
13.5
13.0
12.5
12.0
11.5
11.0
10.5
10.0
ln (Z)
30
35
40
45
50
55
60
65
70
75
80
85
90
95
100
RH %

PROBE # 4

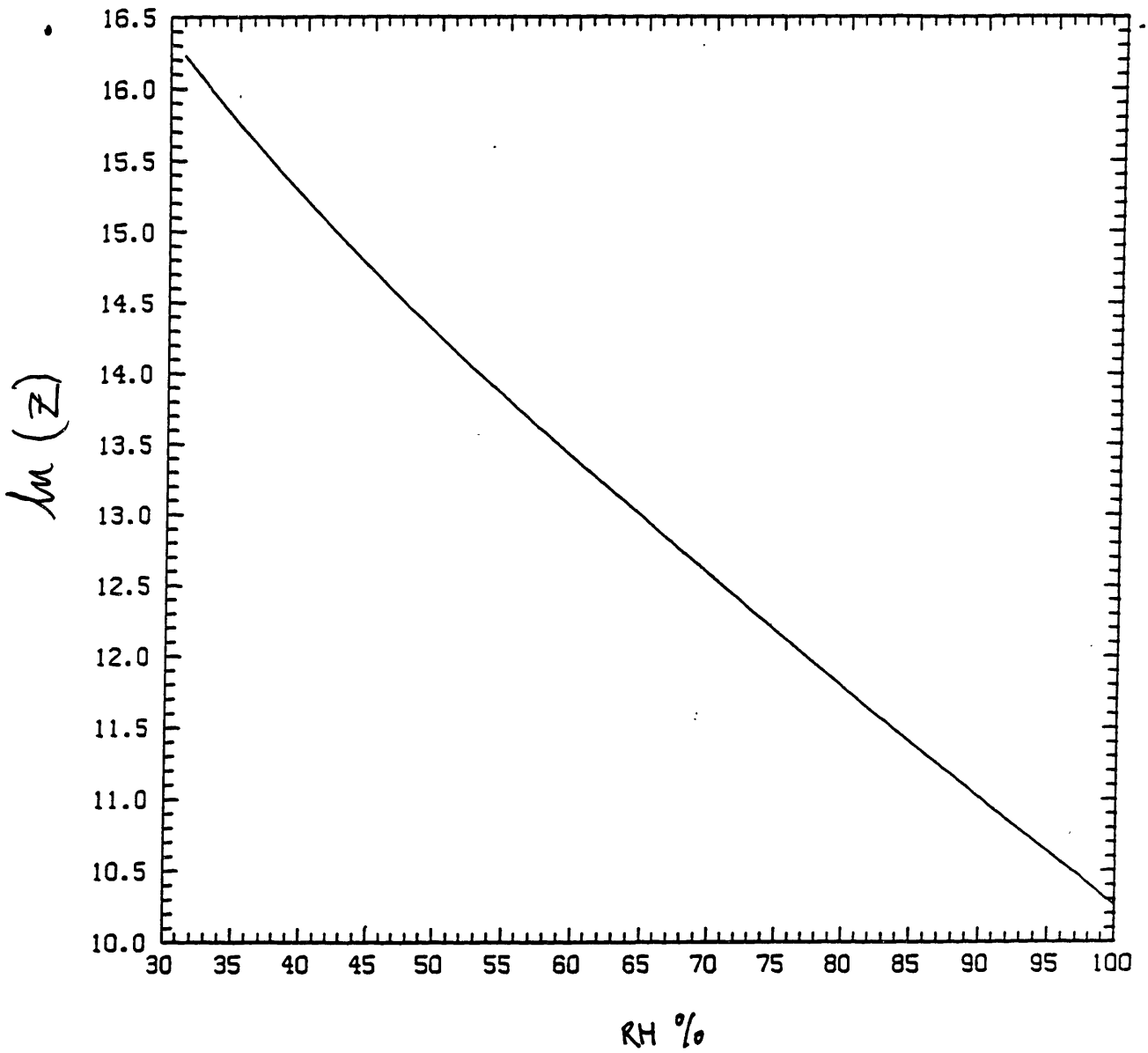
16.5
16.0
15.5
15.0
14.5
14.0
13.5
13.0
12.5
12.0
11.5
11.0
10.5
10.0
ln (Z)
30
35
40
45
50
55
60
65
70
75
80
85
90
95
100
RH %

PROBE # 5

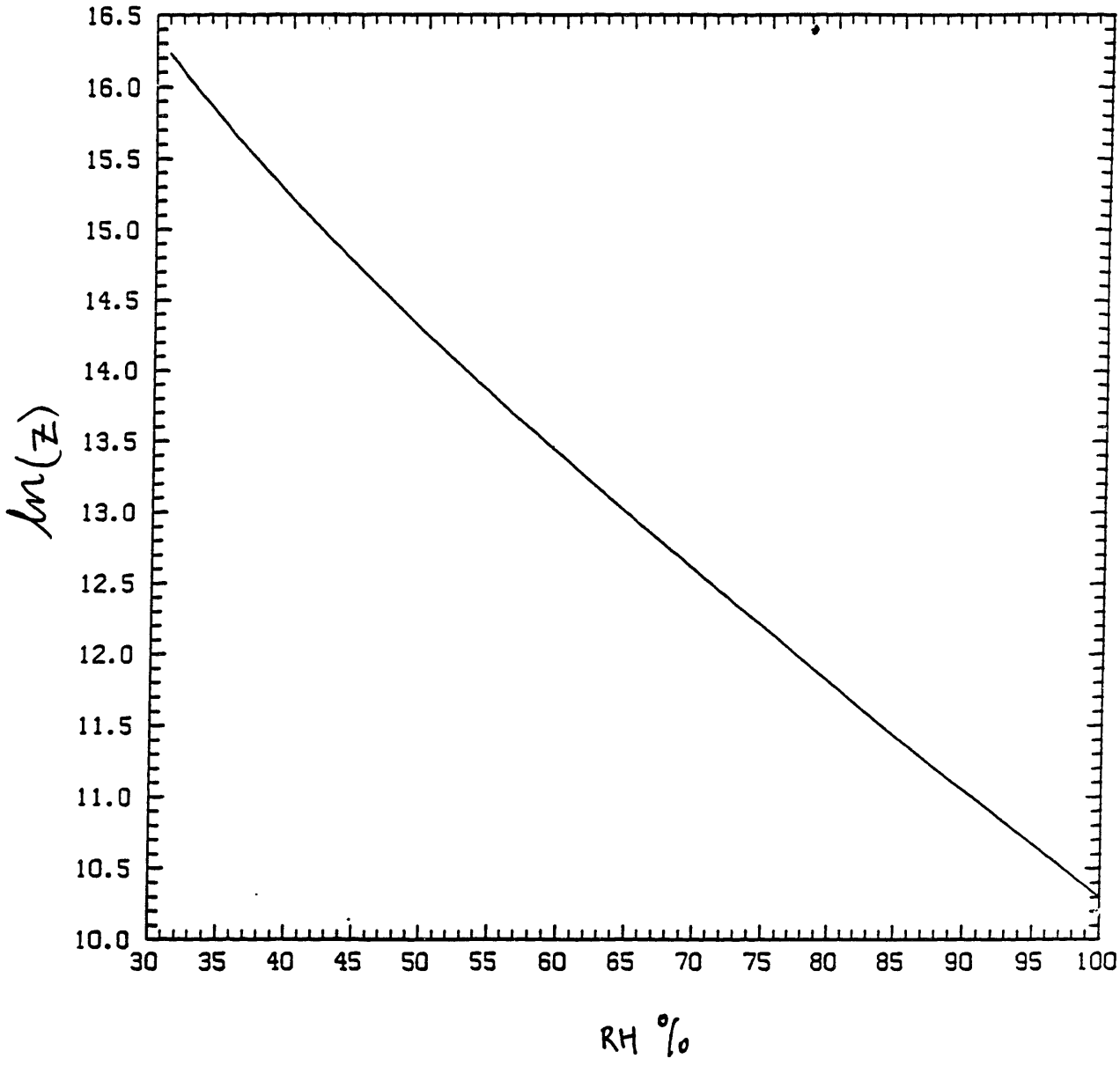
16.5
16.0
15.5
15.0
14.5
14.0
13.5
13.0
12.5
12.0
11.5
11.0
10.5
10.0
ln(Z)
30
35
40
45
50
55
60
65
70
75
80
85
90
95
100
RH %

PROBE # 6

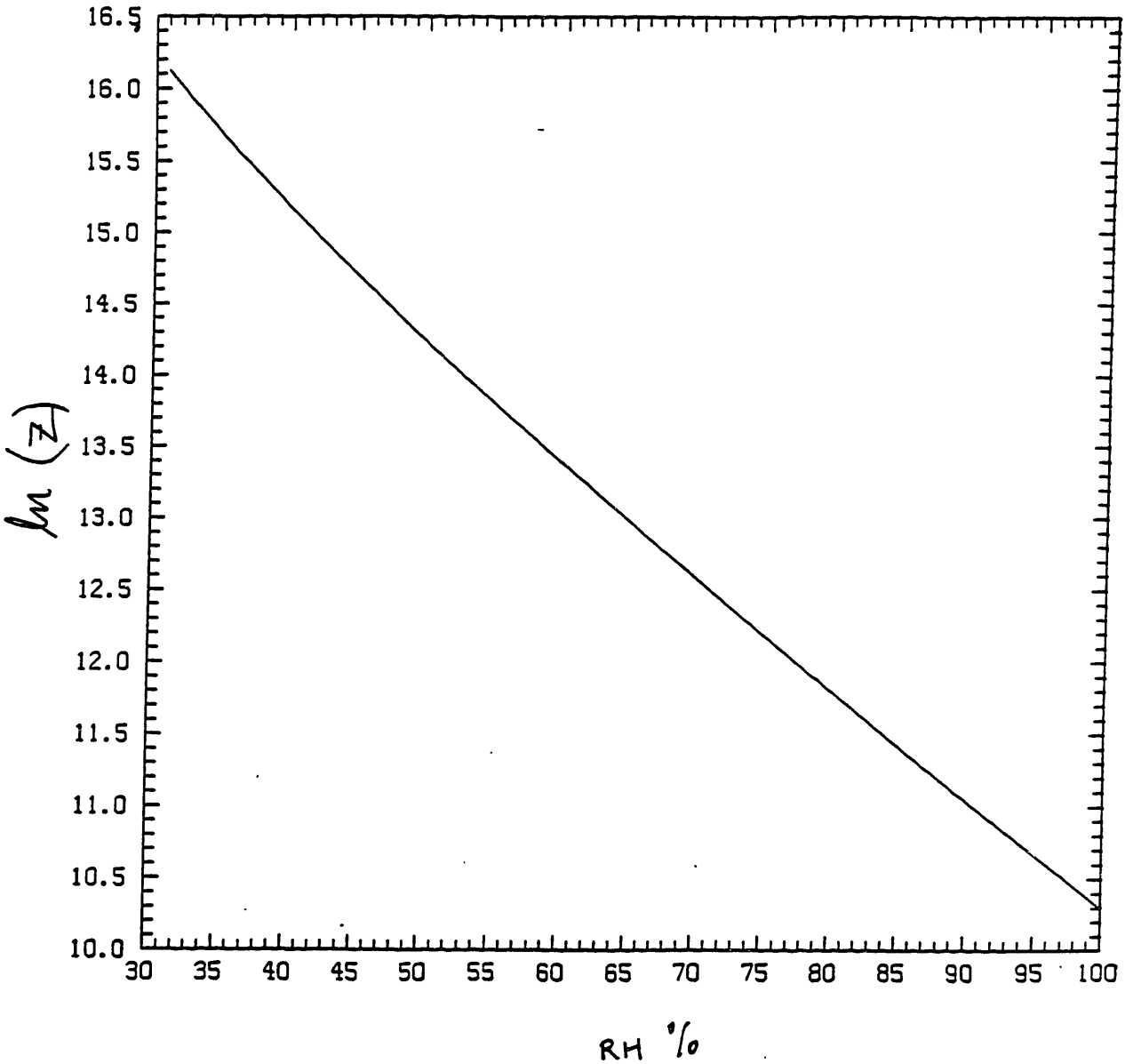
16.5
16.0
15.5
15.0
14.5
14.0
13.5
13.0
12.5
12.0
11.5
11.0
10.5
10.0
ln (Z)
30
35
40
45
50
55
60
65
70
75
80
85
90
95
100
RH %

PROBE # 7

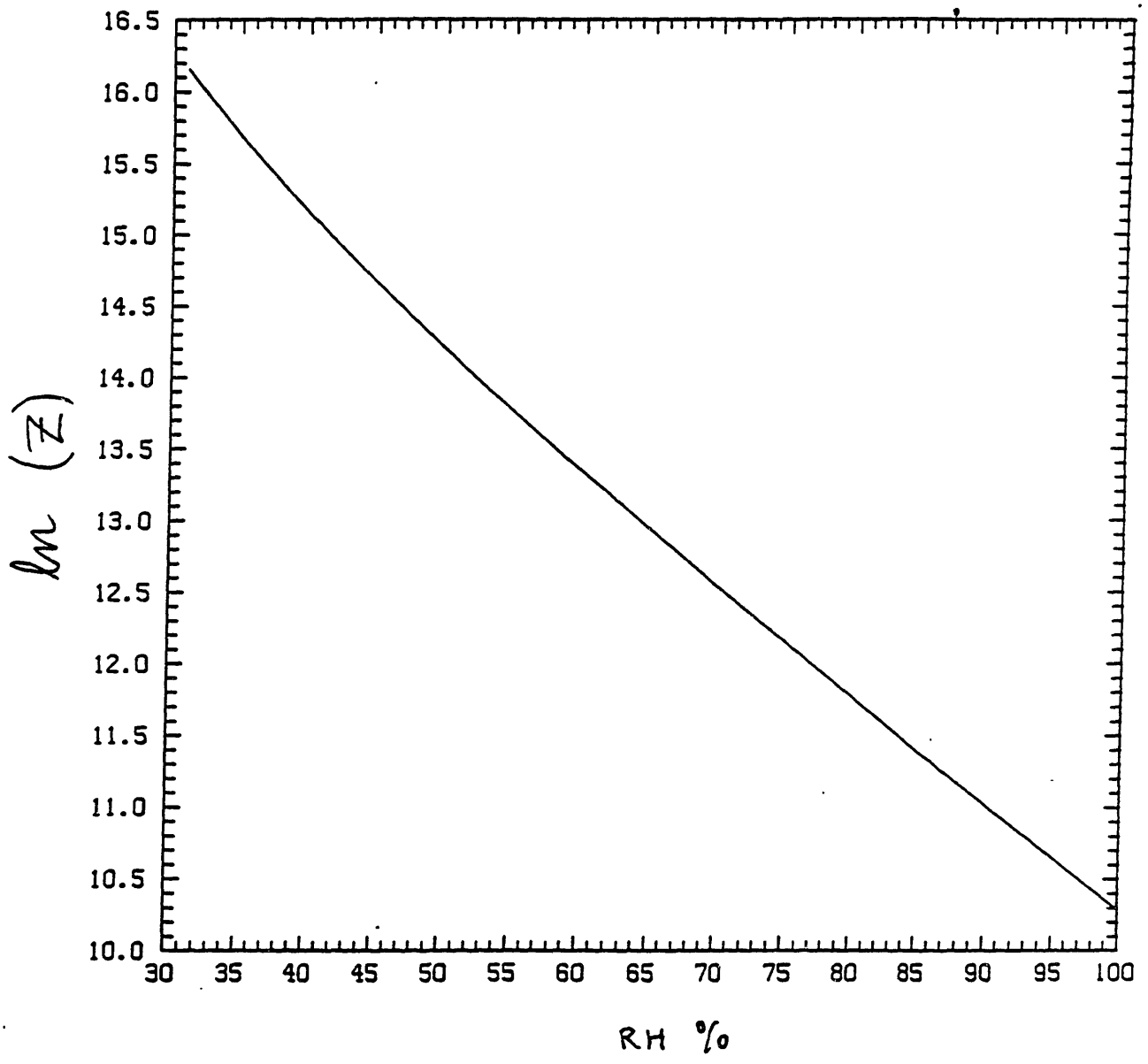
16.5
16.0
15.5
15.0
14.5
14.0
13.5
13.0
12.5
12.0
11.5
11.0
10.5
10.0
ln (Z)
30 35 40 45 50 55 60 65 70 75 80 85 90 95 100
RH %

PROBE # 8

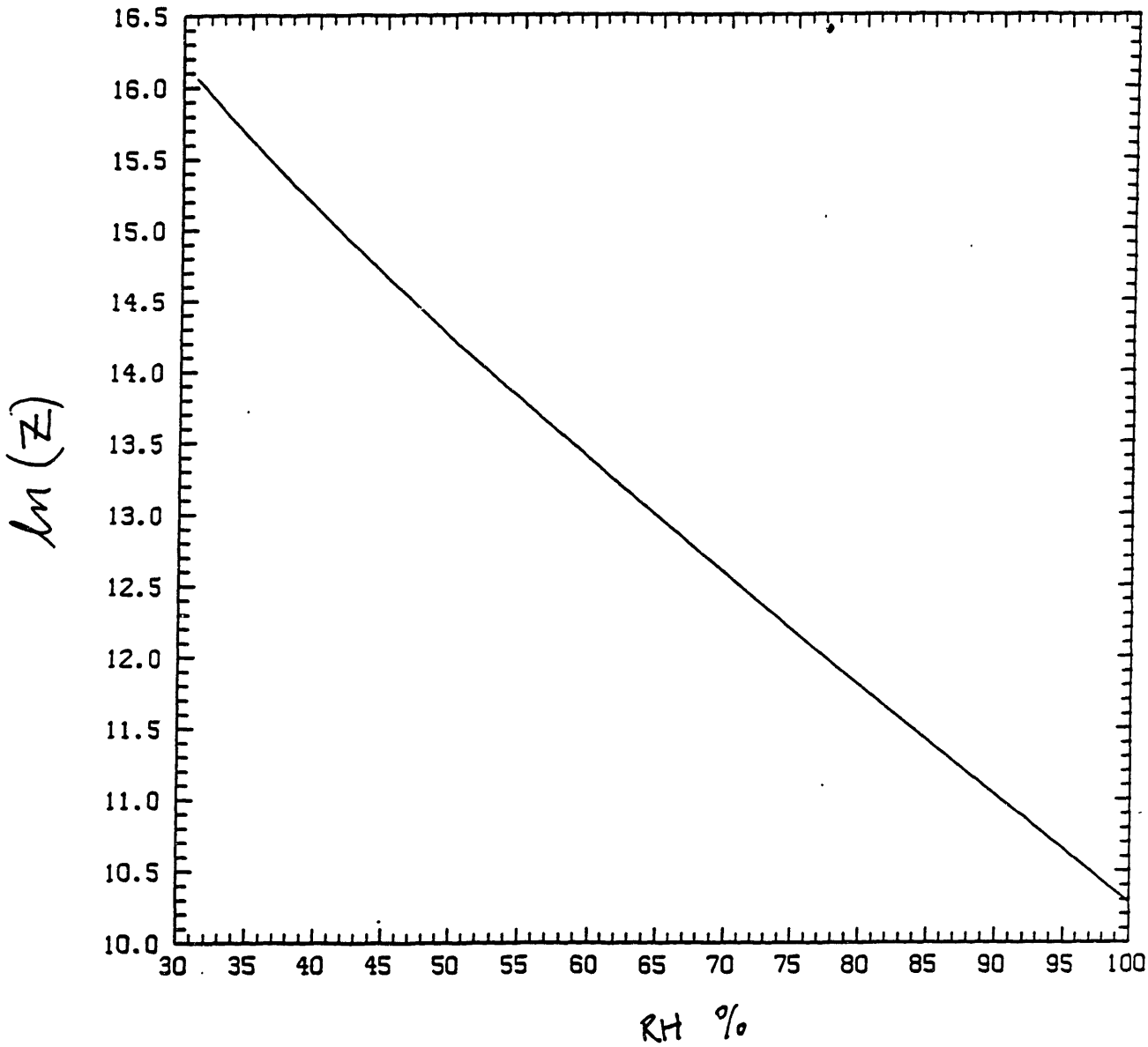
16.5
16.0
15.5
15.0
14.5
14.0
13.5
13.0
12.5
12.0
11.5
11.0
10.5
10.0
ln (Z)
30
35
40
45
50
55
60
65
70
75
80
85
90
95
100
RH %

PROBE # 9

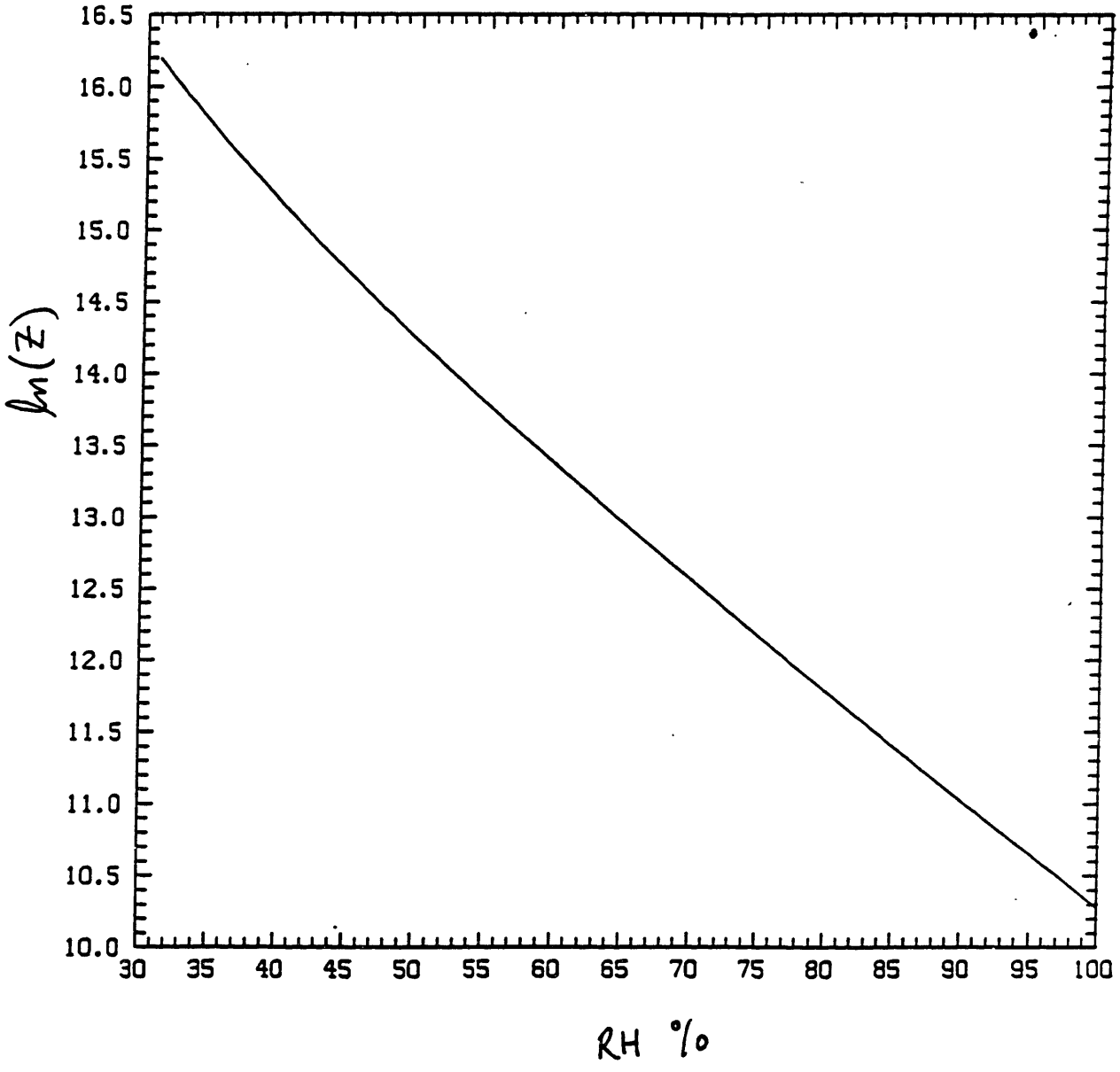
16.5
16.0
15.5
15.0
14.5
14.0
13.5
13.0
12.5
12.0
11.5
11.0
10.5
10.0
ln(Z)
30
35
40
45
50
55
60
65
70
75
80
85
90
95
100
RH %

PROBE # 10

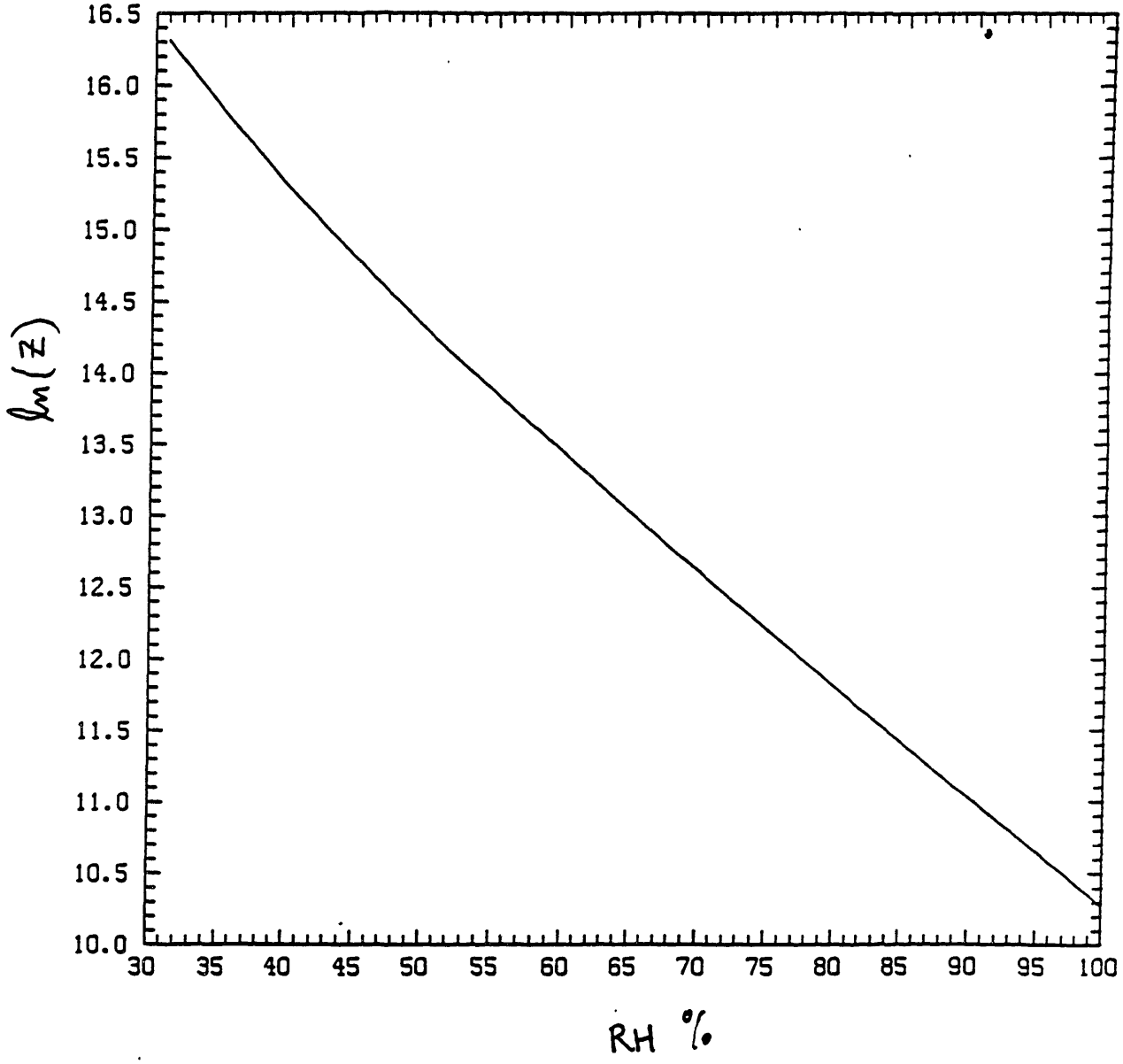
16.5
16.0
15.5
15.0
14.5
14.0
13.5
13.0
12.5
12.0
11.5
11.0
10.5
10.0
ln(Z)
30
35
40
45
50
55
60
65
70
75
80
85
90
95
100
RH %

APPENDIX B

Computer Program Listings

Quasi- Steady Transient Model

```
C
PROGRAM TRANS1
C WRITTEN BY ANDY SHAPIRO
C       REVISION DATE 10 SEPT 1986
  COMMON/param/tr,cr,dv,hfg,R,kw,gama,beta,A1,E1,E2
  REAL*8 T(101),A1(12),E1(7),E2(7),Jacoby(2,2),theta(101),gamma(101)
  REAL*8 tr,cr,hfg,R,kw,kd,gama,beta,t0,nt0,t1,nt1,dcdt,error
  REAL*8 g1,g2,g1p,g2p,dx0,phi,th,tc,dt0,c0,c1,kratio,alpha
  REAL*8 rho,cp,le,dtp,trp,betap,hfgrp,crp,x,dt1,tratio,dcp
  REAL*8 omegap,gamap,lambdap,dtime,ddtdx0dt,ddtdx1dt,lwp,b1
  REAL*8 J0,J1,dtdx0,dcdx0,dtdx1,dcdx1,dcdt1,dcdt0,err,lw,time
  REAL*8 const,dv,dtdx1p,hh,hc,cc,ch,det,dtdx0p,x0,x1,a1,a0
  REAL*8 conc,h,ssn,tfinal,lt
  INTEGER i,i2,flag,ans,n,iter,iter2
  CHARACTER*10 file$,file1$,file2$

 data A1/10.4592,-.00404897,-.41752E-4,.36851E-6,-.10152E-8,
     &  .86531E-12,.903668E-15,-.19969E-17,.779287E-21,.191482E-24,
     &  -.396806E4,.395735E2/
  data E1/-8.9751114,-.4384553,-19.179576,36.765319,-19.462437,0.,0./
  data E2/-3.87446,2.94553,-8.06395,11.5633,-6.02884,0.,0./
  PRINT *,'** This program calculates the temperature and vapor **'
  PRINT *,'**   concentration profiles in a slab of fiberglass  **'
  PRINT *,'**          with transient boundary conditions        **'
  PRINT *,'**                  and liquid diffusion              **'
  PRINT *,' '
  PRINT *,' '
  PRINT *,'ENTER INITIAL LIQUID CONTENT FILE'
  READ *, file$
  OPEN (unit=10,file=file$//'.dat',status='old')
  PRINT *,'ENTER Th,Tc (K)'
  READ *,th,tc
  PRINT *,'ENTER RHh,RHc'
  READ *,hh,hc
  PRINT *,'ENTER kd/kw'
  READ *,kratio
  PRINT *,'ENTER run label'
  READ *,file$
  PRINT *,'ENTER alpha,error'
  READ *,alpha,error
  PRINT *,'ENTER time step, print interval,simulation time'
  READ *,dtime,pint,tfinal
  print *,'enter slab thickness'
  read *,lt
  file1$='temp'//file$//'.dat'
  file2$='conc'//file$//'.dat'
  OPEN(unit=20,file=file1$,status='new')
  OPEN(unit=30,file=file2$,status='new')
C physical properties
  dv=1.6E-5
  kd=.026
  kw=kratio*kd
  R=461.8
  rho = 1.16
  cp = 1007.
  le=kw/(rho*cp*dv)
C find ch & c
C
  READ (10,*),x0,x1
  do 10 i=1,20

read(10,*),theta(i)
10
continue
```

```
      print *,th,tc
      x0=x0*lt
      x1=x1*lt
      if (x0 .lt. 0.01*lt) x0=.01*lt
      if (x1 .gt. 0.99*lt) x1=.99*lt
      print *,x0,x1,lt
      ch=hh*(CONC(th))
      cc=hc*(CONC(tc))
      t0=th-x0*(th-tc)/lt
      t1=th-x1*(th-tc)/lt
      lw=x1-x0
      lwp=lw
      iter2=0
      time=0
      pflag=-.01
   80
   format(' ',g10.5,'   ',g10.5,'  ',g10.5,'  ',g10.5,
     &  '  ',g10.5'  ',g10.4,'  ',g10.4)
     PRINT *,'TIME          T0          T1          X0          X1
     &         Qin         Qout'
   90
   if (time .gt. pflag) then
   c
   qi=(th-t0)*lt/(x0*(th-tc))
   c
   q0=(t1-tc)*lt/((lt-x1)*(th-tc))

   write(6,80),time,t0,t1,x0,x1,qi,q0

   pflag =pflag + pint
     end if
     if (time .gt. tfinal) goto 290
     iter = 0
   100
   dtp=t0-t1
     trp=(t0+t1)/2
     betap=dtp/trp
     hfg=H(trp)
     crp=CONC(trp)
   c dtime = (x0**2*theta(1)**.5+(lt-x1)**2*theta(20)**.5)/
   c     &          (2*dv*crp**.5)
     c0=conc(t0)
     c1=conc(t1)
     dcp=c0-c1
     omegap=hfg*(c0-c1)/(rho*cp*trp)
     gamap=hfg/(r*trp)
     b1=hfg*dv/kd
     lambdap=2*gamap**2*betap*omegap/(1e+gamap*omegap)
     dtdx0p=dtdx0
     dtdx1p=dtdx1
     const=dtp/lw
     dtdx0=-.5*(1+lambdap/(dexp(lambdap)-1))*const
     dtdx1=-.5*(1+lambdap*dexp(lambdap)/(dexp(lambdap)-1))*const
     dcdt0=(conc(t0+.001)-c0)/.001
     dcdt1=(conc(t1+.001)-c1)/.001
     g1=(th-t0)/x0+dtdx0+b1*((ch-c0)/x0 + dcdt0*dtdx0)
     g2=(t1-tc)/(lt-x1)+dtdx1+b1*((c1-cc)/(lt-x1)+dcdt1*dtdx1)
     if (iter .gt. 0) goto 200

dtdx0p=dtdx0

dtdx1p=dtdx1

g1p=g1

g2=g2
```

```
t0=t0+.01
t1=t1+.01
dt0=.01
dt1=.01
dtp=t0-t1
```

```
      dtdx0=-.5*(1+lambdap/(dexp(lambdap)-1)*dtp-1)
      dtdx1=-.5*(1+lambdap*dexp/lambdap)/(dexp(lambdap)-1)*dtp-1)
            g1=(th-t0)/x0+dtdx0+b1*((ch-c0)/x0 + dcdt0*dtdx0)
        g2=(t1-tc)/(lt-x1)+dtdx1+b1*((c1-cc)/(lt-x1)+dcdt1*dtdx1)
200
ddtdx0dt= (dtdx0-dtdx0p)/dt0
  ddtdx1dt= (dtdx1-dtdx1p)/dt1
c Jacoby(1,1)=(1+hfg*dv/kd*dcdt0)*(ddtdx0dt-1/x0)
c Jacoby(1,2)=(g1-g1p)/dt1
c Jacoby(2,1)=(g2-g2p)/dt0
c Jacoby(2,2)=(1+hfg*dv/kd*dcdt1)*(ddtdx1dt+1/(1-x1))
  iter=iter +1
  dt0=-alpha*dt0*g1/(g1-g1p)
  dt1=-alpha*dt1*g2/(g2-g2p)
  g1p=g1
  g2p=g2
c det=1/(Jacoby(1,1)*Jacoby(2,2)-Jacoby(1,2)*Jacoby(2,1))
c dt0=-alpha*(Jacoby(2,2)*g1-Jacoby(2,1)*g2)*det
c dt1=alpha*(Jacoby(1,2)*g1-Jacoby(1,1)*g2)*det
  if (dabs(dt0).gt. .10) dt0=.1*sgn(dt0)
  if (dabs(dt1).gt. .10) dt1=.1*sgn(dt1)
  t0=t0+dt0
  t1=t1+dt1
  err=MAX(dabs(g1),dabs(g2))
  if (err .gt. error) goto 100
  do 250 i=1,20
     x=i
     const=dtp/lw**2*kd/hfg*.5*lambdap**2/(dexp(lambdap)-1)
     &                  *crp/dcp
     gamma(i)=const*dexp(lambdap*x/20)
     x=(20*dx0+x*lw)/lwp
     i2=x
    theta(i)=theta(i2)+(theta(i2+1)-theta(i2))*(x-i2)
     &  +gamma(i)*dtime
250
continue
  dx0=-dtime*dv/theta(1)*((ch-c0)/x0+dcdt0*dtdx0)
  x0=x0+dx0
  x1=x1-dtime*dv/theta(20)*((c1-cc)/(lt-x1)+dcdt1*dtdx1)
  lwp=lw
  lw=x1-x0
  if (lw .lt. .0005) then

print *,'dryout occurs under these conditions'

write(6,80),time+dtime,t0,t1,x0,x1

goto 290
  end if

  time=time+dtime
  iter2=iter2+1
  if (dx0 .gt. 1e-18*dtime) goto 90
c write solution to temp.dat file
290
dx=(x1-x0)/20
c WRITE(20,350),0.,th
c WRITE(30,360),0.,ch
c DO 300 i=1,101
c    WRITE(20,350),x0+(i-1)*dx,T(i)
c
   ci=CONC(T(i))
c    WRITE(30,360),x0+(i-1)*dx,ci
c300
CONTINUE
```

```
c WRITE(20,350),1.,tc
c WRITE(30,360),1.,cc
350
FORMAT('  ',F6.4,'  ',F8.4)
360
FORMAT('  ',F6.4,'  ',F8.7)
```

```
390
PRINT *,'**********************************************************'
  PRINT *,'*****                    OUTPUT                      *****'
  PRINT *,' '
  PRINT *,'RUN LABEL',file$
  PRINT *,' '
  PRINT *,'HEAT ENTERING SLAB =',kd*(th-t0)/x0,'(W/m^2)'
  PRINT *,'HEAT LEAVING SLAB =',kd*(t1-tc)/(1-x1),'(W/m^2)'
  PRINT *,'VAPOR ENTERING SLAB =',dv*(ch-c0)/x0,'(kg/m^2 s)'
  PRINT *,'VAPOR LEAVING SLAB =',dv*(c1-cc)/(1-x1),'(kg/m^2 s)'
  PRINT *,' '
  PRINT *,'WET ZONE BOUNDARIES:',x0,x1
  PRINT *,' '
  PRINT *,'EVAPORATION RATE AT HOT SIDE =',J0,'(kg/m^2 s)'
  PRINT *,'EVAPORATION RATE AT COLD SIDE =',J1,'(kg/m^2 s)'
  PRINT *,' '
  PRINT *,'lambdap =',lambdap
  GOTO 450
400
PRINT *,' NO CONVERGENCE !!'
  goto 450
425
PRINT *,' NO CONDENSATION WITH THESE BOUNDARY CONDITIONS'
450
STOP
  END
c function CONC
  REAL*8 function CONC(T)
  COMMON/param/tr,cr,dv,hfg,R,kw,gama,beta,A1,E1,E2
  REAL*8 t,x,lgp,tnon,vg,A1(12),E1(7),E2(7),tr,cr,dv,hfg,R,kw,gama,beta
  integer*4 n
  lgp=a1(11)/(t-a1(12))
  DO 10 n=1,10
     x=DFLOTJ(n)
     lgp=lgp +sgn(a1(n))*dexp(dlog(dabs(A1(n)))+(x-1)*dlog(T))
10      CONTINUE
  tnon=(647.3-T)/647.3
  vg=1.+1.6351057*tnon**(1./3.)+52.584599*tnon**(5./6.)-
     &   44.694653*tnon**(7./8.)
  DO 20 n=1,7
     vg=vg+E1(n)*tnon**n
20
CONTINUE
  vg=vg*22.089*.003155/dexp(lgp)
  CONC=1./vg
  RETURN
  END
C function H
  REAL*8 function H(T)
  COMMON/param/tr,cr,dv,hfg,R,kw,gama,beta,A1,E1,E2
  REAL*8 t,hfg1,tnon,A1(12),E1(7),E2(7),tr,cr,dv,hfg,R,kw,gama,beta
  INTEGER n
  tnon=(647.3-T)/647.3
  hfg1=.779221*tnon**(1./3.)+4.62668*tnon**(5./6.)-1.07931*tnon**(7./8.)
  DO 10 n=1,7
     hfg1=hfg1+E2(n)*tnon**n
10
continue
  H=hfg1*2.5009E6
  RETURN
  end
c function sgn
  real*8 function sgn(t)
  real*8 a,t
  if (t .lt.0) then
```

```
a=-1
else
a=1
end if
sgn=a
return
end
```

Numerical Transient Model

```
c                    program trans12
c       program solves for the transient temperature -
c       vapor concentration and liquid content profiles
c in a porous slab with heat conduction, vapor diffusion
c
and phase change with constant boundary conditions
  real*8 eta(102),deta(102),cnc(102),dcnc(102)
  real*8 eta2(102),cnc2(102),theta(102),dcdt(102),cnc0(102)
  real*8 alpha,dv,dtime,dx,hfg,dc,dt,tave,rho,cair,r
  real*8 th,tc,hh,hc,x,x0,x1,c0,c1,ch,cc,const,b1,b2
  real*8 conc,h,pint,time,tfinal,tflag,d2tdx2,d2cdx2
  integer i,j,iteration,i0,i1,i0p,i1p,flag,flag2
  character * 10 file$,file1$,file2$
  print *,'enter data output filename'
  read *,file1$
  print *,'enter data file with initial temperature and'
  print *,'liquid distribution:'
  read *, file$
  file$=file$//'.dat.'
  file1$=file1$//'.dat.'
  open(unit=10,file=file$,status='old')
  open(unit=20,file='temp'//file1$,status='new')
  open(unit=30,file='conc'//file1$,status='new')
  open(unit=40,file='theta'//file1$,status='new')
  print *,'enter Th,Tc (K)'
  read *,th,tc
  print *,'enter hh,hc'
  read *,hh,hc
  print *,'enter timestep,print interval,time of simulation'
  read *,dtime,pint,tfinal
c
c PHYSICAL PROPERTIES
  dx=.001
  alpha=2.32E-5
  dv=1.6E-5
  rho=1.16
  cair=1007
  r=461.8
c
c read initial conditions
  time=0
  i0=3
  i1=1
  do 10 i=1 ,101,2

read(10,*),eta(i),cnc(i),theta(i)

cnc0(i)=cnc(i)

if(i0.eq.3) then

if (theta(i) .ne. 0) i0=i

else

if (i1 .eq.1) then

  if (theta(i) .eq. 0) i1=i

end if

end if
10
continue
```

```
      if (i1.le.10) then
      print *,'dryout occurs'
      endif
c
c
c
c set new boundary conditions
```

```
      eta(1)=th
      eta(101)=tc
      eta2(1)=th
      eta2(101)=tc
      ch=hh*conc(th)
      cc=hc*conc(tc)
      cnc(1)=ch
      cnc(101)=cc
      cnc2(1)=ch
      cnc2(101)=cc
      dt=th-tc
      tave=(th+tc)*.5
      dc=ch-cc
      i0p=i0
      i1p=i1
      flag2=0
      print *,i0,i1
   55
   hfg=H(eta(51))
   c step in dry zone
      const=dtime/((2*dx)**2)
      flag=0
      if (i0 .gt.3) then
      do  60 i=3,i0-2,2

   call fnc(d2tdx2,eta,i,i0,i1,flag)

   call fnc(d2cdx2,cnc,i,i0,i1,flag)

   deta(i)=alpha*const*d2tdx2

   dcnc(i)=dv*const*d2cdx2

   eta2(i)=eta(i)+deta(i)

   cnc2(i)=cnc(i)+dcnc(i)

   if (cnc2(i) .gt. 1.01*conc(eta2(i))) then

   cnc2(i)=conc(eta2(i))

   i0p=i

   endif
   60
   continue
     endif
   75
   if (i1 .lt. 99) then
     do 80 i=99,i1+2,-2

   call fnc(d2tdx2,eta,i,i0,i1,flag)

   call fnc(d2cdx2,cnc,i,i0,i1,flag)

   deta(i)=alpha*const*d2tdx2

   dcnc(i)=dv*const*d2cdx2

   eta2(i)=eta(i)+deta(i)

   cnc2(i)=cnc(i)+dcnc(i)

   if (cnc2(i) .gt. 1.01*conc(eta2(i))) then
```

```
cnc2(i)=conc(eta2(i))

ip=1

endif
80
continue
  endif
  b1 =  hfg/(rho*cair)
  flag=1
  if (i0 .le. i1) then

do 100 i=i0,i1,2

call fnc(d2tdx2,eta,i,i0,i1,flag)

d2tdx2=d2tdx2/(2*dx)**2

dtdx=(eta(i+2)-eta(i-2))/(4*dx)

b2=hfg*cnc(i)/(r*eta(i)**2)

b3=1+b1*b2

call fnc(d2cdx2,cnc,i,i0,i1,flag)

d2cdx2=d2cdx2/(2*dx)**2
```

```
     d2cdx2+d2tdx2*b2+dtdx**2*(b2/cnc(i))
c    &                *(b2-2*cnc(i)/eta(i))

     deta(i)=dtime*(alpha*d2tdx2+b1*dv*d2cdx2)/b3

     eta2(i)=eta(i)+deta(i)

     cnc2(i)=conc(eta2(i))

     dcnc(i)=cnc2(i)-cnc(i)

     if (theta(i).eq.0 .and. dtime*dv*d2cdx2.lt.dcnc(i))then
                        deta(i)=dtime*alpha*d2tdx2

       dcnc(i)=dtime*dv*d2cdx2

       eta2(i)=eta(i)+deta(i)

       cnc2(i)=cnc(i)+dcnc(i)
                      endif

     theta(i)=theta(i)+dtime*dv*d2cdx2-dcnc(i)

     if(theta(i) .lt. 1E-6) then

     theta(i)=0.
c
     print *,i,i0,i1

     if (i.eq.i0) i0p=i0+2

     if (i.eq.i1) i1p=i1-2

     end if
     100
     continue
       endif
c
c
       i0=i0p
       i1=i1p
       if (i0.gt.i1) then
       if (flag2 .eq.0) then

     print *,'******** d r y o u t   o c c u r s **********'
       write(6,140),time,i0,i1,eta(i0),eta(i1)
          &     ,(eta(1)-eta(3))*50/dt, (eta(99)-eta(101))*50/dt
       write(6,150),theta(i0),theta(i1),cnc(i0),cnc(i1)
          &         ,(cnc(1)-cnc(3))*50/dc,(cnc(99)-cnc(101))*50/dc

     flag2=1
       endif

     i0=3

     i1=i0-2
       endif
c
       do 105 i=3,99,2

     if (dabs(eta2(i)-tave).gt.100) print *,i

     eta(i)=eta2(i)
```

```
      cnc(i)=cnc2(i)
  105
      continue
      c
        time=time+dtime
      c print output
        if (time .gt. tflag) then

      tflag=tflag+print
        write(6,140),time,i0,i1,eta(i0),eta(i1)
           &     ,(eta(1)-eta(3))*50/dt, (eta(99)-eta(101))*50/dt
        write(6,150),theta(i0),theta(i1),cnc(i0),cnc(i1)
           &         ,(cnc(1)-cnc(3))*50/dc,(cnc(99)-cnc(101))*50/dc
        endif
        if (time .gt. tfinal) then
        do 130 i=1,101,2
        write(20,160),i,eta(i)
        write(30,160),i,cnc(i)
        write(40,160),i,theta(i)
      130
      continue
        goto 200
```

```
      endif
      goto 55
  140
  format(' ',f12.5,'    'i3,'  ',i3,'       ',g10.5,'  ',g10.5,
     &      '   ',f10.5, '  ',f10.5)
  150
  format(' ',f10.5,'    ',f10.5, '     ',g10.5,'  ',g10.5,
     &      '   ',f10.5, '  ',f10.5)
  160
  format('  ',i3,'  ',f10.5)
  200
  end
  c function fnc returns second derivative
    subroutine fnc(b,a,i,J,k,flag)
    real*8 b
    real*8 a(102)
    integer i,J,k,flag
    if (i.ne.3 .and. i.ne.99)
       &
      b=(-a(i-4)+16.*a(i-2)-30.*a(i)+16.*a(i+2)-a(i+4))/12.
    if (i.eq.J+2 .or. i.eq.k+2) then
              if ((k-i).lt.6 .or. i.gt.95) then
        b=(a(i-2)-2.*a(i)+a(i+2))


      else

  b=(11.*a(i-2)-20.*a(i)+6.*a(i+2)+4.*a(i+4)-a(i+6))/12.
        endif
    endif
    if (i.eq.k-2 .or. i.eq.J-2) then
        if ((i-J).lt.6 .or. (i.lt.7)) then
           b=(a(i-2)-2.*a(i)+a(i+2))

      else
           b=(-a(i-6)+4.*a(i-4)+6.*a(i-2)-20.*a(i)+11.*a(i+2))/12.
        endif
    endif
    if ((i.eq.J).or.(i.eq.k)) then

   b=(a(i-2)-2*a(i)+a(i+2))
    endif
    if (i.eq.3 .or. i.eq.99 ) b=(a(i-2)-2.*a(i)+a(i+2))
    return
    end
```

Quasi-Steady Transient Model
With Two Vapor Barriers

SOME TEXT ON THE FOLLOWING PAGE(S) IS
ILLEGIBLE ON THE ORIGINAL MATERIAL.

```
C
      PROGRAM moflux1
C           WRITTEN BY ANDY SHAPIRO
C           REVISION DATE 10 SEPT 1986
        COMMON/param/tr,cr,dv,hfg,R,kw,gama,beta,A1,E1,E2
        REAL*8 T(10),A1(12),E1(7),E2(7),Jacoby(2,2),theta(101),gamma(101)
        REAL*8 tr,cr,hfg,R,kw,kd,gama,beta,t0,nt0,t1,nt1,dcdt,error
        REAL*8 g1,g2,g1p,g2p,dx0,phi,th,tc,dt0,c0,c1,kratio,alpha
        REAL*8 rho,cp,le,dtp,trp,betap,hfgrp,crp,x,dt1,tratio,dcp
        REAL*8 omegap,gamap,lambdap,dtime,ddtdx0dt,ddtdx1dt,lwp,b1
        REAL*8 J0,J1,dtdx0,dcdx0,dtdx1,dcdx1,dcdt1,dcdt0,err,lw,time
        REAL*8 const,dv,dtdx1p,hh,hc,cc,ch,det,dtdx0p,x0,x1,ai,a0
        REAL*8 conc,h,sgn,tfinal,region(6),ratio,L(10),lt
        INTEGER i,i2,flag,ans,n,iter,iter2
        CHARACTER*10 file$,file1$,file2$

      data A1/10.4592,-.00404897,-.41752E-4,.36851E-6,-.10152E-8,
     &   .86531E-12,.903668E-15,-.19969E-17,.779287E-21,.191482E-24,
     &   -.396806E4,.395735E2/
        data E1/-9.9751114,-.4384553,-19.179576,36.765319,-19.462437,0.,0./
        data E2/-3.87446,2.94553,-8.06393,11.5633,-6.02884,0.,0./
        PRINT *,'** This program calculates the temperature and vapor **'
        PRINT *,'**   concentration profiles in a slab of fiberglass  **'
        PRINT *,'**          with transient boundary conditions       **'
        PRINT *,'**                and liquid diffusion               **'
        PRINT *,' '
        PRINT *,' '
        PRINT *,'ENTER INITIAL LIQUID CONTENT FILE'
        READ *, file$
        OPEN (unit=10,file=file$//'.dat',status='old')
        PRINT *,'ENTER Th,Tc (K)'
        READ *,th,tc
        PRINT *,'enter slab thickness'
        read *,lt
        PRINT *,'ENTER kd/kw'
        READ *,kratio
        PRINT *,'ENTER run label'
        READ *,file$
        PRINT *,'ENTER alpha,error'
        READ *,alpha,error
        PRINT *,'ENTER print interval,simulation time'
        READ *,pint,tfinal
        file1$='temp'//file$//'.dat'
        file2$='liquid'//file$//'.dat'
        OPEN(unit=20,file=file1$,status='new')
        OPEN(unit=30,file=file2$,status='new')
C physical properties
        dv=1.6E-5
        kd=.026
        kw=kratio*kd
        R=461.8
        rho = 1.16
        cp = 1007.
        le=kw/(rho*cp*dv)
C find ch & c
C
              read(10,*),x0,x1
        if (x0.lt. .01) x0=.01
        do 10 i=1,20

      read(10,*),theta(i)
      10
      continue
        print *,th,t
         *
```

```
      x0=x0*lt
      x1=x1*lt
      t0=th
      t1=tc
      lw=x1-x0
      lwp=lw
      region(1)=.1*lt
      region(2)=.22*lt
      region(3)=.31*lt
      region(4)=.59*lt
      region(5)=.87*lt
             region(6)=1.0*lt
      iter2=0
      time=0
      pflag=.01
 80
 format(' ',g10.5,'    ',g10.5,'   ',g10.5,'   ',g10.5,' ',g10.5)
 85
 format(' ',g9.4,'  ',g9.4,'  ',g9.4,'  ',g9.4,'  ',g9.4,'  ',g9.4)
 87       format(' ',g9.4,'  ',g9.4,'  ',g9.4,'  ',g9.4,'  ',g9.4,'  '
      &  ,g9.4,'  ',g9.4,'  ',g9.4,'  ',g9.4)
      PRINT *,'TIME           T0             T1            X0            X1'
      write(20,*),'time   x0    x1    T(1)    T(2)    T(3)    T(4)    T(5)
      &  T(6)'
 90
 if (time .gt. pflag) then

 write(6,80),time,t0,t1,x0,x1

 do 95 i=1,6
 95
   if (x0.lt.region(i)) goto 96
 96
 do 97 j=1,i-1,1

   L(j)=0
 97
   T(j)=th-region(j)/x0*(th-t0)

 do 98 j=i,6

   x=(region(j)-x0)/lw

   L(j)=theta(int(1+19*x))

   eta=.5*(1-x-(exp(lambdap*x)-1)/(exp(lambdap)-1))

   T(j)=eta*dtp+trp
 98
 continue
   write (6,85),T(1),T(2),T(3),T(4),T(5),T(6)
   write(20,87),time,x0,x1,T(1),T(2),T(3),T(4),T(5),T(6)
   write(30,87),time,x0,x1,L(1),L(2),L(3),L(4),L(5),L(6)
   pflag =pflag + pint
   end if
   if (time .gt. tfinal) goto 290
   iter = 0
100
dtp=t0-t1
   trp=(t0+t1)/2
   betap=dtp/trp
   hfg=H(trp)
   crp=CONC(trp)
   [illegible]
```

```
c0=conc(t0)
c1=conc(t1)
dcp=c0-c1
omegap=hfg*(c0-c1)/(rho*cp*trp)
gamap=hfg/(r*trp)
bi=hfg*dv/kd
lambdap=2*gamap**2*betap*omegap/(1e+gamap*omegap)
dtdx0p=dtdx0
dtdx1p=dtdx1
const=dtp/lw
dtdx0=-.5*(1+lambdap/(dexp(lambdap)-1))*const
dtdx1=-.5*(1+lambdap*dexp(lambdap)/(dexp(lambdap)-1))*const
```

```
      dcdt0=(conc(t0+.001)-c0)/.001
      dcdt1=(conc(t1+.001)-c1)/.001
      if (x0.gt.0) then

    g1=(th-t0)/x0+dtdx0*(1+b1*dcdt0)
      else
                    goto 260
      endif

    if (iter .gt. 0) goto 200

    dtdx0p=dtdx0

    dtdx1p=dtdx1

    g1p=g1

    t0=t0+.01

    dt0=.01

    dtp=t0-t1

    dtdx0=-.5*(1+lambdap/(dexp(lambdap)-1))*dtp/lw
          dtdx1=-.5*(1+lambdap*dexp(lambdap)/(dexp(lambdap)-1))*dtp/lw
      g1=(th-t0)/x0+dtdx0*(1+b1*dcdt0)
    200
    iter=iter +1
      dt0=-alpha*dt0*g1/(g1-g1p)
      g1p=g1
      if (dabs(dt0).gt. .10) dt0=.1*sgn(dt0)
      t0=t0+dt0
      err=dabs(g1)
      if (err .gt. error) goto 100
      do 250 i=1,20
         ratio=19/lwp*(dx0+(i-1)*(lw-lwp)/19)
        theta(i)=theta(i)+(theta(i+1)-theta(i))*ratio
    250
    continue
         const=dtp/lw**2*kd/hfg*.5*lambdap**2/(dexp(lambdap)-1)
         &                  *crp/dcp
         sum=0
      do 255 i=1,19
         gamma(i)=const*dexp(lambdap*(i-1)/19)
         theta(i)=theta(i)+gamma(i)*dtime
         sum=sum+theta(i)*lw/19
    255      continue
      theta(20)=theta(20)-dv*(dcdt1*dtdx1)*dtime*20/lw
      sum=sum+theta(20)*lw/19
    c print *,sum,'liquid content'
    260
    dx0=-dtime*dv/theta(1)*(dcdt0*dtdx0)
      x0=x0+dx0
    c if (x1 .lt.lt) x1=x1-dtime*dv/theta(20)*(dcdt1*dtdx1)
      lwp=lw
      lw=x1-x0
      if (lw .lt. .005*lt) then

    print *,'dryout occurs under these conditions'

    write(6,80),time+dtime,t0,t1,x0,x1

    goto 290
      end if
```

```
      time=time+dtime
      iter2=iter2+1
      if (dx>0 .gt. 1e-18*dtime) goto 90
c write solution to temp.dat file
290
dx=(x1-x0)/20
c WRITE(20,350),0.,th
c WRITE(30,360),0.,ch
c DO 300 i=1,101
c     WRITE(20,350),x0+(i-1)*dx,T(i)
c
       ci=CONC(T(i))
c     WRITE(30,360),x0+(i-1)*dx,ci
```

```
c300
CONTINUE
c WRITE(20,350),1.,tc
c WRITE(30,360),1.,cc
350
FORMAT('  ',F6.4,'  ',F8.4)
360
FORMAT('  ',F6.4,'  ',F8.7)
390
PRINT *,'*****************************************************'
  PRINT *,'*****                    OUTPUT                    *****'
  PRINT *,' '
  PRINT *,'RUN LABEL',file$
  PRINT *,' '
  PRINT *,'HEAT ENTERING SLAB =',kd*(th-t0)/x0,'(W/m^2)'
  PRINT *,'HEAT LEAVING SLAB =',kd*(t1-tc)/(1-x1),'(W/m^2)'
  PRINT *,'VAPOR ENTERING SLAB =',dv*(ch-c0)/x0,'(kg/m^2 s)'
  PRINT *,'VAPOR LEAVING SLAB =',dv*(c1-cc)/(1-x1),'(kg/m^2 s)'
  PRINT *,' '
  PRINT *,'WET ZONE BOUNDARIES:',x0,x1
  PRINT *,' '
  PRINT *,'EVAPORATION RATE AT HOT SIDE =',J0,'(kg/m^2 s)'
  PRINT *,'EVAPORATION RATE AT COLD SIDE =',J1,'(kg/m^2 s)'
  PRINT *,' '
  PRINT *,'lambdap =',lambdap
  GOTO 450
400
PRINT *,' NO CONVERGENCE !!'
  goto 450
425
PRINT *,' NO CONDENSATION WITH THESE BOUNDARY CONDITIONS'
450
STOP
  END
c function CONC
  REAL*8 function CONC(T)
  COMMON/param/tr,cr,dv,hfg,R,kw,gama,beta,A1,E1,E2
  REAL*8 t,x,lgp,tnon,vg,A1(12),E1(7),E2(7),tr,cr,dv,hfg,R,kw,gama,beta
  integer*4 n
  lgp=a1(11)/(t-a1(12))
  DO 10 n=1,10
     x=DFLOTJ(n)
     lgp=lgp +sign(a1(n))*dexp(dlog(dabs(A1(n)))+(x-1)*dlog(T))
10      CONTINUE
  tnon=(647.3-T)/647.3
  vg=1.+1.6351057*tnon**(1./3.)+52.584599*tnon**(5./6.)-
     &   44.694653*tnon**(7./8.)
  DO 20 n=1,7
     vg=vg+E1(n)*tnon**n
20
CONTINUE
  vg=vg*22.089*.003155/dexp(lgp)
  CONC=1./vg
  RETURN
  END
C function H
  REAL*8 function H(T)
  COMMON/param/tr,cr,dv,hfg,R,kw,gama,beta,A1,E1,E2
  REAL*8 t,hfg1,tnon,A1(12),E1(7),E2(7),tr,cr,dv,hfg,R,kw,gama,beta
  INTEGER n
  tnon=(647.3-T)/647.3
  hfg1=.779221*tnon**(1./3.)+4.62668*tnon**(5./6.)-1.07931*tnon**(7./8.)
  DO 10 n=1,7
     hfg1=hfg1+E2(n)*tnon**n
```

```
10
continue
  H=hf31*2.5000E8
  RETURN
  end


c function sgn
  real*8 function sgn(t)
  real*8 a,t
  if (t .lt.0) then

a=-1
  else
          a=1
  end if
  sgn=a
  return
  end
```